NATIONAL UNIVERSITY OF SCIENCE AND
TECHNOLOGY POLITEHNICA BUCHAREST
Doctoral School of Biotechnical Systems Engineering

ABSTRACT OF THE PHD THESIS

DIRECTOR OF THESIS:
Prof. PhD. Eng. habil. Andrei CRAIFALEANU

PhD STUDENT:
Eng. Ștefan DUMITRU

2024

NATIONAL UNIVERSITY OF SCIENCE AND
TEHNOLOGY POLITEHNICA BUCHAREST
Doctoral School of Biotechnical Systems Engineering

ABSTRACT OF THE PHD THESIS

MECHANICAL ANALISYS OF A ROBOTIC HAND-ARM SYSTEM

DIRECTOR OF THESIS:
Prof. PhD. Eng. habil. Andrei CRAIFALEANU

PhD STUDENT:
Eng. Ștefan DUMITRU

2024

Contents

1. Introduction

1.1. Importance of the theme and motivation behind its study

The study of robotic systems continues to be an area of interest, where new methods for their simulation [52], [72] and control [37] are being investigated. Various researchers generally study simple robotic systems without applications for the common man in his everyday life [22], [61]. A first obstacle that a home user, or an elderly person might face in using a robotic system, would be its adversity to a classical robotic arm with a simple prehension system. For this reason, the robot studied in this PhD thesis attempts to mimic a human arm as closely as possible, both in the movement it is intended to perform and in the size of the system.

Above all, the method of prehension is very important as it can attract or repel potential home users. The human hand is a complex biological mechanism [26], [29], [55], difficult to replicate at low cost, which is why, in general, classical graspers have a small number of degrees of freedom and no possibility to manipulate an already grasped object [34], [69], [73]. There are also studies on anthropomorphic graspers with a large number of degrees of freedom [2], [46], but they are difficult to operate by an inexperienced user.

The literature often studies either only the robotic arm [17] or only the prehensor [25], without considering the influence that one has on the other.

The prices of anthropomorphic robotic arms are generally high [79], [80], [81] In the present work, the aim is to produce a model that can be practically realized at a low cost, built from prefabricated parts that can be printed using a 3D printer. By following this design strategy, modifications can be subsequently made to the robotic arm designed and presented in this paper.

This PhD thesis aims to conduct a full kinematic and dynamic study of an original anthropomorphic hand-arm system for domestic use.

1.2. General knowledge

The study of robotic systems consisting of an arm and a prehension system is an important field of study which, although addressed by many researchers, is still of interest and offers a wide range of research directions.

This PhD thesis studied an anthropomorphic robotic arm with 7 degrees of freedom corresponding to the three joints of the human arm (shoulder - 3 degrees of freedom, elbow - 1 degree of freedom, wrist - 2 degrees of freedom), plus an additional degree of freedom from the movement of the forearm around its longitudinal axis.

An anthropomorphic prehensor (a robotic hand) with 5 fingers and 6 mobilities has been placed at the end of this robotic arm. The main reason for using such a complicated mechanism is to be able to make a robot that can be used for domestic use, in which case the shape and visual proximity of the robot hand to a human hand is an advantage for use by different people.

1.3. Study methods

Two problems are studied in robot dynamics [18] [45]. The first is that of direct dynamics, in which the laws of variation of forces and moments are taken to be known and the motion to be performed by the robot is determined. The second problem is that of inverse dynamics, in which the

motion to be performed by the robot is taken to be known and the forces and moments required to perform it are determined.

Buondonno and De Luca [5] used a Newton-Euler algorithm to solve the inverse dynamics problem of a robot with elastic joints. Sutanto et al [60] used a recursive Newton-Euler algorithm to control a robotic arm with 7 degrees of freedom. Gonçalves et al. [20] used a Newton-Euler algorithm to dynamically model a robot consisting of 24 bodies, with 19 degrees of freedom, driven by 4 linear motors and 15 revolution servomotors. Zhang et al [74] studied a robotic arm dynamically using the Newton-Euler algorithm to determine the moments in the joints of the XB7 robotic arm.

Wang et al [71] analyzed the dynamic behavior of the joints of an industrial robot using theory from multibody system dynamics.

1.4. Paper structure

This paper contains nine chapters.

The first chapter, Introduction, gives some general background on the importance of the topic, justifies the choice of this topic, and states the aims and objectives of the paper.

The second chapter, Current Status, presents a brief history of the topic, reviews the literature in the field of robotic arms and hands, and frames the topic within current research directions.

The third chapter, Presentation of the studied system, highlights the modifications to the anthropomorphic prehensor underlying the study and the design of the robotic arm studied in the PhD thesis.

The fourth chapter, System configuration study, presents how to determine the positions of the significant points of the robotic hand-arm system (joints and centers of mass), considering known values of the active joint parameters. Laws of variation of these parameters are also defined and considered later in numerical applications.

In the fifth chapter, entitled Kinematic study, methods for calculating the angular velocities and accelerations of the elements of the hand-arm robotic system, as well as the velocities and accelerations of significant points, are presented.

The sixth chapter, Inverse Dynamics, is devoted to determining the forces and moments in the joints when the motion of the robot is known, as well as the external forces. The formulas and equations used are deduced by the methods of classical mechanics (based on the impulse theorem and the kinetic momentum theorem). Alternatively, the driving forces and moments are also determined by the methods of analytical mechanics (based on D'Alembert's principle and the principle of virtual powers).

In the seventh chapter, Direct Dynamics is studied, where, knowing the driving forces and moments of each actuator, the motion of the elements of the hand-arm system is determined.

The eighth chapter, entitled Vibrations, deals with the determination of the proper pulsations of the fingers of the robotic hand as well as of the whole hand.

The concluding chapter presents the conclusions of this PhD thesis, the original contributions made by the author and the potential future directions of development of the topic.

2. Current status

2.1. A Brief history of robotics

Robots can be defined as machines that can operate either automatically or remotely [8] and can perform manipulation and motion tasks [75], being operable along two or more axes [76].

The popularity of robotic manipulators has steadily increased since their launch, and their ability to work in hazardous or toxic conditions [11], as well as their propensity to perform cyclic operations, has led to their increasing use in industrial applications.

2.2. Current status in robotic arms

Most robotic arms in existence today use two types of kinematic couplings with one degree of freedom each [58]:

- of rotation (of revolution) (fig. 2.1 a);
- of translation (prismatic) (fig. 2.1 b).

Fig. 2.1. Types of kinematic couplings used for manipulators

Both types of couples have one degree of freedom each. The revolution coupling only allows rotation through an angle θ about the axis of the joint (Fig. 2.1 a). The prismatic coupling allows only rectilinear motion with a displacement x along its axis (fig. 2.1 b).

In addition to prismatic and revolution couplings, the following types of joints are also used in practice [58]:

- helical coupling;
- cylindrical coupling;
- universal coupling;
- spherical couplings.

The movements allowed by revolution and prismatic couplings are plane, while the movements allowed by helical, cylindrical, universal, or spherical couplings are three-dimensional.

A classification of industrial manipulators can be made according to the presence of closed or open kinematic chains. Thus, there are two broad categories of industrial robots:

- serial manipulators; this category includes robots with an open kinematic coupling chain and independent joint coordinates;
- parallel manipulators; this category includes robots with a closed kinematic torque chain, the joint coordinates being linked by dependency relations [64].

2.3. Current status in robotic hands

The prehensor, or robotic hand, is the end effector of any robotic arm, with the function of grasping the object and manipulating it, which is why many research centers are interested and investigating the entire process [42].

Most grippers currently used in industry are simple mechanisms designed to perform simple repetitive operations of grasping and releasing objects [8]. However, they do not allow the manipulation of already grasped objects, which is essential for a robot with a wide range of

Anthropomorphic graspers or anthropomorphic mechanical hands have become an increasingly interesting topic for many researchers due to the versatility they have, unlike the currently used pincer or clamp-type graspers [43] [63].

The human hand is a complex biological mechanism, consisting of 27 bones (14 phalanges, 5 metacarpal and 8 carpal) and can be modelled as a system of rigid bodies, single joints and double joints with 25 degrees of freedom [1], [53] (Fig. 2.10).

Many examples of anthropomorphic robotic hands with a large number of degrees of freedom can be found in the literature, such as the Gifu II hand [28] or the OCU I hand [38], which have 16 and 19 degrees of freedom, respectively.

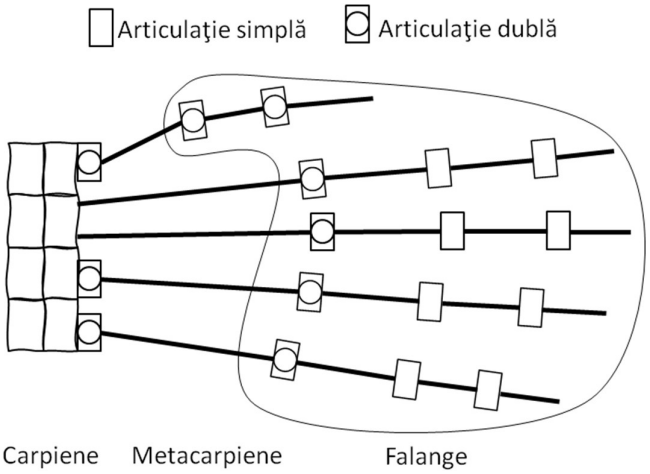

Fig. 2.10. The human hand in Abdel-Malek's proposed model

Such mechanisms are complex and difficult to use effectively because of the substantial number of actuators required to control them. To reduce the weight and complexity of such robotic hands, a system with a reduced number of actuators can be used, where some elements are connected by additional links. In the literature [12] there are many such robotic hands with a reduced number of degrees of freedom, designed to limit the size of the systems, such as the HRI hand [47] or the Alaris hand [44], both with 6 degrees of freedom.

3. Presentation of the studied system

To realize a hand-arm robotic system with a wide range of use, in the present work an anthropomorphic gripper was chosen, realized by improving the uHand robotic hand [78], [83], (Fig. 3.1).

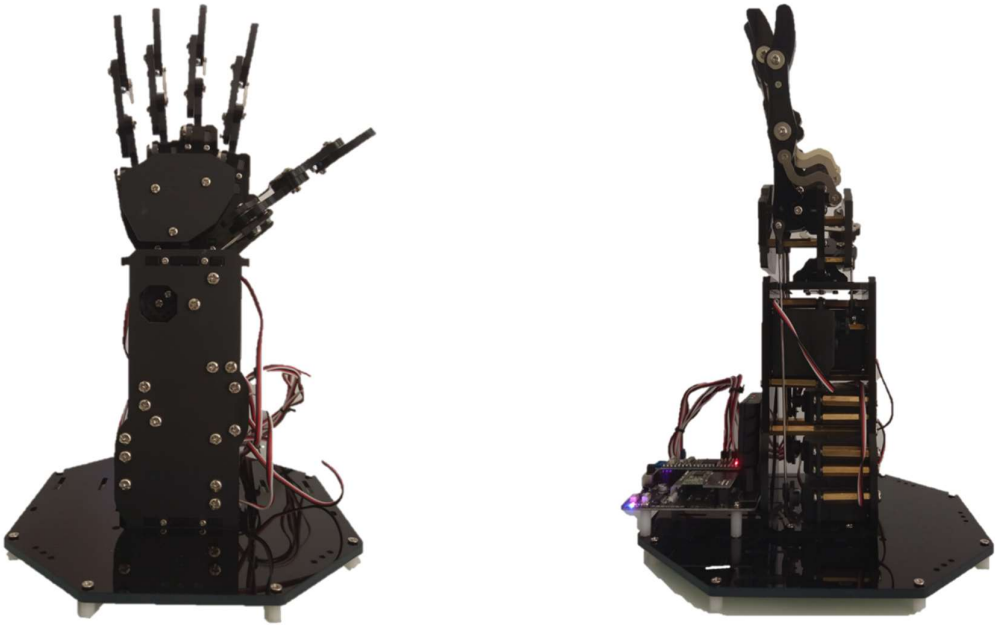

a) b)

Fig. 3.1. uHand robotic hand

3.1. uHand robotic hand

The uHand anthropomorphic robotic hand was made by Lobot. The prehensor has been studied in references [23], [24], but both works were limited to determining the positions of significant points of the system.

a) b)

Fig. 3.5. Grasping two spherical objects

An advantage of an anthropomorphic gripper is the ability to distribute the normal force applied to objects over a larger area, thus reducing the pressure applied to them.

Figure 3.5 shows the gripping of two spherical objects of varied sizes using the anthropomorphic robotic hand shown.

As can be seen, because the two objects have varied sizes, the gripping method applied to them is also different. Only three fingers are needed to grasp the object in figure 3.5 a), with the first finger being the supporting base and the other two fingers balancing it. For the object in figure 3.5 b), the first finger is the balancing finger, while the other three fingers and the palm acting on the object take over the degrees of freedom of the object.

Although the anthropomorphic robotic hand can easily grasp objects of varied sizes and shapes, as can be seen from the analysis of Figure 3.5, one problem with this anthropomorphic gripper is the impossibility of manipulating the object once it has been grasped.

Considering these issues, a number of modifications were made to the uHand to improve its grasp ability and to reduce the mass of the system.

3.2. Improvements brought to the uHand robotic hand

A first improvement that can be made to the uHand is the implementation of an additional degree of freedom for the thumb to rotate around an axis perpendicular to the palm of the hand. In this way, the functionality of this mechanical thumb approaches that of the human thumb.

However, the servomotors occupy most of the interior of the casing, which limits or even prevents the possibility of placing the components of the additional degree of freedom control mechanism. To this end, servomotors can be replaced by linear actuators, which are characterized by smaller volumes and masses.

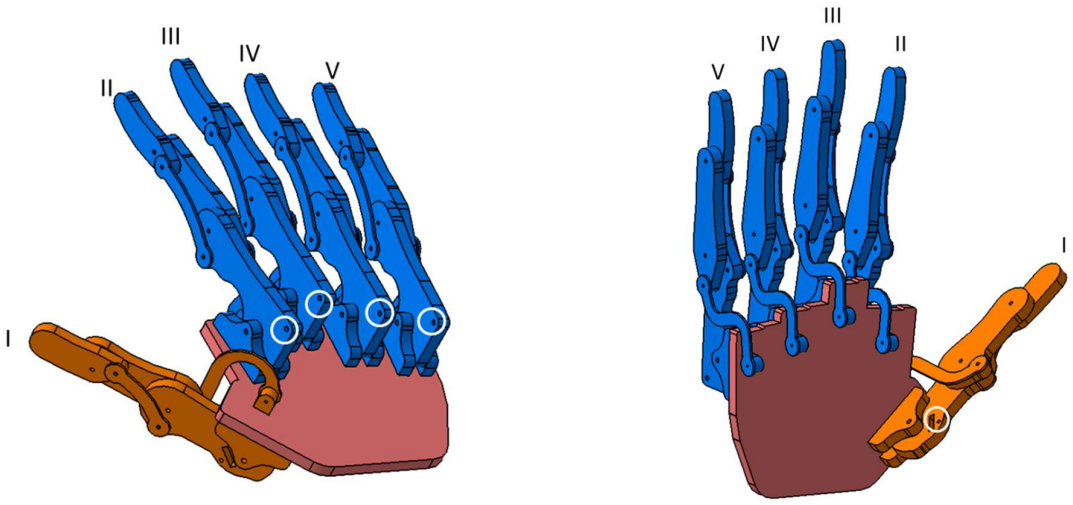

a) b)

Fig. 3.8. 3D model of the anthropomorphic prehensor

The housing of the linear actuator is made of plastic, while the actuator system (actuator rod) is made of duralumin. The maximum elongation of the chosen actuator is 21 mm and its nominal speed is 15 mm/s at a nominal voltage of 12 V. The motor speed can be changed by changing the motor supply voltage accordingly. Once the upper elongation or lower contraction

limit is reached, the motor automatically disconnects the power supply. Reversing the polarity of the current can change the direction of the drive. The nominal force that the linear actuator produces is 64 N. The 3D geometry of the anthropomorphic uHand is shown in Figure 3.8. Taking as reference finger III, finger II is rotated by 5^o and finger I by 45^o with respect to an axis perpendicular to the finger attachment plate. Relative to the same axis, but in the opposite direction, fingers IV and V are rotated by 3^o and 6^o, respectively. The axes of the rod grippers transmitting motion from the actuator yoke to the fingers are marked on the figure with white circles.

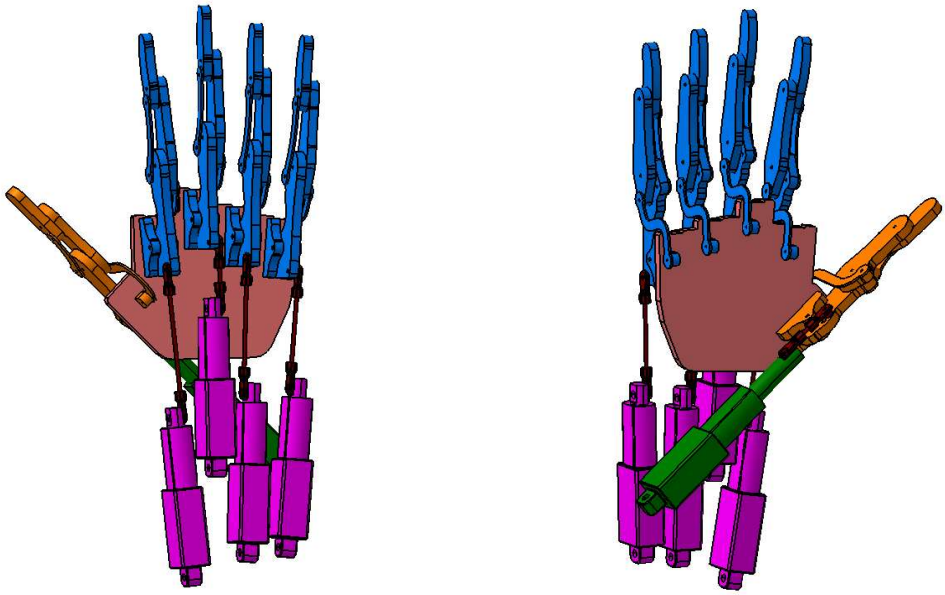

a) b)

Fig. 3.9. Position of linear actuators

The location of each actuator was chosen so that the movements of the yoke, rod and phalanges were in parallel planes (Fig. 3.9).

To flex fingers II-V the corresponding linear actuators must be extended, while due to the geometry of the system the actuator corresponding to finger I must have an opposite, restricting movement.

The thumb, together with its flexing mechanism (linear actuator and motion transmitting rod) is placed on a plate (fig. 3.11), which can be rotated by the additional degree of freedom control mechanism.

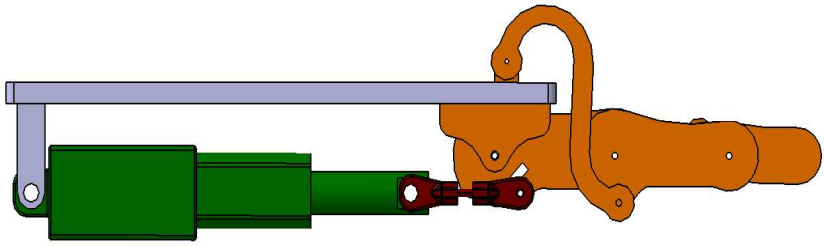

Fig. 3.11. Finger I assembly

The additional degree of freedom control mechanism is operated by an LFD-06 type servomotor, taken from those that have been replaced by linear actuators (fig. 3.12).

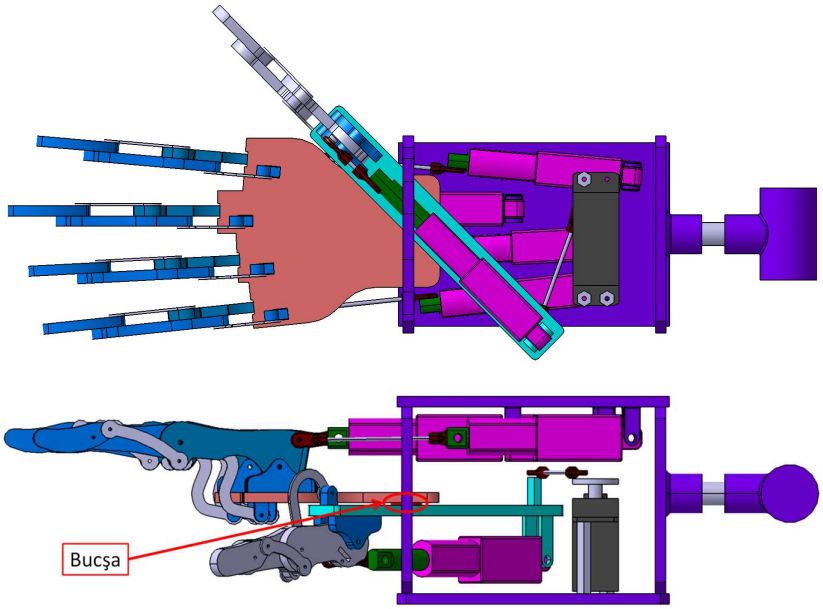

Fig. 3.12. Anthropomorphic hand assembly with 6 mobilities

3.3. Robotic arm

The modified anthropomorphic prehensor, shown in the previous paragraphs, was attached to an anthropomorphic robotic arm. It was designed by the author to be made of prefabricated materials with 3D printable joints. It was also intended that any changes to the design could be easily made, again using a 3D printer.

Such a human-like robotic arm was chosen to make a familiar-looking device for the home user, who is inexperienced in using robots.

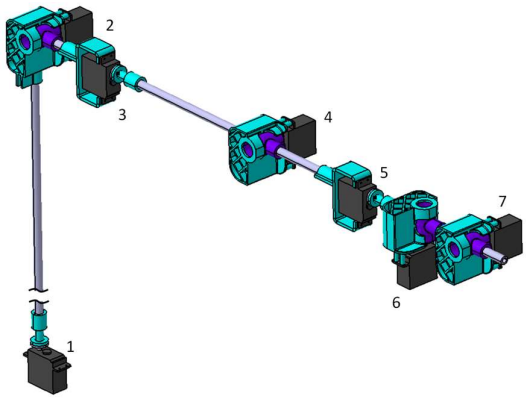

Fig. 3.13. 3D model of the robotic arm

In the designed robotic arm model (Fig. 3.13), servomotors 1-3 of type LFD-06 play the role of the ball joint present in the human shoulder. Servomotors 4 and 5, allow a system movement like that of the human forearm. Thus, the rotation allowed by the elbow joint is performed by servomotor 4 and the movement around the longitudinal axis of the forearm, produced by the ulna

and radius bones, is performed by servomotor 5. Servomotors 6 and 7 allow a movement such as that performed by the double wrist joint in two transverse directions.

The joints connect 10 mm diameter duralumin rods, which perform the role of bones in the human arm.

Three types of joints were used, whose 3D models are shown in Figure 3.14.

Joints 1, 3 and 5 (Fig. 3.13 a) allow rotation around the axes of the bars they connect. Joints 2, 4, 6 and 7 (Fig. 3.13 b, c) allow rotational movements about axes perpendicular to the directions of the bars, with the proviso that joint 2 connects initially perpendicular bars and joints 4, 6 and 7 connect initially parallel bars. The different geometry of hinge 2 from that of hinges 4, 6 and 7 is necessary because of the limitation of the rotational possibilities of these devices as well as of the servomotors.

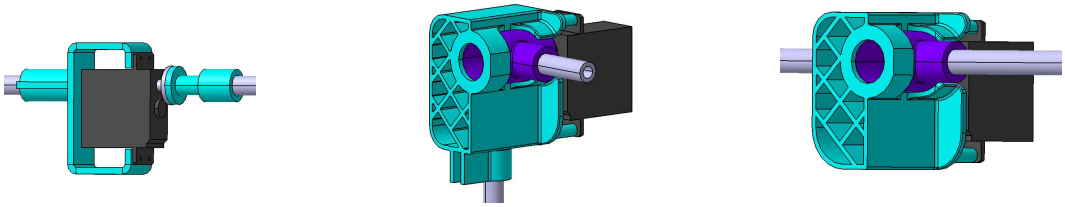

a) Joints 1, 3 and 5 b) Joint 2 c) Joints 4, 6 and 7

Fig. 3.14. 3D models of the joints (details)

At the end of the arm, attach the robotic hand with 6 degrees of mobility shown in the previous paragraph, resulting in a robotic hand-arm system (Fig. 3.15). This system is studied geometrically, kinematically, and dynamically in the following chapters.

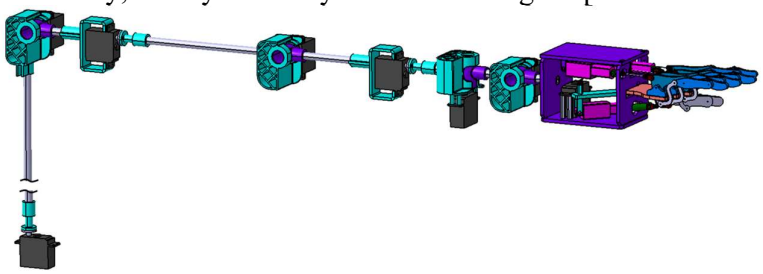

Fig. 3.15. 3D Model of the hand-arm system

4. Study of system configuration

In modelling the system, the following types of body-to-body connections were used:

- free, cylindrical joints - allowing rotation about the axis of symmetry;
- universal free joints - allowing rotation about the axis of symmetry as well as about an axis perpendicular thereto, locking rotation about the other perpendicular axis, generally in the longitudinal direction of the following body;
- free, spherical joints - allowing rotation about all three axes;
- controlled, cylindrical joints - imparting rotation about the axis of symmetry;
- controlled joints, prismatic ¬- which impart translation along the longitudinal axis.

The choice of link types was made in such a way as to avoid both under- and overstressing of the mechanical system, and therefore so that the system of dynamic equations calculating the forces and moments in the links is compatible and determinate.

4.1. Mechanical modelling of the hand-arm robotic system

The human arm, has three joints, all controlled:

- a ball joint (shoulder joint),
- a double joint (elbow joint and a joint corresponding to the movement of the ulna and radius bones rotating the forearm around its longitudinal axis),
- a double joint (wrist joint).

The spherical and double ball-and-socket joints are difficult to produce in practice by 3D printing and to put into operation accurately, which is why it was decided to replace them with cylindrical joint systems, driven independently by rotary servomotors (Fig. 3.13). This results in the cylindrical ball-and-socket joints of O_1, O_2, O_3, O_4, O_5, O_6 and O_7 (fig. 4.1).

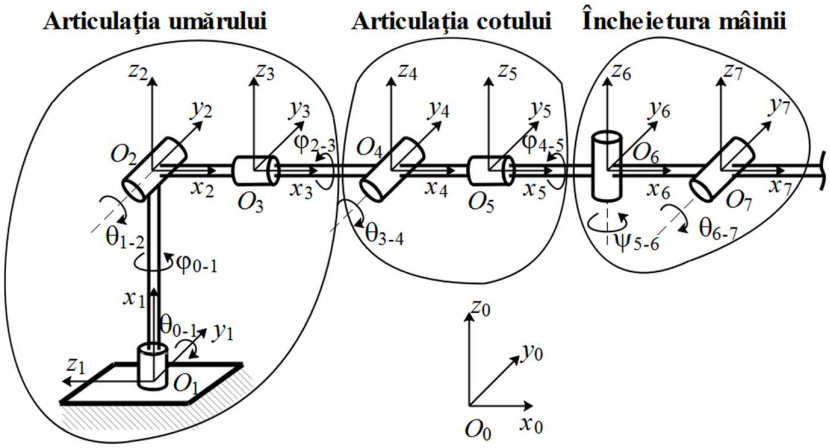

Fig. 4.1. Mechanical model of the studied robotic arm

The resulting mechanical model (Fig. 4.1) has 7 degrees of freedom of rotation, defined by the angles $\varphi_{0\text{-}1}$, $\theta_{1\text{-}2}$, $\varphi_{2\text{-}3}$, $\theta_{3\text{-}4}$, $\varphi_{4\text{-}5}$, $\psi_{5\text{-}6}$, and $\theta_{6\text{-}7}$, around the axes x_1, y_2, x_3, y_4, x_5, z_6, and y_7, respectively.

The reference system attached to the i-element was chosen with its origin in the joint O_i and with the axis Ox directed to the next joint in the kinematic chain. Coordinate system $O_1x_1y_1z_1$.

The coordinate system of the first element of the mechanical model was rotated relative to the global reference system $O_0x_0y_0z_0$, around the axis y_0 with the angle $\theta_{0\text{-}1}$=-90°.

The anthropomorphic prehension system shown in paragraph 3.2 attaches to the robotic arm at the joint O_7.

The thumb additional degree of freedom control system (fig. 4.2 a - 3D model, fig. 4.2 b - mechanical model) has three fixed points relative to the reference system 7 (O_7, O_8 and O_{10}) and two mobile points (O_9 and F). The degree of freedom added to the thumb is rotation about an axis perpendicular to the plate to which fingers 2-5 are attached.

The links of the additional freedom control system are modelled as follows:

- in O_8 – controlled, cylindrical joint;
- in O_9 – free, universal joint;
- in F – free, spherical joint;
- in O_{10} – free, cylindrical joint.

For all five fingers, reference system 10 is rotated by an angle $\psi_{7\text{-}10}$ compared to reference system 7. For the thumb, this angle is variable and is controlled by means of the quadrilateral mechanism, $O_8O_9FO_{10}$, allowing the body FO_{10} to rotate, relative to the axis z_{10}. For fingers 2-5, this angle is constant and the mechanism $O_8O_9FO_{10}$ is not present. Thus, in the case of these fingers systems 8, 9 and 10 coincide.

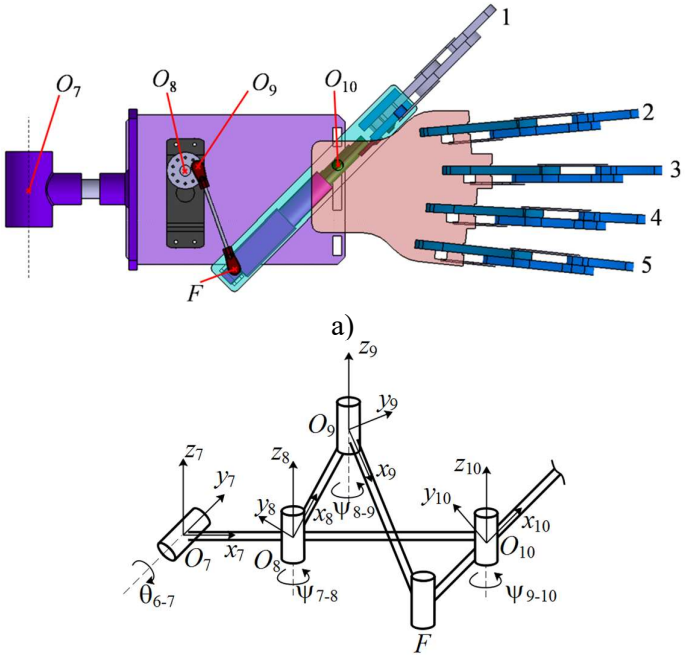

Fig. 4.2. System controlling the additional degree of freedom of the thumb

The geometry of fingers 2-5 (fig. 4.3 a) is like that of finger 1 (fig. 4.3 b). All five fingers can be mechanically modelled by the single-mobility system shown in figure 4.3 c. This system is composed of a crank rod mechanism with eccentricity ($O_{11}O_{12}AO_{13}$) and two inverted quadrilateral mechanisms ($O_{13}O_{14}BO_{15}$ and $O_{14}O_{16}DO_{17}$The distal phalanx continues to the point of contact with the object to be grasped.

The links between the bodies making up the fingers are shaped as follows [14]:

- in O_{11} – controlled, prismatic joint;
- in O_{12}, O_{15} and O_{17} – free, universal joint;

- in A, B and D – free, spherical joint;
- in O_{13}, O_{14} and O_{16} – free, cylindrical joint.

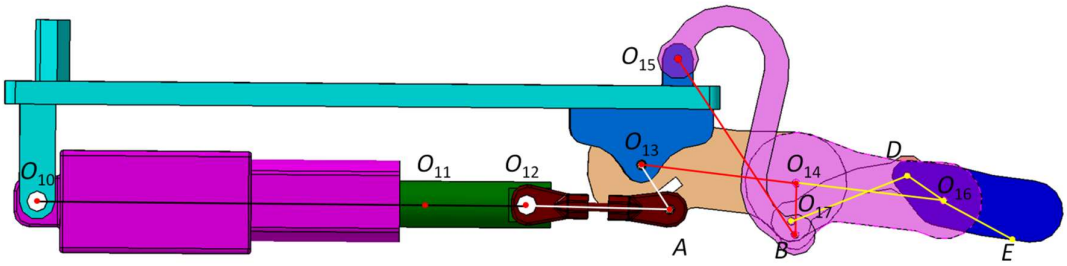

a) 3D model of finger 1

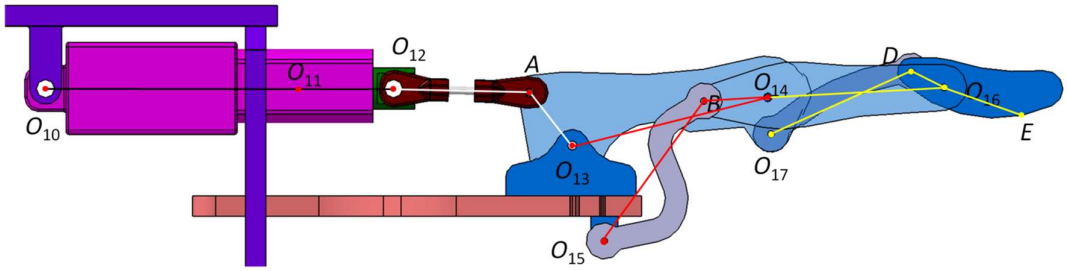

b) 3D model of fingers 2-5

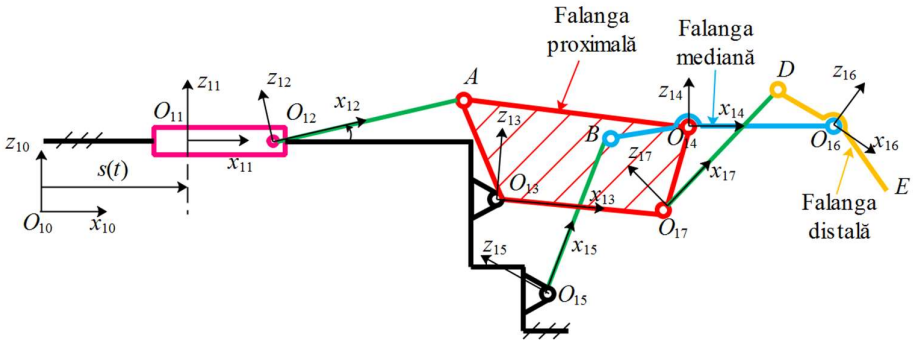

c) mechanical model of fingers 1-5

Fig. 4.3. Finger modelling

4.2. Laws of motion

The eight rotary servomotors and five linear actuators form a system with 13 control parameters ($\varphi_{0\text{-}1}$, $\theta_{1\text{-}2}$, $\varphi_{2\text{-}3}$, $\theta_{3\text{-}4}$, $\varphi_{4\text{-}5}$, $\psi_{5\text{-}6}$, $\theta_{6\text{-}7}$, $\psi_{7\text{-}8}$, s_1, s_2, s_3, s_4 and s_5). Depending on the complexity of the problem to be studied, these parameters may have different values and be described by distinct functions. For the studies in chapters 4-6 known laws of motion of these parameters have been considered.

The laws of motion were chosen as follows:

- for the angular parameters ($\varphi_{0\text{-}1}$, $\theta_{1\text{-}2}$, $\varphi_{2\text{-}3}$, $\theta_{3\text{-}4}$, $\varphi_{4\text{-}5}$, $\psi_{5\text{-}6}$, $\theta_{6\text{-}7}$ and $\psi_{7\text{-}8}$), a law of motion has been sought which starts and ends with zero angular velocity and acceleration; such a law of motion must be expressed by a function with zero first and second derivatives at the initial

and final times, t_1 and t_2; considering the initial and final values of any rotation angle, f1 and f2, a function satisfying these conditions is [77] (fig. 4.4):

$$f(t) = f_1 + (f_2 - f_1) \cdot \left[\frac{t - t_1}{t_2 - t_1} - \frac{\sin\left(2\pi \frac{t - t_1}{t_2 - t_1}\right)}{2\pi} \right]; \tag{4.1}$$

- for the linear parameters (s1, s2, s3, s4 and s5), a simple law of motion was chosen, with constant values of the linear motor speed:

$$s(t) = v_{ml} \cdot t + x_0. \tag{4.2}$$

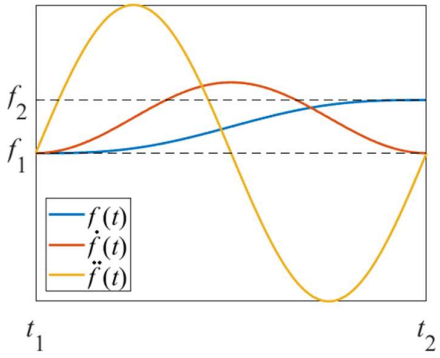

Fig. 4.4. Law of motion and its derivatives for angular parameters

4.3. Rotations. Transformation matrix

Transformation between point coordinate matrices P_1, $\{X_1\}$, respectively $\{X_1'\}$, is a function of the form $\{X_1'\} = f(\{X_1\}, t)$, which is shaped [43]:

$$f(\{X_1\}, t) = [T](t) \cdot \{X_1\}, \tag{4.3}$$

where $[T](t)$ is, in the case of Euclidean space, a time-dependent transformation matrix defined in $\mathbb{R}^{3x3}$.

If the rotation occurs at an angle φ about the *Ox* axis, the transformation matrix is [3], [15], [43], [48]:

$$[T_x](\varphi) = \begin{bmatrix} 1 & 0 & 0 \\ 0 & cos\,\varphi & -sin\,\varphi \\ 0 & sin\,\varphi & cos\,\varphi \end{bmatrix}. \tag{4.4}$$

Similarly, if the rotation occurs at an angle θ about the *Oy* axis, the transformation matrix is:

$$[T_y](\theta) = \begin{bmatrix} cos\,\theta & 0 & sin\,\theta \\ 0 & 1 & 0 \\ -sin\,\theta & 0 & cos\,\theta \end{bmatrix}. \tag{4.5}$$

Similarly, if the rotation occurs with angle ψ around the *Oz* axis, the transformation matrix is:

$$[T_z](\psi) = \begin{bmatrix} cos\,\psi & -sin\,\psi & 0 \\ sin\,\psi & cos\,\psi & 0 \\ 0 & 0 & 1 \end{bmatrix}. \tag{4.6}$$

4.4. Determination of coordinates and angles

The coordinates $\{X\}$ of a point in any reference system j can be determined using the coordinate rotation matrix transformation with respect to a known reference system k,

$$\{X\}_j = [T]_{jk}\{X\}_k, \tag{4.7}$$

where:

- the reference system j is obtained by rotating the reference system k, first by the angle φ about the *Ox* axis, then by the angle θ about the *Oy* axis, and finally by the angle ψ about the *Oz* axis;
- $\{X\}$ is the column matrix of coordinates,

$$\{X\} = \begin{Bmatrix} x \\ y \\ z \end{Bmatrix}, \tag{4.8}$$

- $[T]_{jk}$ is the rotation matrix from reference system k to reference system *j* [15], [48], [59],

$$[T]_{jk} = T_x(\varphi)T_y(\theta)T_z(\psi) = \\ = \begin{bmatrix} c\theta \cdot c\psi & -c\theta \cdot s\psi & s\theta \\ c\varphi \cdot s\psi + s\varphi \cdot s\theta \cdot c\psi & c\varphi \cdot c\psi - s\varphi \cdot s\theta \cdot s\psi & -s\varphi \cdot c\theta \\ s\varphi \cdot s\psi - c\varphi \cdot s\theta \cdot c\psi & s\varphi \cdot c\psi + s\theta \cdot s\psi & c\varphi \cdot c\theta \end{bmatrix} \tag{4.9}$$

- *c* and *s* are the cosine and sine functions applied to the angles of rotation,

$$\begin{cases} s\varphi = \sin\varphi_{jk} & s\theta = \sin\theta_{jk} & s\psi = \sin\psi_{jk} \\ c\varphi = \cos\varphi_{jk} & c\theta = \cos\theta_{jk} & c\psi = \cos\psi_{jk} \end{cases}. \tag{4.10}$$

At some point in time, the angles $\varphi_{0\text{-}1}$, $\theta_{1\text{-}2}$, $\varphi_{2\text{-}3}$, $\theta_{3\text{-}4}$, $\varphi_{4\text{-}5}$, $\psi_{5\text{-}6}$, $\theta_{6\text{-}7}$, and $\psi_{7\text{-}8}$ have known values, resulting from the laws of motion presented above. Thus, the coordinates of *Oi* points are determined using the formulae (4.7)-(4.10).

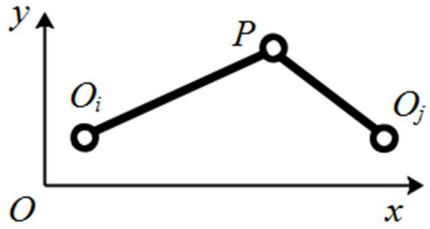

Fig. 4.6. System with two articulated rods

For the solution of the quadrilateral and eccentricity crank rod systems presented above, it can be seen that in the general case of two articulated rods O_iP and O_jP, moving parallel to the plane *Oxy* (fig. 4.6), the x and y coordinates of point *P* are determined using the system of equations:

$$\begin{cases} (x_P - x_{O_i})^2 + (y_P - y_{O_i})^2 = O_iP^2 \\ (x_P - x_{O_j})^2 + (y_P - y_{O_j})^2 = O_jP^2. \end{cases} \tag{4.11}$$

4.5. Numerical applications

In the numerical applications the laws of motion presented in paragraph 4.1 were used, considering the following input data:

- the time interval in which the movement takes place, $t = 0 \ldots 0.8$ s;
- speed of the linear actuator of finger 1, $v_{ML\,1} = -12.75$ mm/s;

- speed of the linear actuator of fingers 2-5, $v_{ML\,2-5} = 15\,\mathrm{mm/s}$.

The time step value was chosen by trial and error to identify an acceptable compromise between the accuracy of the numerical integration results and the runtime of MATLAB

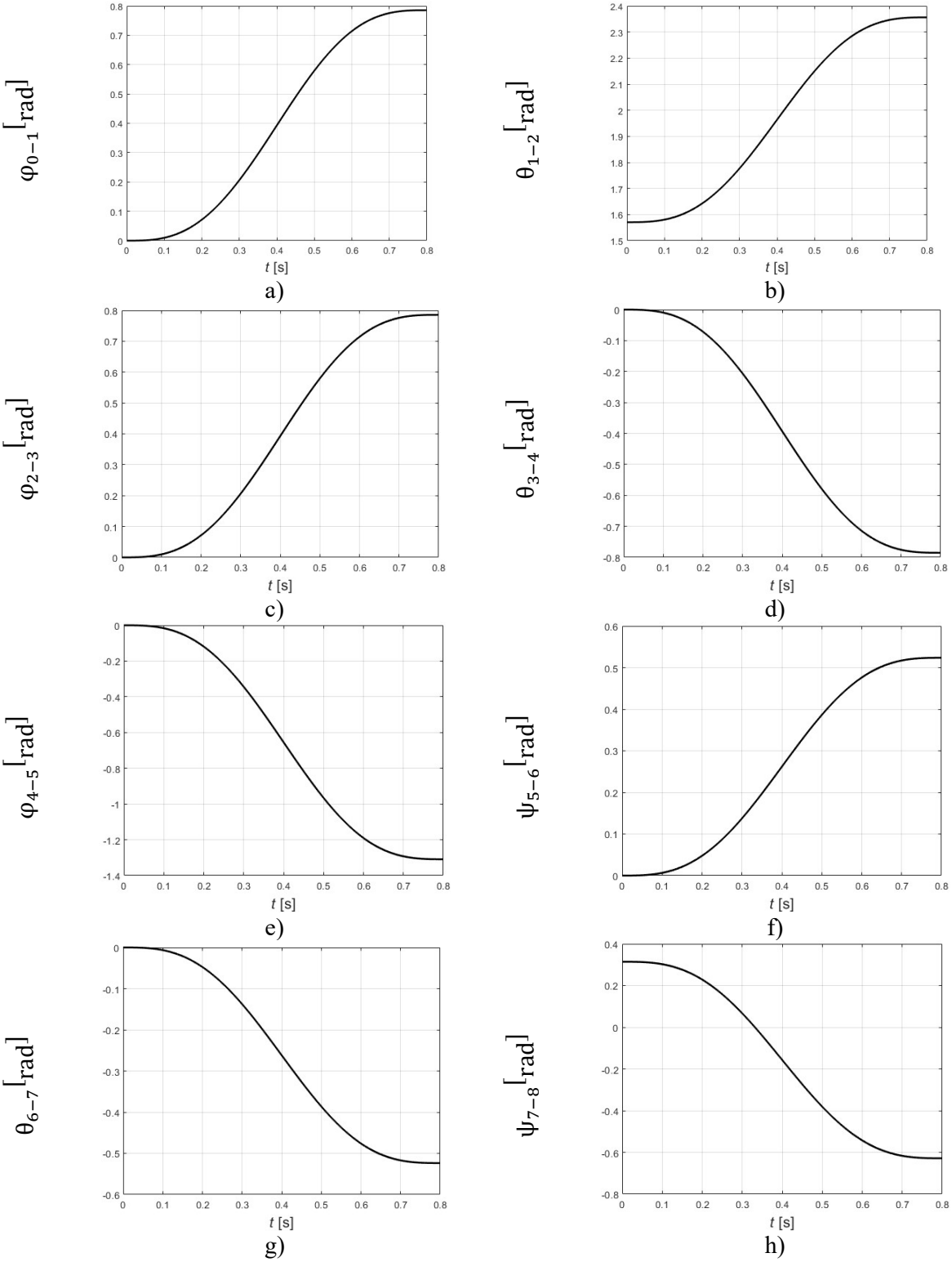

Fig. 4.7. Variations of rotation angles in driving joints

The speed of the linear actuator of finger 1 was imposed by the operating limits of the finger mechanism. The speed of the linear actuators of fingers 2-5 is equal to their nominal speed.

The ranges of variation of the angles corresponding to the arm actuators are given in Table 4.1.

Tab. 4.1: Angles of rotation of the drive joints of the robotic arm

Angle	$\varphi_{0\text{-}1}$	$\theta_{1\text{-}2}$	$\varphi_{2\text{-}3}$	$\theta_{3\text{-}4}$	$\varphi_{4\text{-}5}$	$\psi_{5\text{-}6}$	$\theta_{6\text{-}7}$
Value	$0 \dots \frac{\pi}{4}$	$\frac{\pi}{2} \dots \frac{3\pi}{4}$	$0 \dots \frac{\pi}{4}$	$0 \dots -\frac{\pi}{4}$	$0 \dots -\frac{5\pi}{12}$	$0 \dots \frac{\pi}{6}$	$0 \dots -\frac{\pi}{6}$

Table 4.2 shows the rotation angles between reference system 7 and reference system 8.

Tab. 4.2: Angles of rotation $\psi_{7\text{-}8}$ of each finger

Finger	1	2	3	4	5
Value	$\frac{\pi}{10} \dots -\frac{\pi}{5}$	$\frac{\pi}{36}$	0	$-\frac{\pi}{60}$	$-\frac{\pi}{30}$

The variations of the relative rotation angles of coordinate systems 1-8 are illustrated in Figure 4.7.

The variations of the function s(t) for finger 1 and fingers 2-5 respectively are plotted in Figure 4.8.

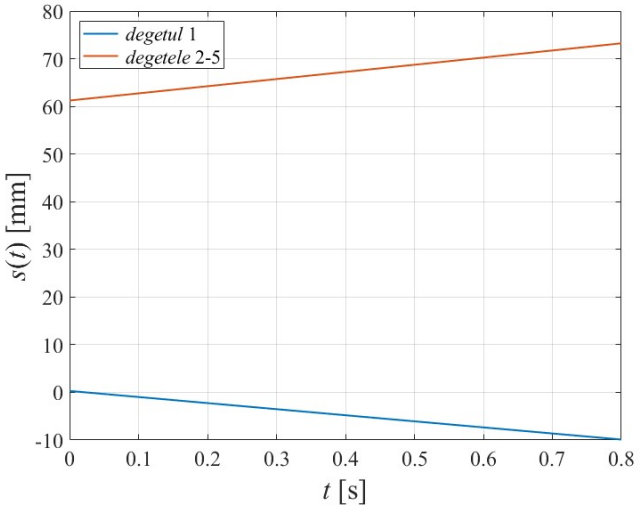

Fig. 4.8. Variations of displacements of prismatic couplings $O_{10}O_{11}$

Figure 4.10 shows the variations of the joint coordinates O_2, ..., O_7, with respect to the $O_1x_0y_0z_0$ reference system.

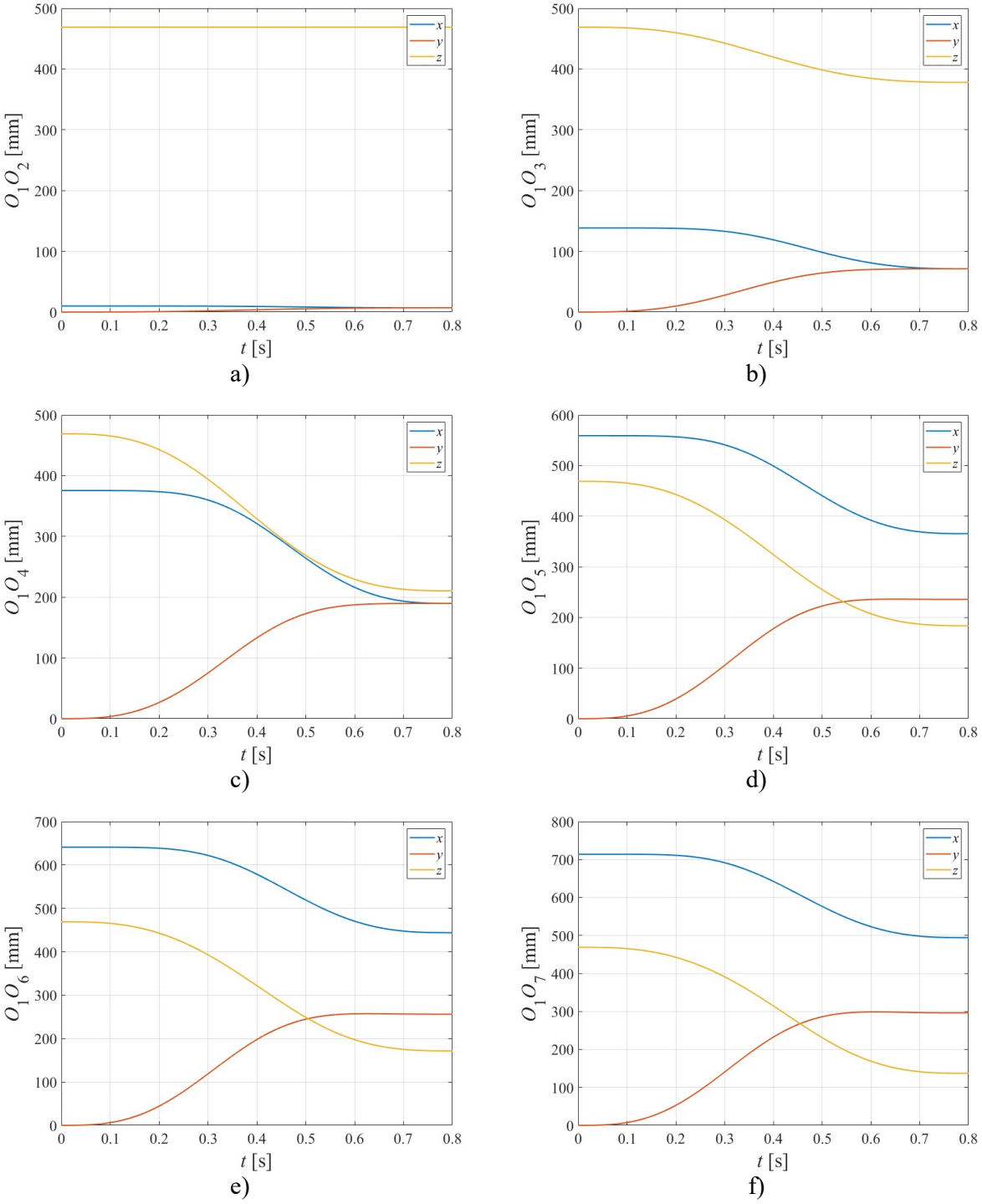

Fig. 4.10. Variations of the arm joint coordinates

Figure 4.12 shows the coordinate variations, in the global reference system, of the joints of the assembly of which this finger is composed, O_8, ..., O_{17}, A, B, D, E, F.

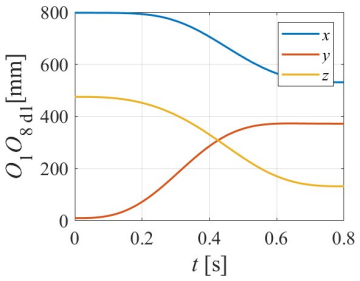
$O_1O_{8\,d1}$ [mm]
t [s]
x
y
z

a)

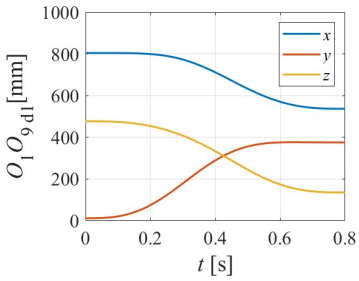
$O_1O_{9\,d1}$ [mm]
t [s]
x
y
z

b)

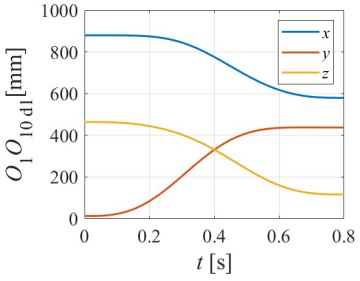
$O_1O_{10\,d1}$ [mm]
t [s]
x
y
z

c)

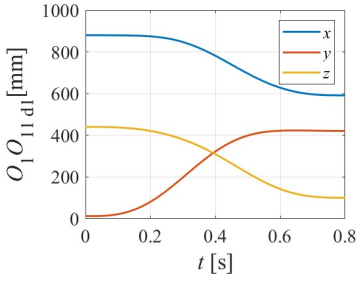
$O_1O_{11\,d1}$ [mm]
t [s]
x
y
z

d)

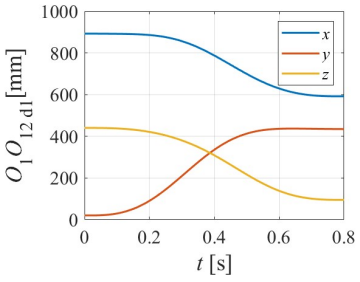
$O_1O_{12\,d1}$ [mm]
t [s]
x
y
z

e)

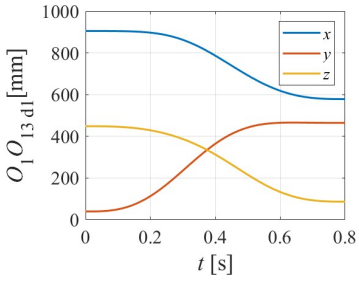
$O_1O_{13\,d1}$ [mm]
t [s]
x
y
z

f)

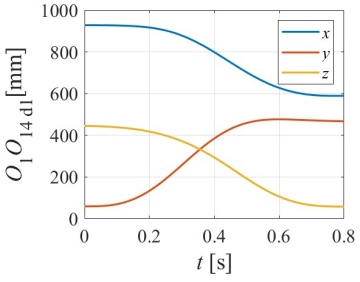
$O_1O_{14\,d1}$ [mm]
t [s]
x
y
z

g)

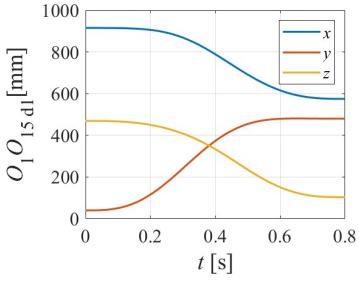
$O_1O_{15\,d1}$ [mm]
t [s]
x
y
z

h)

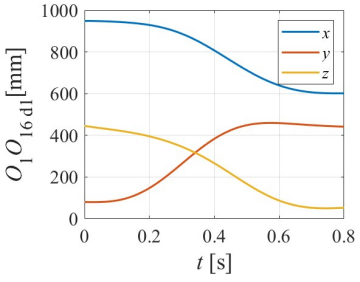
$O_1O_{16\,d1}$ [mm]
t [s]
x
y
z

i)

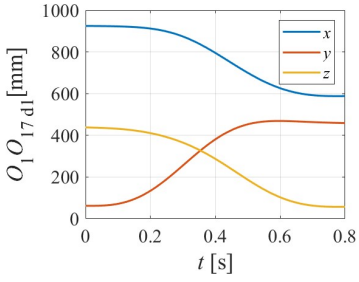
$O_1O_{17\,d1}$ [mm]
t [s]
x
y
z

j)

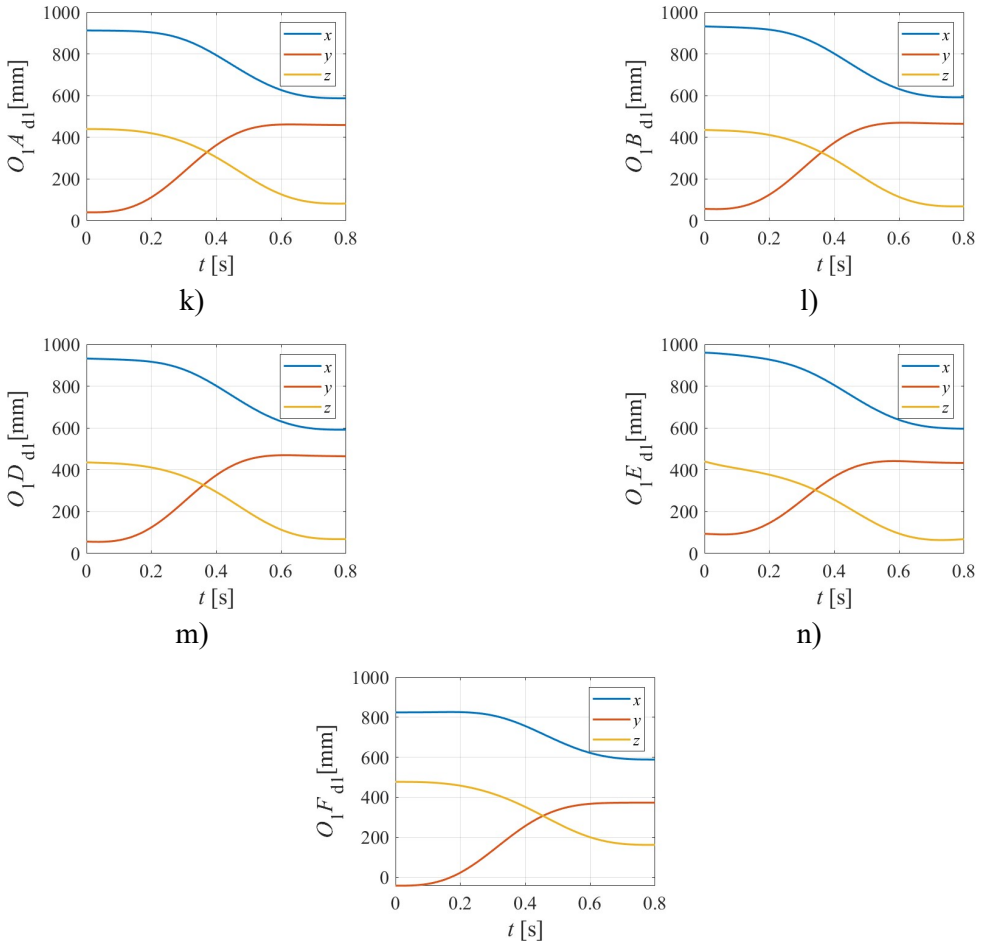

Fig. 4.12. Variation of the coordinates of the joints of finger 1

4.6. Conclusions

The movement of the hand-arm robotic system was visualized through an animated graphical representation of its significant points, made with the help of a program developed to determine the kinematic and dynamic calculations.

The variations of the arm and finger joint coordinates, presented in the previous paragraph, occur within a plausible range, not exceeding the physical limitations of the hand-arm robotic system.

5. Kinematic study

In this chapter the velocities and accelerations of the significant points of the bodies of the hand-arm system and the angular velocities and accelerations of these bodies are determined.

5.1. Velocity and angular velocities

In the general case of a Cartesian coordinate system, rotated first by the angle φ around the axis *Ox*, then with the angle θ around the new *Oy* axis and finally with the angle ψ around the new *Oz* axis, the column matrix corresponding to the angular velocity vector with respect to the initial system is [48], [59]:

$$\begin{Bmatrix}\omega_x\\ \omega_y\\ \omega_z\end{Bmatrix} = \begin{bmatrix} cos(\theta)\cdot cos(\psi) & sin(\psi) & 0\\ -cos(\theta)\cdot sin(\psi) & cos(\psi) & 0\\ sin(\theta) & 0 & 1\end{bmatrix}\begin{Bmatrix}\dot{\varphi}\\ \dot{\theta}\\ \dot{\psi}\end{Bmatrix}. \quad (5.1)$$

Considering the angular velocity vector of system *i* with respect to system *j* and that of system *j* with respect to system *k*, the angular velocity vector of system *i* with respect to system *k* can be written as [9], [51], [68]:

$$\bar{\omega}_{i,k} = \bar{\omega}_{i,j} + \bar{\omega}_{j,k} \quad (5.2)$$

The velocity of any point, *P*, of rigid *i*, relative to reference system *j*, can be determined with the formula [[9], [51], [68]:

$$\bar{v}_{P,j} = \bar{v}_{O_i,j} + \bar{\omega}_{i,j} \times \overline{O_iP}. \quad (5.3)$$

The velocity of the point O_{11} of the linear motor rod is determined using the known formulas from the kinematics of the relative motion of the [9], [51], [68]:

$$\bar{v}_{O_{11},j} = \bar{v}_{O_{11},10} + \bar{v}_{O_{10},j} + \bar{\omega}_{j,10} \times \overline{O_{10}O_{11}}. \quad (5.4)$$

In the case of two articulated bars O_iP and O_jP moving in the plane (fig. 4.6), if the speeds of the points O_i and O_j are known, the angular velocities of the bars as well as the velocity of point *P* can be determined using the formula (5.6):

$$\bar{v}_P = \bar{v}_{O_i} + \bar{\omega}_i \times \overline{O_iP} = \bar{v}_{O_j} + \bar{\omega}_j \times \overline{O_jP}. \quad (5.5)$$

This calculation method applies to systems $O_8O_9FO_{10}$, $O_{11}O_{12}AO_{13}$, $O_{13}O_{14}BO_{15}$ and $O_{14}O_{16}DO_{17}$, to determine the velocities of the points *F*, *A*, *B* and *D*, as well as the angular velocities of bodies 9, 10 and 12-17, respectively.

5.2. Accelerations and angular accelerations

The angular acceleration vector is the derivative of the angular velocity vector [9], [51], [68]:

$$\begin{Bmatrix}\varepsilon_x\\ \varepsilon_y\\ \varepsilon_z\end{Bmatrix} = \begin{Bmatrix}\dot{\omega}_x\\ \dot{\omega}_y\\ \dot{\omega}_z\end{Bmatrix}. \quad (5.6)$$

Assuming that the velocity and angular acceleration vectors of system *i* with respect to system *j* and of system *j* with respect to system *k* are known, the angular acceleration vector of system *i* with respect to system *k* can be written as [9], [51], [68]:

$$\bar{\varepsilon}_{i,k} = \bar{\varepsilon}_{i,j} + \bar{\varepsilon}_{j,k} + \bar{\omega}_{j,k} \times \bar{\omega}_{i,j}. \quad (5.7)$$

The acceleration of any point, *P*, of rigid *i*, relative to the reference system *j*, can be determined with the formula [9], [51], [68]:

$$\bar{a}_{P,j} = \bar{a}_{O_i,j} + \bar{\varepsilon}_{i,j} \times \overline{O_iP} + \bar{\omega}_{i,j} \times \left(\bar{\omega}_{i,j} \times \overline{O_iP}\right). \quad (5.8)$$

The acceleration of point O_{11} of the linear motor rod is determined using the known formulas from the kinematics of the relative motion of the rigid body[9], [51], [68]:

$$\bar{a}_{O_{11},j} = \bar{a}_{O_{11},10} + \bar{a}_{O_{10},j} + \bar{\varepsilon}_{10,j} \times \overline{O_{10}O_{11}} + \bar{\omega}_{10,j} \times \left(\bar{\omega}_{10,j} \times \overline{O_{10}O_{11}}\right) + 2\bar{\omega}_{10,j} \times \bar{v}_{O_{11},10}. \quad (5.9)$$

In the case of two articulated bars O_iP and O_jP moving in plane (fig. 4.6), if the accelerations of the points O_i and O_j, as well as the angular velocities of the bars are known, , the angular accelerations of the bars can be determined, as well as the acceleration of point P, using the formula (5.16):

$$\bar{a}_P = \bar{a}_{O_i} + \bar{\varepsilon}_i \times \overline{O_iP} + \bar{\omega}_i \times (\bar{\omega}_i \times \overline{O_iP}) = \bar{a}_{O_j} + \bar{\varepsilon}_j \times \overline{O_jP} + \bar{\omega}_j \times \left(\bar{\omega}_j \times \overline{O_jP}\right). \quad (5.10)$$

This calculation method applies to systems $O_8O_9FO_{10}$, $O_{11}O_{12}AO_{13}$, $O_{13}O_{14}BO_{15}$ and $O_{14}O_{16}DO_{17}$, to determine the accelerations of the points F, A, B and D, as well as the angular accelerations of the bodies 9, 10 and 12-17.

5.3. Numerical applications

In the numerical study, the velocities, and accelerations of the significant points of the hand-arm system were determined, as well as the velocities and angular accelerations of the bodies forming this system.

5.3.1. Velocities and angular velocities

The variations of the angular velocities of the bodies that make up the arm, in relation to the reference system 0, are represented in figure 5.2. They start from and return to the value 0. This is due to the chosen law of motion. The variations of the angular velocities of the bodies that make up the assembly of finger 1 (fig. 5.3) follow the same rule mentioned previously, up to body 11. Starting with body 12, this property is no longer preserved, because the influence of the law of motion of the linear motor appears. Another observation would be that the angular velocities of bodies 10 and 11 coincide. This is due to the translational movement of body 11 relative to body 10.

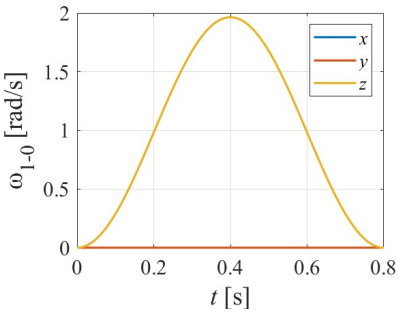

a)

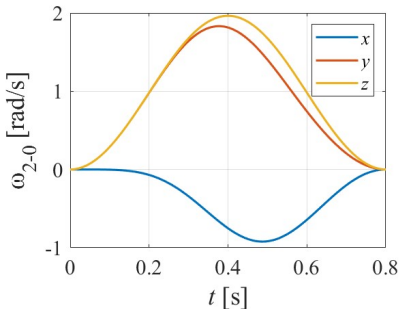

b)

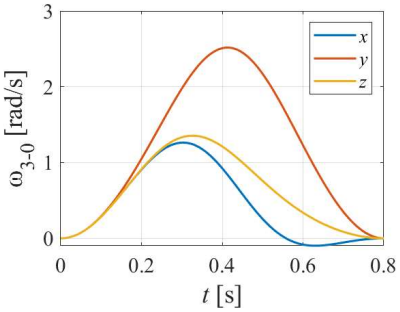

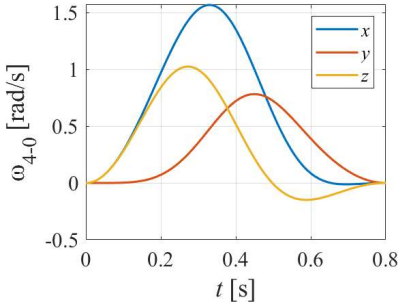

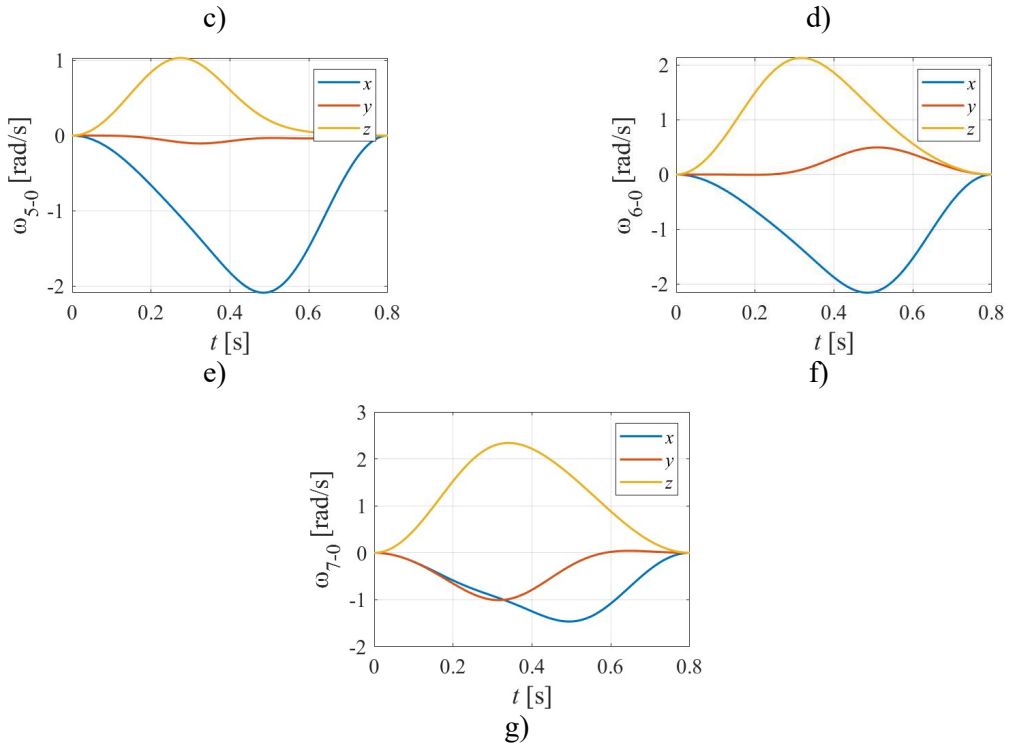

Fig. 5.2. The components of the angular velocity vectors of the arm elements with respect to the global reference system, relative to the axes of this system

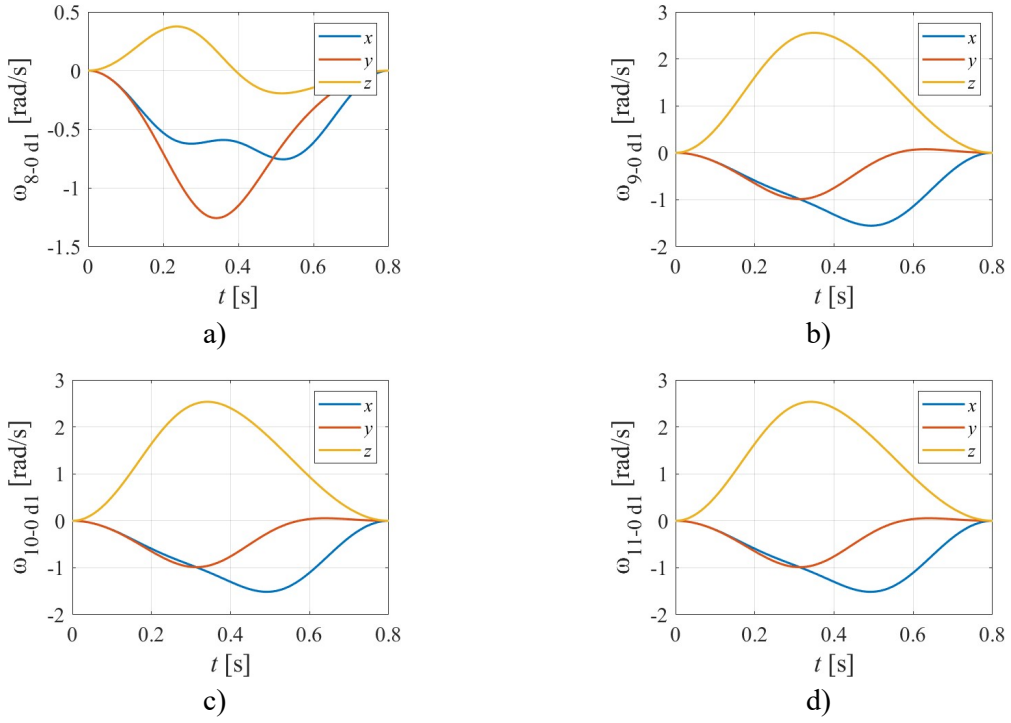

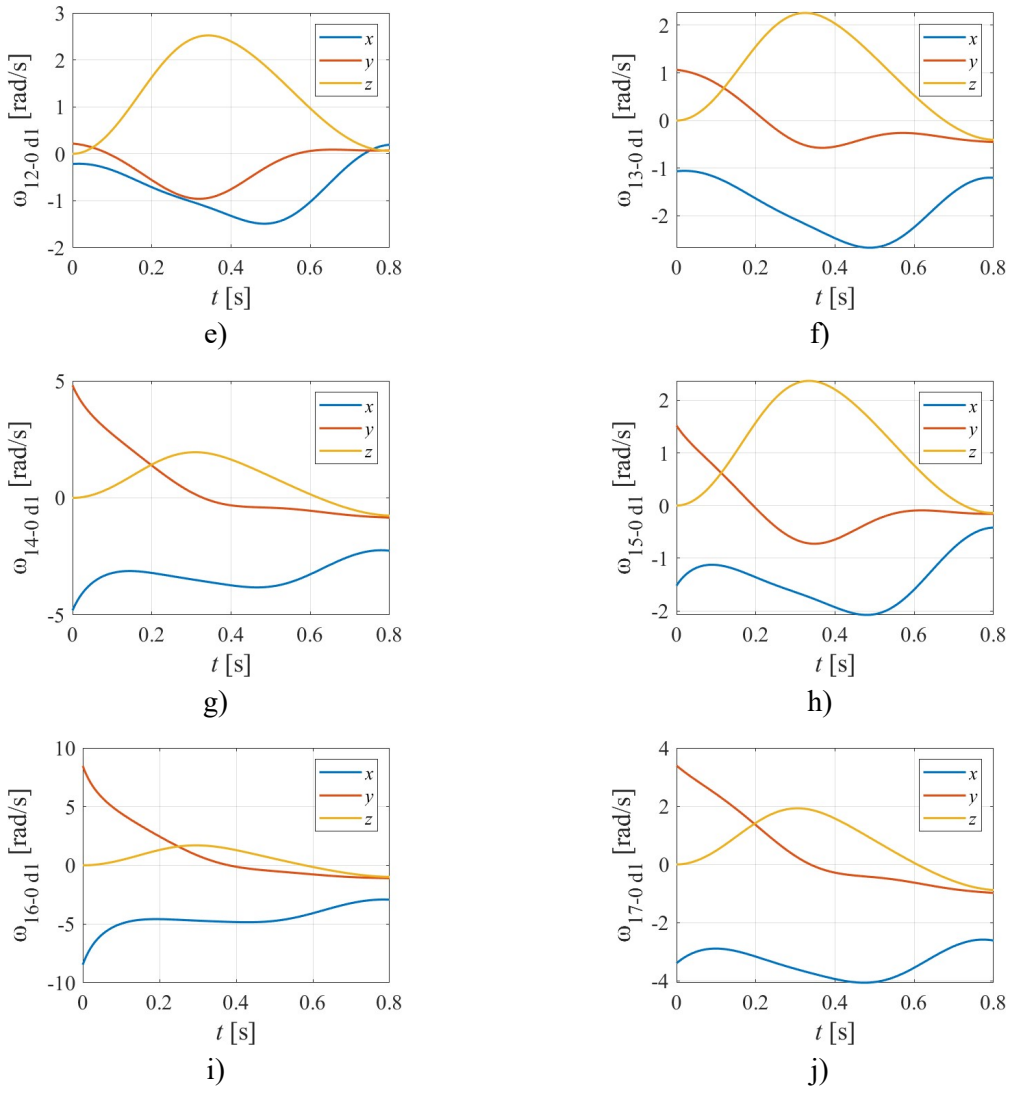

Fig. 5.3. The components of the angular velocity vectors of the elements of finger 1 with respect to the global reference system, relative to the axes of this system

In the following, the variations of the speed components of the points in the joints O_2, ..., O_7 (fig. 5.9) were represented, determined in the global reference system.

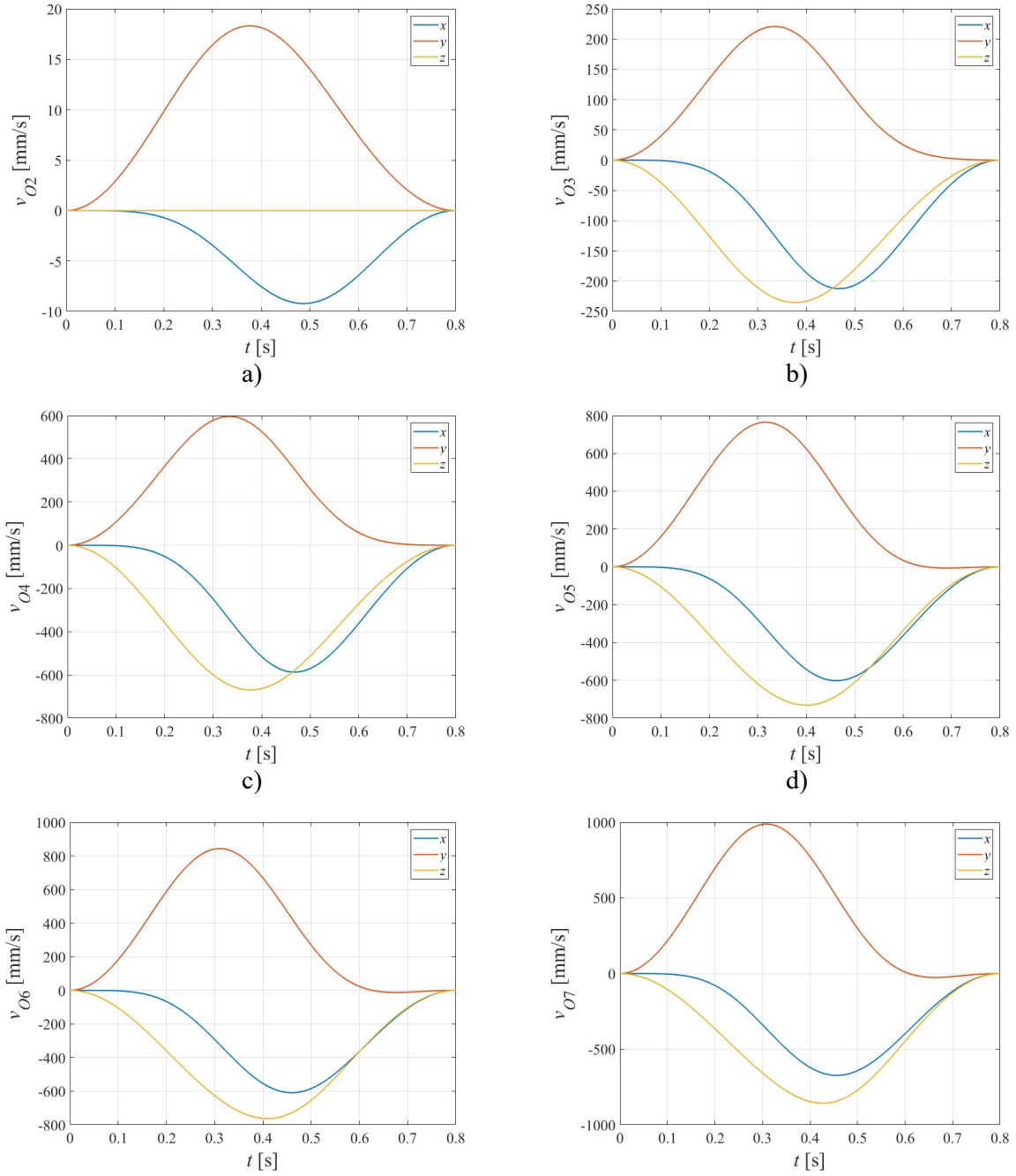

Fig. 5.9. The variation of the components of the velocities of the points in the joints of the arm elements

Figure 5.11 shows the variations of the speed components of the points of interest, O_8, ..., O_{17}, E, of the assembly of which finger 1 is composed, in the global reference system.

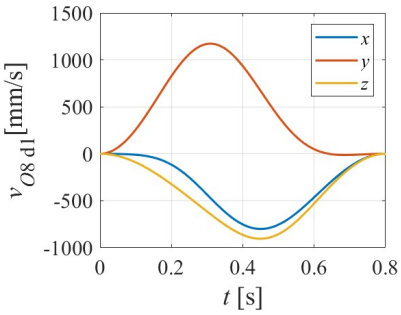
1500
1000
500
0
-500
-1000
0
0.2
0.4
0.6
0.8
t [s]
x
y
z
v_O8 d1 [mm/s]

a)

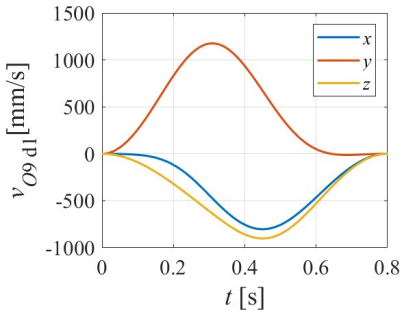
1500
1000
500
0
-500
-1000
0
0.2
0.4
0.6
0.8
t [s]
x
y
z
v_O9 d1 [mm/s]

b)

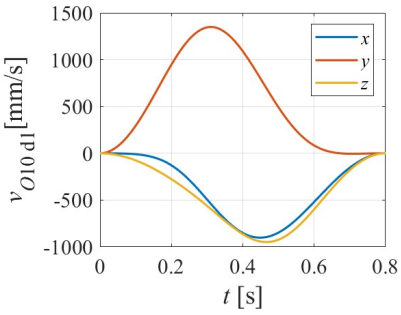
1500
1000
500
0
-500
-1000
0
0.2
0.4
0.6
0.8
t [s]
x
y
z
v_O10 d1 [mm/s]

c)

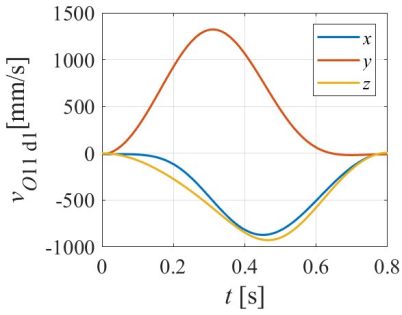
1500
1000
500
0
-500
-1000
0
0.2
0.4
0.6
0.8
t [s]
x
y
z
v_O11 d1 [mm/s]

d)

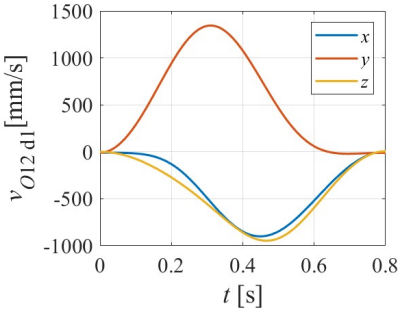
1500
1000
500
0
-500
-1000
0
0.2
0.4
0.6
0.8
t [s]
x
y
z
v_O12 d1 [mm/s]

e)

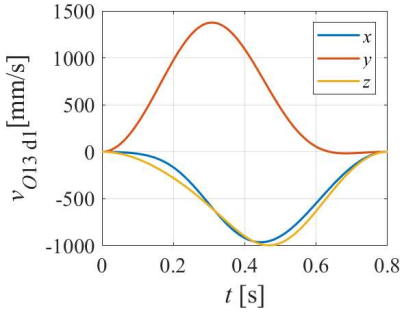
1500
1000
500
0
-500
-1000
0
0.2
0.4
0.6
0.8
t [s]
x
y
z
v_O13 d1 [mm/s]

f)

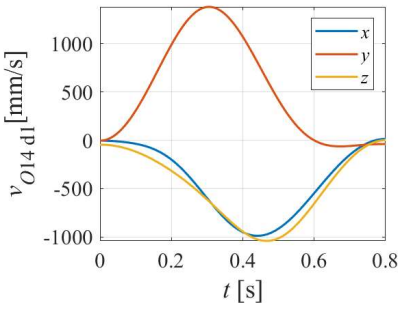
1000
500
0
-500
-1000
0
0.2
0.4
0.6
0.8
t [s]
x
y
z
v_O14 d1 [mm/s]

g)

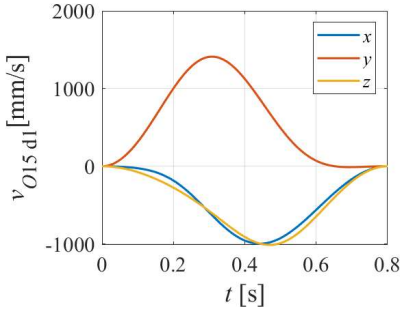
2000
1000
0
-1000
0
0.2
0.4
0.6
0.8
t [s]
x
y
z
v_O15 d1 [mm/s]

h)

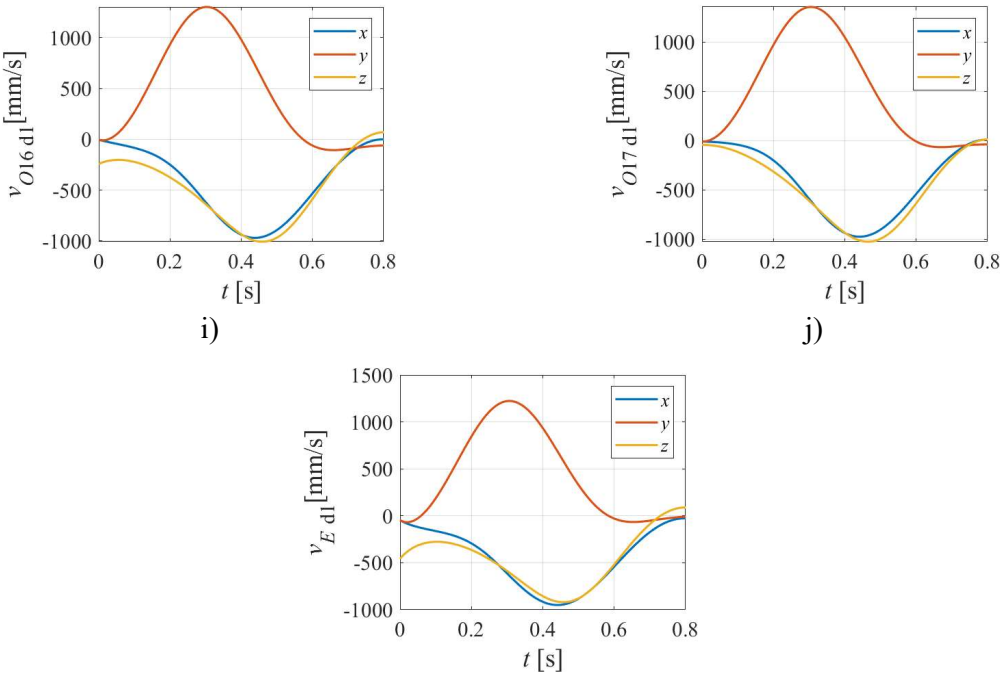

i) j) k)

Fig. 5.11. The variation of the components of the interest point velocities of the finger assembly elements 1

5.3.2. **Accelerations and angular accelerations**

The variations of the angular accelerations of the bodies that make up the arm, in relation to the reference system 0, were represented in figure 5.21. They start and go back to 0. This is due to the chosen law of motion. The variations of the angular accelerations of the bodies that make up the assembly of finger 1 (fig. 5.22) follow the same rule mentioned before, up to body 11. Starting with body 12, this property is no longer preserved, because the influence of the law of motion of the linear motor appears. Another observation would be that the angular accelerations of bodies 10 and 11 coincide. This is due to the translational movement of body 11 relative to body 10.

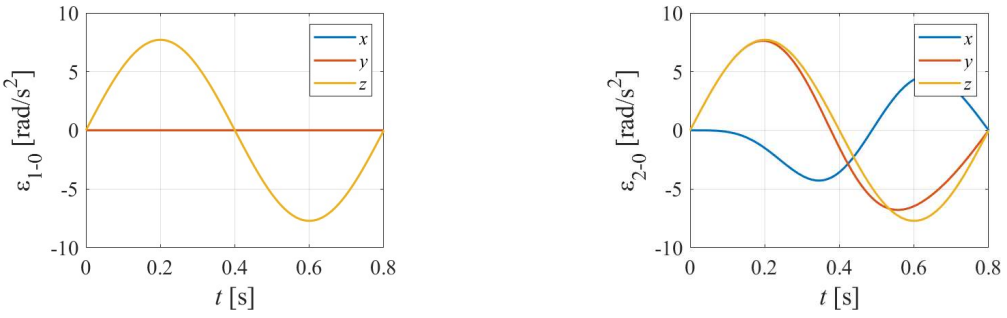

a) b)

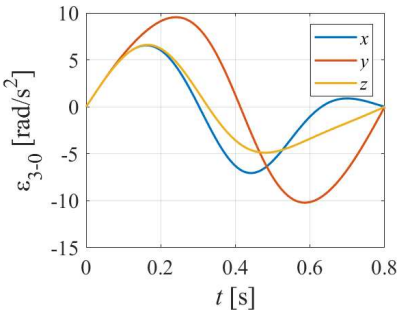

c)

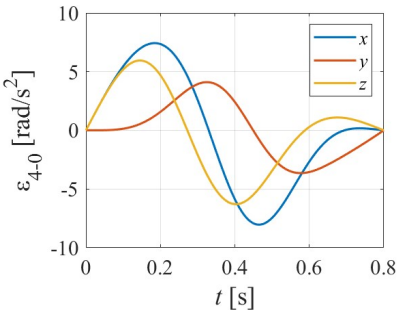

d)

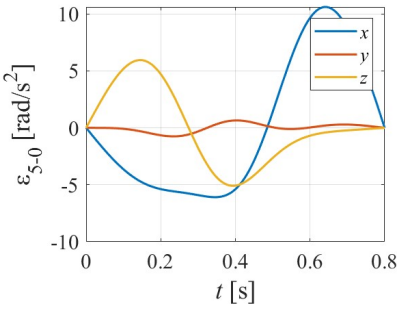

e)

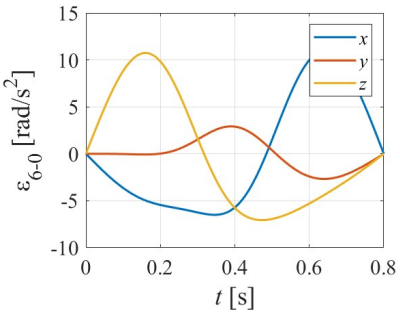

f)

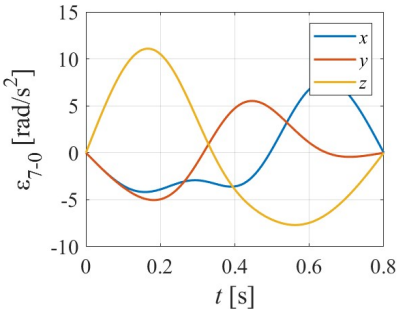

g)

Fig. 5.21. The variation of the components of the angular acceleration vectors of the arm elements with respect to the global reference system, in relation to the axes of this system

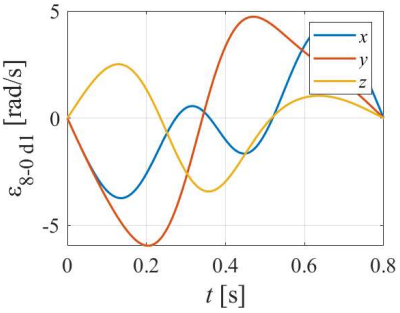

a)

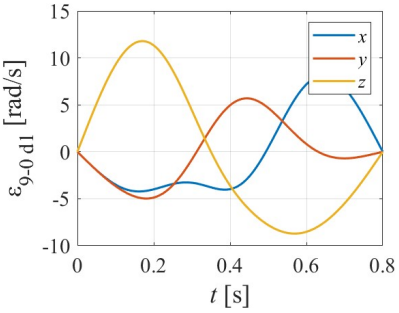

b)

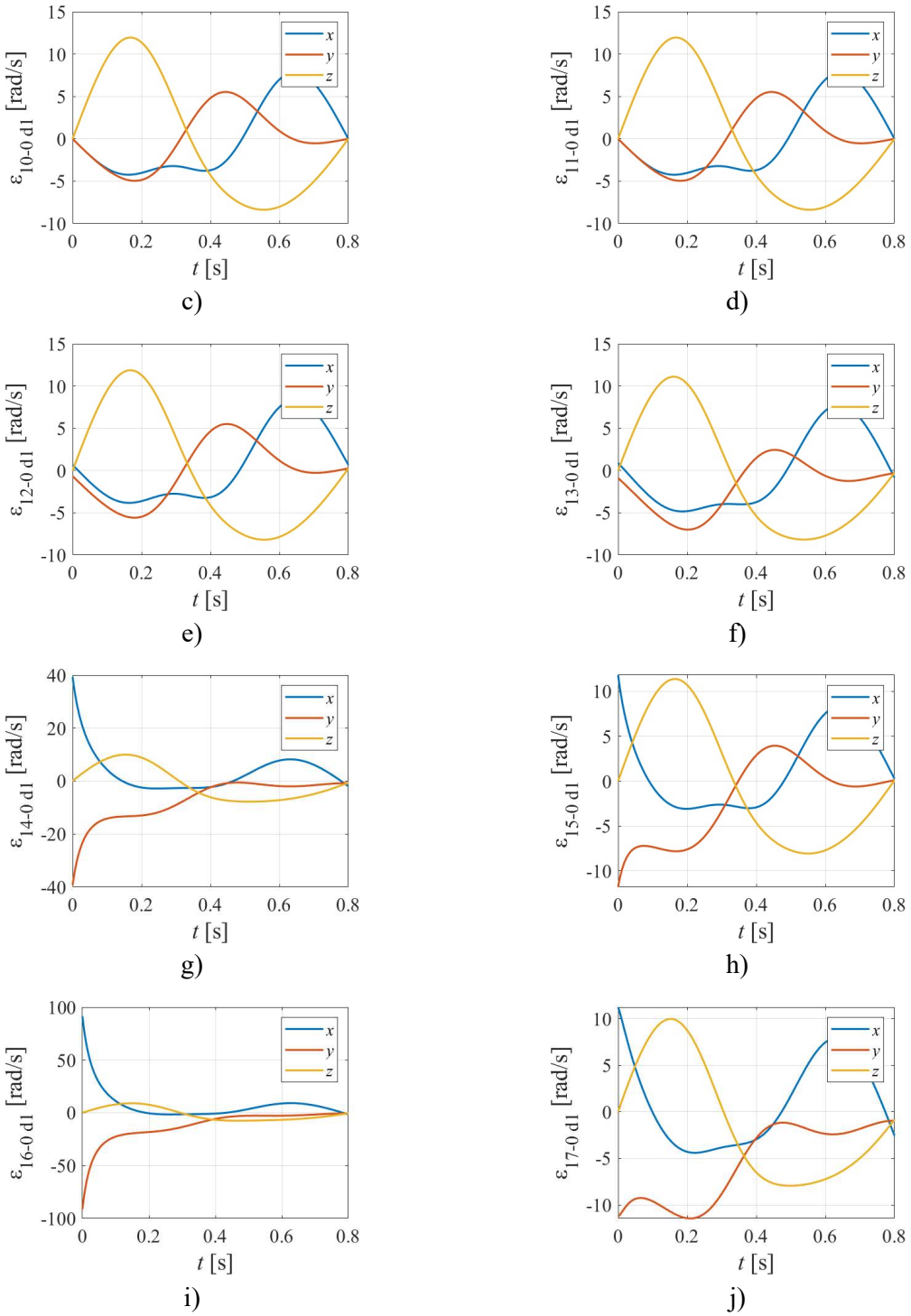

Fig. 5.22. The variation of the components of the angular acceleration vectors of the elements of finger 1 with respect to the global reference system, in relation to the axes of this system

In the following, the variations of the acceleration components of the points in the joints were represented O_2, ..., O_7(fig. 5.28), determined in the global reference system.

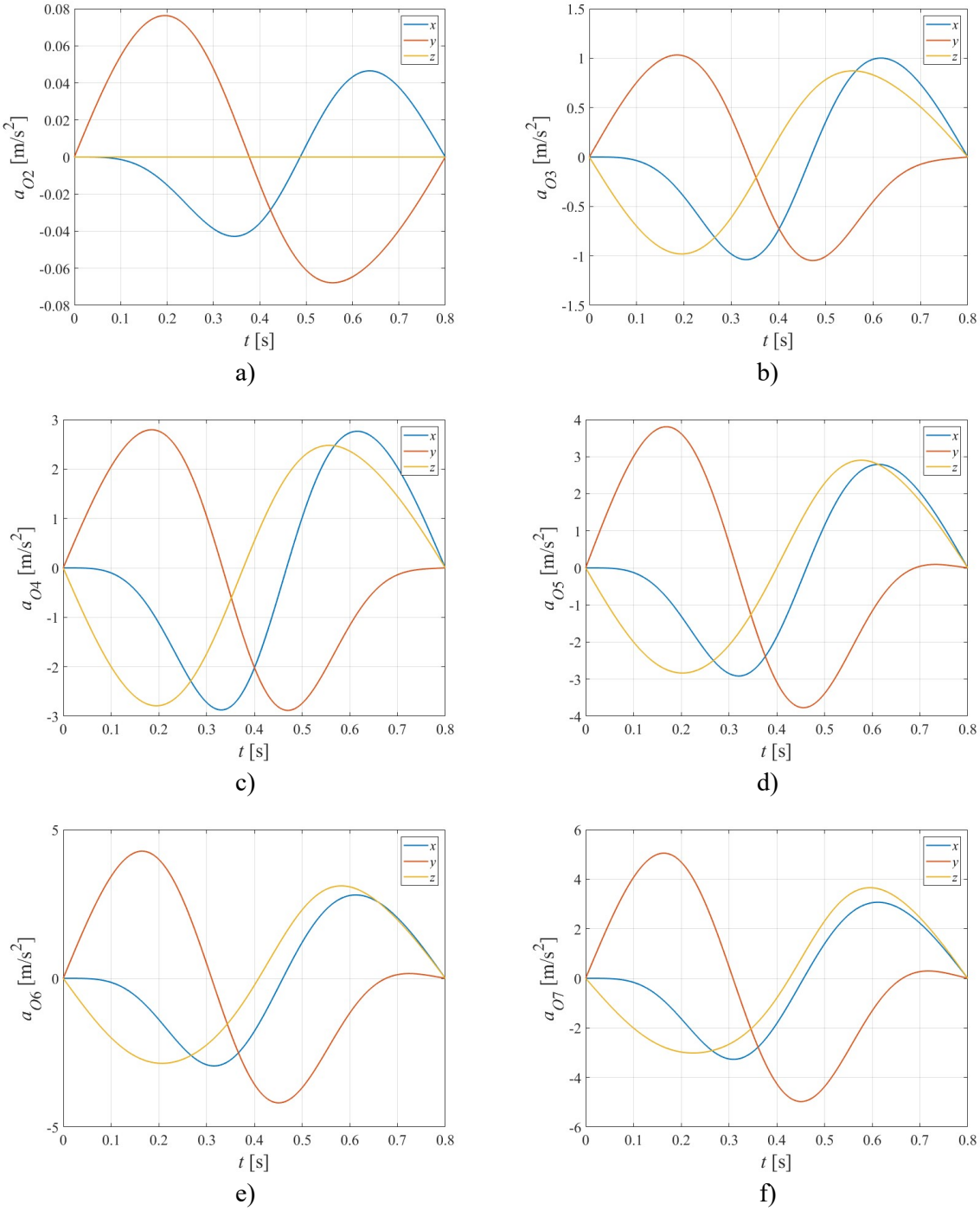

Fig. 5.28. The variation of the components of the accelerations of the points in the joints of the arm elements

In figure 5.30 the variations of the components of the accelerations of the points of interest were represented, O_8, ..., O_{17}, E, of the assembly of which finger 1 is composed, in the global reference system.

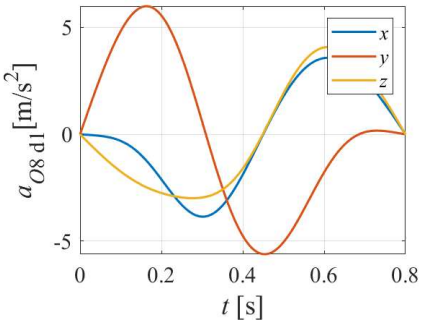
$a_{O8\,\mathrm{d1}}$[m/s^2]
t [s]
x
y
z

a)

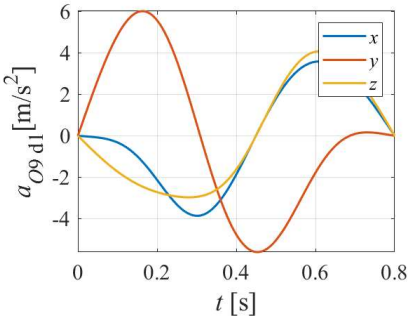
$a_{O9\,\mathrm{d1}}$[m/s^2]
t [s]
x
y
z

b)

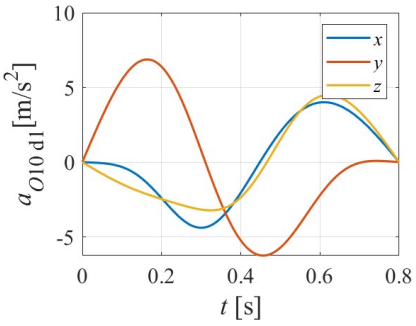
$a_{O10\,\mathrm{d1}}$[m/s^2]
t [s]
x
y
z

c)

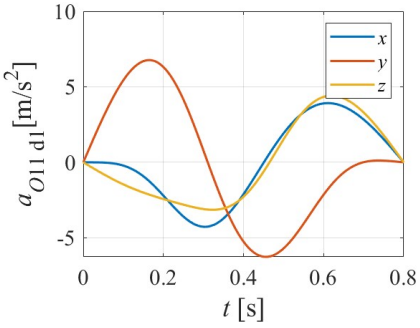
$a_{O11\,\mathrm{d1}}$[m/s^2]
t [s]
x
y
z

d)

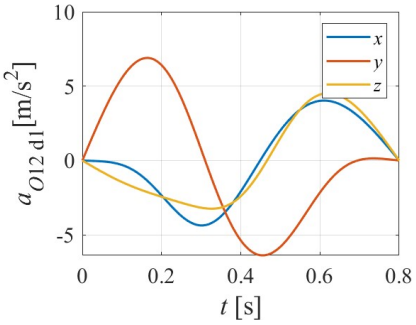
$a_{O12\,\mathrm{d1}}$[m/s^2]
t [s]
x
y
z

e)

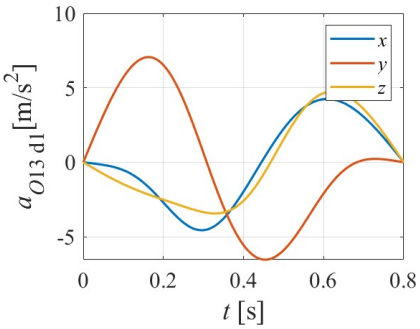
$a_{O13\,\mathrm{d1}}$[m/s^2]
t [s]
x
y
z

f)

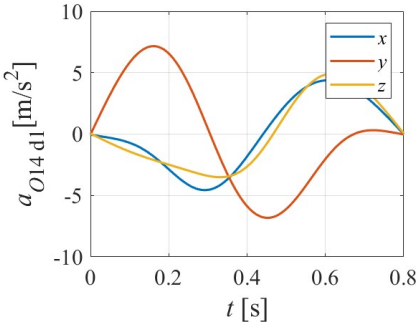
$a_{O14\,\mathrm{d1}}$[m/s^2]
t [s]
x
y
z

g)

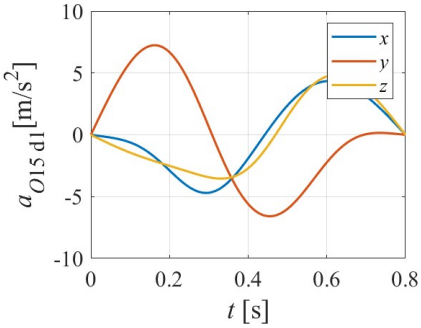
$a_{O15\,\mathrm{d1}}$[m/s^2]
t [s]
x
y
z

h)

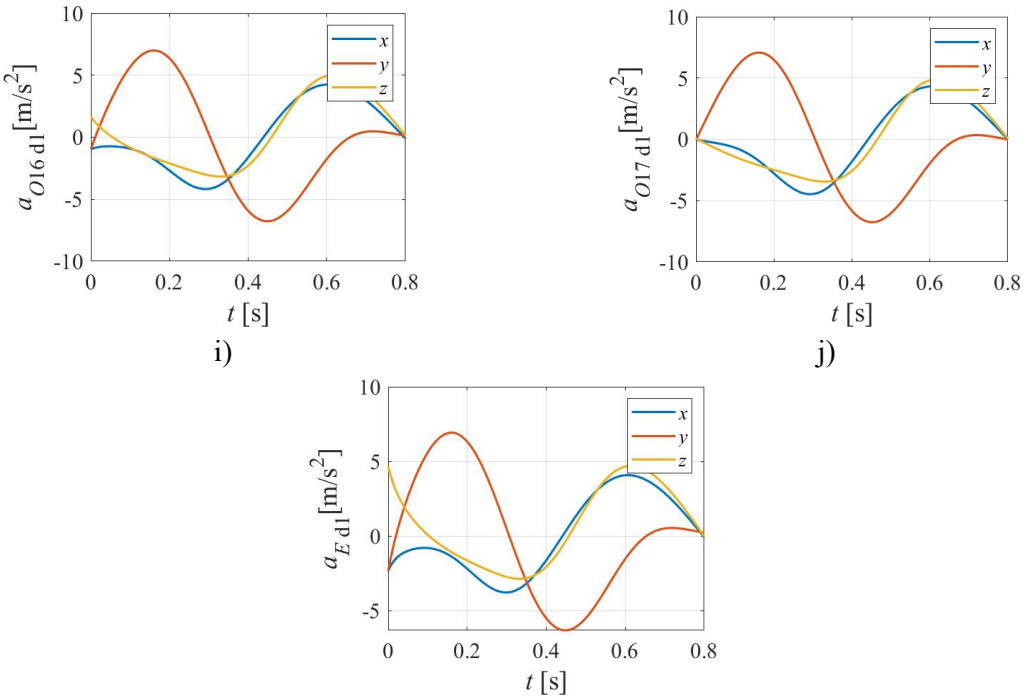

Fig. 5.30. Variation of the components of the accelerations of the points of interest of the elements of the finger assembly 1

5.3.3. **Verifications**

To verify the veracity of the results obtained in subsections 5.3.1 and implicitly 5.3.2, Poisson's formulas were used [9], [51], [66], [67], [68]:

$$\dot{\bar{\imath}} = \bar{\omega} \times \bar{\imath}$$
$$\dot{\bar{\jmath}} = \bar{\omega} \times \bar{\jmath} \qquad (5.11)$$
$$\dot{\bar{k}} = \bar{\omega} \times \bar{k}$$

In figure 5.39 these relationships were verified, projecting them on the global reference system, for reference system 1, and represented on the same graph with two different colors (blue and red), each component of each term of the previously presented equalities.

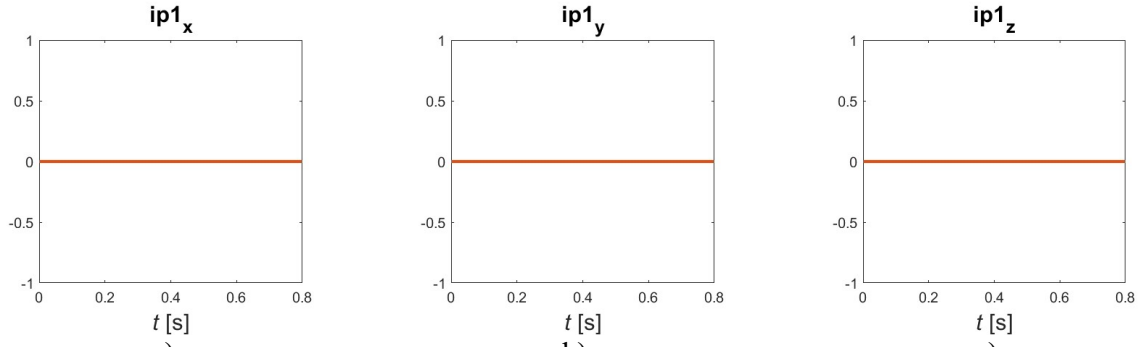

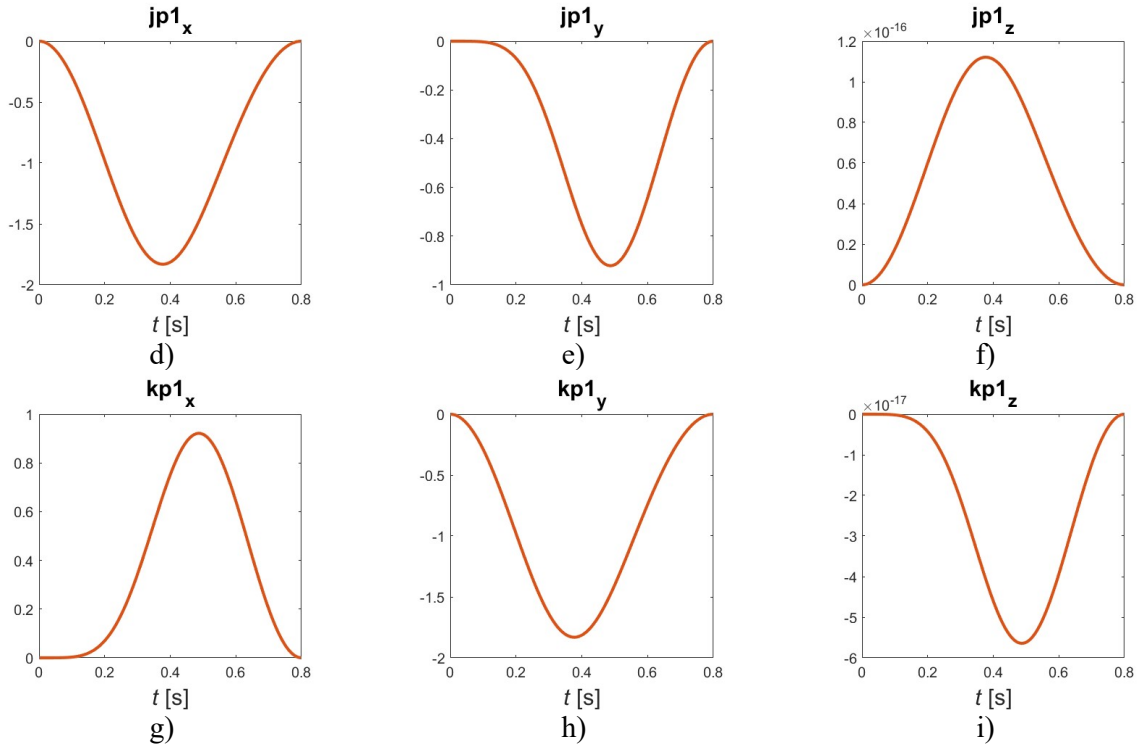

Fig. 5.39. Poisson for system 1

5.4. Conclusions

After performing the kinematic calculations and determining the angular velocities, angular accelerations, as well as the velocities and accelerations of the significant points of the robotic arm system, several sets of checks were performed, as follows:

1. the angular velocities of analytically determined component copes were verified using Poisson's relations, in which the unit vectors $\bar{\imath}, \bar{\jmath}$ and $\bar{k}$ were derived numerically;
2. The analytically determined significant point rates were compared with the values obtained by numerical derivation of position vectors;
3. the angular accelerations of analytically determined component copes were compared with values obtained by numerical derivation of angular velocities;
4. analytically determined accelerations of significant points were compared with values obtained by numerical velocity derivation.

In all four sets of checks, the results obtained by the two methods are very well in agreement.

6. Inverse dynamics

In robotics, inverse dynamics deals with determining forces and moments in joints, when knowing the positions, velocities, and accelerations of points of interest of the system, as well as inertial quantities (masses and moments of inertia).

Two methods have been used in this paper:

- with the help of the methods of classical mechanics, isolating all 55 bodies of the system and using the momentum theorem and angular momentum theorem with respect to the center of mass for each individual body;
- with the help of the methods of analytical mechanics, using D'Alembert's principle and the principle of virtual powers.

6.1. Study with the methods of classical mechanics

In the case of the study based on the methods of classical mechanics, to determine the forces and momenta in the joints of the system, the bodies of the system are isolated and the momentum theorem and the angular momentum theorem are successively applied with respect to the center of mass, for each of them [9], [51], [68].

For simplicity, only the system consisting of the robotic arm and finger 1 of the hand can be analyzed (fig. 6.1), since, as shown in previous chapters, fingers 2-5 have a mechanical pattern similar to finger 1.

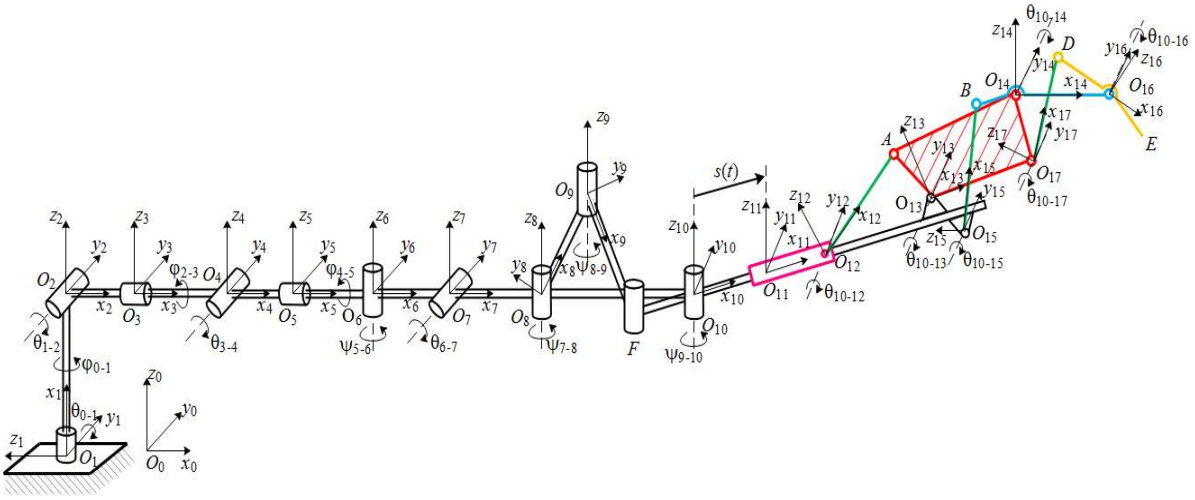

Fig. 6.1. The system consisting of the robotic arm and the prehensor represented with finger 1

In the following, for any body i, it is noted:

- m_i – mass,
- $\overline{\overline{J_{C_i}}}$ – inertia tensor with respect to center of mass C_i,
- $\bar{g}$ – gravitational acceleration,
- $\overline{\varepsilon_i}$ – absolute angular acceleration vector,
- $\overline{a_{C_i}}$ – absolute acceleration of the center of gravity,
- $\overline{\omega_i}$ – absolute angular velocity vector,

- $\bar{R}_i$ – force in the joint O_i,
- $-\bar{R}_{i+1}$ – force in the joint O_{i+1},
- $\bar{M}_i$ – moment in the joint O_i,
- $-\bar{M}_{i+1}$ – moment in the joint O_{i+1},
- $\overline{C_iO_i}$ – positioning vector of the point O_i with respect to the center of gravity C_i,
- $\overline{C_iO_{i+1}}$ – – positioning vector of the point O_{i+1} with respect to the center of gravity C_i.

By virtue of the principle of action and reaction, forces, and moments in the joint O_{i+1} are considered with a plus sign on body i+1 and with a minus sign on body i.

The equations resulting from the application of the two theorems are expressed in relation to the reference frame attached to the respective body, since in relation to it, the matrix $[J_{C_i}]_i$ corresponding to the inertia tensor $\overline{\overline{J_{C_i}}}$ is constant.

6.1.1. **Bodies 1-6 and 8**

The mechanical models of bodies 1-6 and 8 are similar (fig. 6.2). By isolating body i (i=1, 2,..., 6, 8), joint O_i is replaced with the force $\bar{R}_i$ and the moment $\bar{M}_i$, and the joint O_{i+1} with the force $-\bar{R}_{i+1}$ and the moment $-\bar{M}_{i+1}$. The body is also driven by its weight, $m_i\bar{g}$.

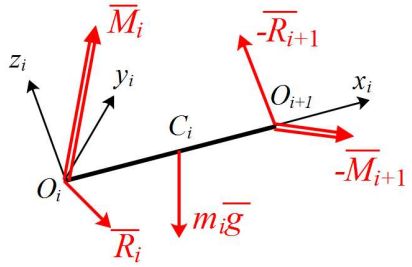

Fig. 6.2. Bodies 1-6 and 8, isolated

Applying the momentum theorem and the angular momentum theorem with respect to the center of mass of the body, the vectorial relations are obtained

$$m_i\overline{a_{C_i}} = \bar{R}_i - \bar{R}_{i+1} + m_i\bar{g}, \tag{6.1}$$

$$\overline{\overline{J_{C_i}}}\cdot\bar{\varepsilon}_i + \bar{\omega}_i \times \overline{\overline{J_{C_i}}}\cdot\bar{\omega}_i = \bar{M}_i - \bar{M}_{i+1} + \overline{C_iO_i}\times\bar{R}_i - \overline{C_iO_{i+1}}\times\bar{R}_{i+1}, \tag{6.2}$$

Equations (6.1), and (6.2), have the following matrix representations:

$$m_i\{a_{C_i}\}_i = \{R_i\}_i - \{R_{i+1}\}_i + m_i\{g\}_i, \tag{6.3}$$

$$[J_{C_i}]_i\{\varepsilon_i\}_i + [\widehat{\omega}_i]_i[J_{C_i}]_i\{\omega_i\}_i = \{M_i\}_i - \{M_{i+1}\}_i + [\widehat{C_iO_i}]_i\{R_i\}_i - [\widehat{C_iO_{i+1}}]_i\{R_{i+1}\}_i. \tag{6.4}$$

The mechanical models of the other bodies are different and are presented below.

6.1.2. **Body 7**

The isolated body 7, is shown in Figure 6.3. By virtue of the principle of action and reaction, the forces, and moments in the joints O_8 and O_{10} are considered with a plus sign on bodies 8 and 10 respectively and with a minus sign on body 7.

Applying the momentum theorem and the angular momentum theorem with respect to the center of mass of the body, the vectorial relations are obtained

$$m_7\overline{a_{C_7}} = \bar{R}_7 - \bar{R}_8 - \sum_{finger} \bar{R}_{10} + m_7\bar{g}, \tag{6.5}$$

$$\overline{\overline{J_{C_7}}} \cdot \overline{\varepsilon_7} + \overline{\omega_7} \times \overline{\overline{J_{C_7}}} \cdot \overline{\omega_7} =$$

$$= \bar{M}_7 - \bar{M}_8 - \sum_{finger} \bar{M}_{10} + \overline{C_7O_7} \times \bar{R}_7 - \overline{C_7O_8} \times \bar{R}_8 - \sum_{finger} \overline{C_7O_{10}} \times \bar{R}_{10}, \tag{6.6}$$

where:

- $-\sum_{finger} \bar{R}_{10}$ – the resultant vector of forces in the joints O_{10}, corresponding to the five fingers, acting on the body *7*,
- $-\sum_{deget} \bar{M}_{10}$ – the resultant vector of moments in the joints O_{10}, corresponding to the five fingers, acting on the body *7*,

$\overline{C_7O_{10}}$ – positioning vector of point O_{10} of each finger, with respect to the center of mass C_7.

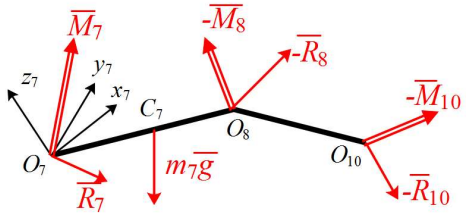

Fig. 6.3. Body 7, isolated

6.1.3. **Body 9**

The isolated body 9, is shown in Figure 6.4.

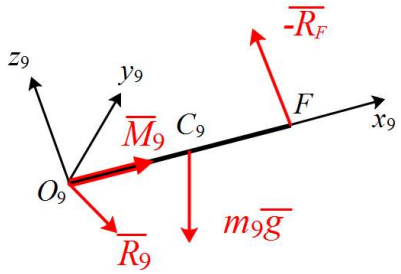

Fig. 6.4. Body 9, isolated

The link in O_9 was considered a universal joint, so the moment in this link has component only on the axis x_9. The link in F was considered a spherical joint, so the moment in this connection is null.

By virtue of the principle of action and reaction, the force in the joint F is considered with a plus sign on body 10 and a minus sign on body 9.

Applying the momentum theorem and the angular momentum theorem with respect to the center of mass of the body, the vectorial relations are obtained:

$$m_9\overline{a_{C_9}} = \bar{R}_9 - \bar{R}_F + m_9\bar{g}, \tag{6.7}$$

$$\overline{\overline{J_{C_9}}} \cdot \overline{\varepsilon_9} + \overline{\omega_9} \times \overline{\overline{J_{C_9}}} \cdot \overline{\omega_9} = \bar{M}_9 + \overline{C_9O_9} \times \bar{R}_9 - \overline{C_9F} \times \bar{R}_F, \tag{6.8}$$

where:

- $-\bar{R}_F$ – the force from the joint F of body 9,
- $\overline{C_9F}$ – positioning vector of point F with respect to the center of mass C_9.

6.1.4. **Body 10**

The isolated body 10, is shown in Figure 6.5. By virtue of the principle of action and reaction, the forces, and moments in the joints O_{11}, O_{13} and O_{15} are considered with a plus sign on bodies 11, 13 and 15 and with a minus sign on body 10.

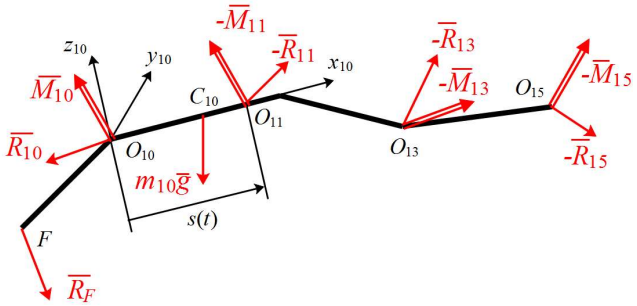

Fig. 6.5. Body 10, isolated

Applying the momentum theorem and the angular momentum theorem with respect to the center of mass of the body, the vectorial relations are obtained:

$$m_{10}\overline{a_{C_{10}}} = \bar{R}_{10} + \bar{R}_F - \bar{R}_{11} - \bar{R}_{13} - \bar{R}_{15} + m_{10}\bar{g}, \tag{6.9}$$

$$\overline{\overline{J_{C_{10}}}} \cdot \overline{\varepsilon_{10}} + \overline{\omega_{10}} \times \overline{\overline{J_{C_{10}}}} \cdot \overline{\omega_{10}} = \\ = \bar{M}_{10} - \bar{M}_{11} - \bar{M}_{13} - \bar{M}_{15} + \\ + \overline{C_{10}O_{10}} \times \bar{R}_{10} + \overline{C_{10}F} \times \bar{R}_F - \overline{C_{10}O_{11}} \times \bar{R}_{11} - \overline{C_{10}O_{13}} \times \bar{R}_{13} - \overline{C_{10}O_{15}} \times \bar{R}_{15}, \tag{6.10}$$

where:

- $\bar{R}_F$ – the force from the joint F of body 10,
- $-\bar{R}_{13}$ – the force from the joint O_{13} of body 10,
- $-\bar{R}_{15}$ – the force from the joint O_{15} of body 10,
- $-\bar{M}_{13}$ – the moment from the joint O_{13} of body 10,
- $-\bar{M}_{15}$ – the moment from the joint O_{15} of body 10,
- $\overline{C_{10}F}$ – positioning vector of point F with respect to the center of mass C_{10},
- $\overline{C_{10}O_{13}}$ – positioning vector of point O_{13} with respect to the center of mass C_{10},
- $\overline{C_{10}O_{15}}$ – positioning vector of point O_{15} with respect to the center of mass C_{10}.

6.1.5. **Body 11**

The isolated body 11, is presented in Figure 6.6.

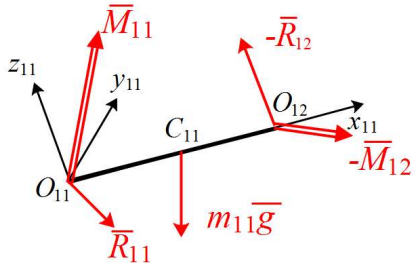

Fig. 6.6. Body 11, isolated

Applying the momentum theorem and the angular momentum theorem with respect to the center of mass of the body, the vectorial relations are obtained:

$$m_{11}\overline{a_{C_{11}}} = \bar{R}_{11} - \bar{R}_{12} + m_{11}\bar{g}, \tag{6.11}$$

$$\overline{\overline{J_{C_{11}}}} \cdot \overline{\varepsilon_{11}} + \overline{\omega_{11}} \times \overline{\overline{J_{C_{11}}}} \cdot \overline{\omega_{11}} = \bar{M}_{11} - \bar{M}_{12} + \overline{C_{11}O_{11}} \times \bar{R}_{11} - \overline{C_{11}O_{12}} \times \bar{R}_{12}. \tag{6.12}$$

6.1.6. **Body 12**

The isolated body 12, is presented in Figure 6.7.

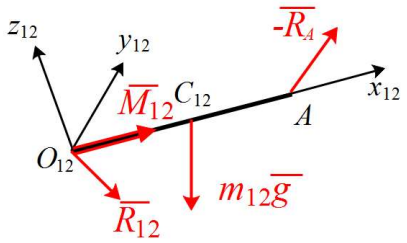

Fig. 6.7. Body 12, isolated

The link in O_{12} was considered a universal joint, so the moment in this link has component only on the axis x_{12}. The link in A was considered a spherical joint, so the moment in this connection is null.

By virtue of the principle of action and reaction, the force in the joint A is considered with a plus sign on body 13 and a minus sign on body 12.

Applying the momentum theorem and the angular momentum theorem with respect to the center of mass of the body, the vectorial relations are obtained:

$$m_{12}\overline{a_{C_{12}}} = \bar{R}_{12} - \bar{R}_A + m_{12}\bar{g}, \tag{6.13}$$

$$\overline{\overline{J_{C_{12}}}} \cdot \overline{\varepsilon_{12}} + \overline{\omega_{12}} \times \overline{\overline{J_{C_{12}}}} \cdot \overline{\omega_{12}} = \bar{M}_{12} + \overline{C_{12}O_{12}} \times \bar{R}_{12} - \overline{C_{12}A} \times \bar{R}_A, \tag{6.14}$$

where:

- $-\bar{R}_A$ – the force from the joint A of body 12,
- $\overline{C_{12}A}$ – positioning vector of point A with respect to the center of mass C_{12}.

6.1.7. **Body 13**

The isolated body 13, is presented in Figure 6.8.

By virtue of the principle of action and reaction, the forces, and moments in the joints O_{14} and O_{17} are considered with a plus sign on bodies 14 and 17 and a minus sign on body 13.

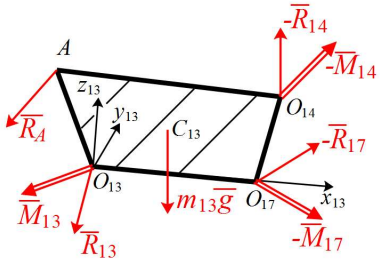

Fig. 6.8. Body 13, isolated

Applying the momentum theorem and the angular momentum theorem with respect to the center of mass of the body, the vectorial relations are obtained:

$$m_{13}\overline{a_{C_{13}}} = \bar{R}_{13} + \bar{R}_A - \bar{R}_{14} - \bar{R}_{17} + m_{13}\bar{g}, \tag{6.15}$$

$$\overline{\overline{J_{C_{13}}}} \cdot \overline{\varepsilon_{13}} + \overline{\omega_{13}} \times \overline{\overline{J_{C_{13}}}} \cdot \overline{\omega_{13}} = \\ = \bar{M}_{13} - \bar{M}_{14} - \bar{M}_{17} + \overline{C_{13}O_{13}} \times \bar{R}_{13} + \overline{C_{13}A} \times \bar{R}_A - \overline{C_{13}O_{14}} \times \bar{R}_{14} - \overline{C_{13}O_{17}} \times \bar{R}_{17}, \quad (6.16)$$

where:

- $\bar{R}_A$ – the force from the joint A of body 13,
- $-\bar{R}_{17}$ – the force from the joint O_{17} of body 13,
- $-\bar{M}_{17}$ – the moment from the joint O_{17} of body 13,
- $\overline{C_{13}A}$ – positioning vector of point A with respect to the center of mass C_{13},
- $\overline{C_{13}O_{17}}$ – positioning vector of point O_{17} with respect to the center of mass C_{13}.

6.1.8. **Body 14**

The isolated body 14, is presented in Figure 6.9. By virtue of the principle of action and reaction, the force and moment in joint O_{16} are considered with the plus sign on body 16 and a minus sign on body 14.

The link in B was considered a spherical joint, so the moment in this connection is null.

Applying the momentum theorem and the angular momentum theorem with respect to the center of mass of the body, the vectorial relations are obtained:

$$m_{14}\overline{a_{C_{14}}} = \bar{R}_{14} + \bar{R}_B - \bar{R}_{16} + m_{14}\bar{g}, \quad (6.17)$$

$$\overline{\overline{J_{C_{14}}}} \cdot \overline{\varepsilon_{14}} + \overline{\omega_{14}} \times \overline{\overline{J_{C_{14}}}} \cdot \overline{\omega_{14}} = \\ = \bar{M}_{14} - \bar{M}_{16} + \overline{C_{14}O_{14}} \times \bar{R}_{14} + \overline{C_{14}B} \times \bar{R}_B - \overline{C_{14}O_{16}} \times \bar{R}_{16}, \quad (6.18)$$

where:

- $\bar{R}_B$ – the force from the joint B of body 14,
- $-\bar{R}_{16}$ – the force from the joint O_{16} of body 14,
- $-\bar{M}_{16}$ – the moment from the joint O_{16} of body 14,
- $\overline{C_{14}B}$ – positioning vector of point B with respect to the center of mass C_{14},
- $\overline{C_{14}O_{16}}$ – positioning vector of point O_{16} with respect to the center of mass C_{14}.

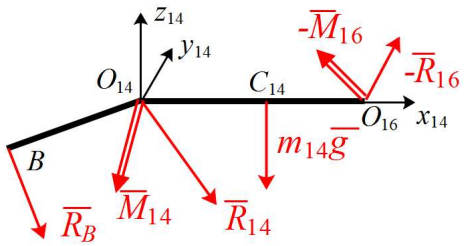

Fig. 6.9. Body 14, isolated

6.1.9. **Body 15**

The isolated body 15, is presented in Figure 6.10.

The link in O_{15} was considered a universal joint, so the moment in this link has component only on the axis x_{15}.

Applying the momentum theorem and the angular momentum theorem with respect to the center of mass of the body, the vectorial relations are obtained:

$$m_{15}\overline{a_{C_{15}}} = \bar{R}_{15} - \bar{R}_B + m_{15}\bar{g}, \quad (6.19)$$

$$\overline{\overline{J_{C_{15}}}} \cdot \overline{\varepsilon_{15}} + \overline{\omega_{15}} \times \overline{\overline{J_{C_{15}}}} \cdot \overline{\omega_{15}} = \bar{M}_{15} + \overline{C_{15}O_{15}} \times \bar{R}_{15} - \overline{C_{15}B} \times \bar{R}_B, \tag{6.20}$$

where:

- $-\bar{R}_B$ – the force from the joint B of body 15,
- $\overline{C_{15}B}$ – positioning vector of point B with respect to the center of mass C_{15}.

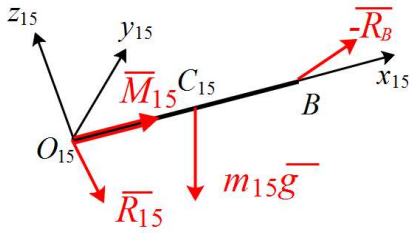

Fig. 6.10. Body 15, isolated

6.1.10. **Body 16**

The isolated body 16, is presented in Figure 6.11.

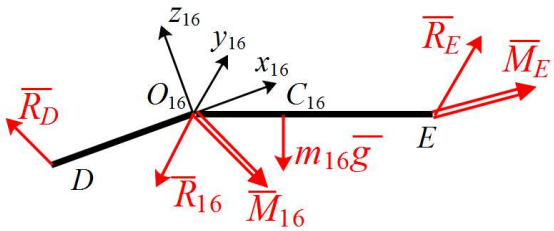

Fig. 6.11. Body 16, isolated

The link in D was considered a spherical joint, so the moment in this connection is null.

Applying the momentum theorem and the angular momentum theorem with respect to the center of mass of the body, the vectorial relations are obtained:

$$m_{16}\overline{a_{C_{16}}} = \bar{R}_{16} + \bar{R}_D + \bar{R}_E + m_{16}\bar{g}, \tag{6.21}$$

$$\overline{\overline{J_{C_{16}}}} \cdot \overline{\varepsilon_{16}} + \overline{\omega_{16}} \times \overline{\overline{J_{C_{16}}}} \cdot \overline{\omega_{16}} = \\ = \bar{M}_{16} + \bar{M}_E + \overline{C_{16}O_{16}} \times \bar{R}_{16} + \overline{C_{16}D} \times \bar{R}_D + \overline{C_{16}E} \times \bar{R}_E, \tag{6.22}$$

where:

- $\bar{R}_D$ – the force from the joint D of body 16,
- $\bar{R}_E$ – the external force applied in point E of body 16,
- $\bar{M}_E$ – the external moment applied in point E of body 16,
- $\overline{C_{16}D}$ – positioning vector of point D with respect to the center of mass C_{16},
- $\overline{C_{16}E}$ – positioning vector of point E with respect to the center of mass C_{16}.

6.1.11. **Body 17**

The isolated body 17, is presented in Figure 6.12.

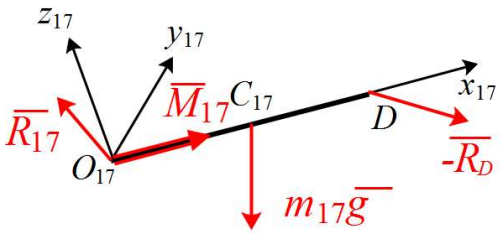

Fig. 6.12. Body 17, isolated

Applying the momentum theorem and the angular momentum theorem with respect to the center of mass of the body, the vectorial relations are obtained:

$$m_{17}\overline{a_{C_{17}}} = \bar{R}_{17} - \bar{R}_E + m_{17}\bar{g}, \tag{6.23}$$

$$\overline{\overline{J_{C_{17}}}} \cdot \overline{\varepsilon_{17}} + \overline{\omega_{17}} \times \overline{\overline{J_{C_{17}}}} \cdot \overline{\omega_{17}} = \bar{M}_{17} + \overline{C_{17}O_{17}} \times \bar{R}_{17} - \overline{C_{17}D} \times \bar{R}_D, \tag{6.24}$$

where:

- $-\bar{R}_D$ the force from the joint D of body 17,
- $\overline{C_{17}D}$ positioning vector of point D with respect to the center of mass C_{17},

6.1.12. **Analysis of the resulting system of equations**

The equations obtained by isolating the fields and applying the momentum theorem and the angular momentum theorem form a linear algebraic system of 270 equations, with 270 unknowns.

This system must be solved for each moment of time, which requires a high calculation time, proportional to the number of discretization points of the time interval in which the movement occurs.

To reduce execution time and increase precision, the resulting system can be decoupled into:

- 8 subsystems of 6 equations, with 6 unknowns, corresponding to bodies 1-8;
- 5 subsystems of 6 equations, with 6 unknowns, corresponding to body 11 of each finger;
- 1 subsystem of 12 equations, with 12 unknowns, corresponding to the mechanism O_9FO_{10}, present only on finger 1;
- 15 subsystems of 12 equations, with 12 unknowns, corresponding to mechanisms $O_{12}AO_{13}$, $O_{14}BO_{15}$ and $O_{16}DO_{17}$ of each finger.

Torques and driving forces are certain components of moments and forces, respectively, in the links, as follows:

- components in relation to the axes of rotation in the joints O_1, O_2, O_3, O_4, O_5, O_6, O_7, as well as from the joint O_8 of finger 1, of moments, respectively M_{1x}, M_{2y}, M_{3x}, M_{4y}, M_{5x}, M_{6z}, M_{7y}, M_{8z};
- components in relation to axes corresponding x_{11}, of the forces applied to the rods 11, on the five fingers, respectively F_{11dx} (d = 1, 2,…, 5).

6.2. Study with methods of analytical mechanics

If only motor forces and moments are concerned, the calculation can be made even more efficient by using the principle of virtual powers and the principle of D'Alembert.

In the following, these principles are presented, as well as how they are used in this paper

The principle of virtual powers in case of equilibrium of a system of material points

6.2.1. The principle of virtual powers in case of equilibrium of a system of material points

The principle of virtual powers is known from literature [9], [51], [68], by virtue of which a discrete system of material points P_i (i=1, 2,…, n), of masses m_i, subjected to ideal bonds, it is in equilibrium if and only if the virtual power performed by directly applied forces $\bar{F}_i$,

$$P' = \sum_i \bar{F}_i \cdot \bar{v}_i' \tag{6.25}$$

is null, for any virtual speeds $\bar{v}_i'$ given to the points o the system:

$$P' = 0. \tag{6.26}$$

6.2.2. D'Alembert principle in the case of a material point system

We also know from literature D'Alembert's principle [9], [51], [68], according to which a discrete system of material points P_i (i=1, 2,…, n), of masses m_i, in motion due to the action of the directly applied forces $\bar{F}_i$, is equivalent to the system in equilibrium under the action of directly applied forces as well as forces of inertia, $\bar{F}_i^{in} = -m_i \bar{a}_i$.

6.2.3. The principle of virtual powers in case of movement of a system of material points

Combining D'Alembert's principle with the principle of virtual powers, it follows that the motion of a discrete system of material points is governed by the equation (6.26), in which, however, virtual power takes form

$$P' = \sum_i \left(\bar{F}_i - m_i \bar{a}_i\right) \cdot \bar{v}_i'. \tag{6.27}$$

6.2.4. The principle of virtual powers in case of movement of a system of rigid solids

The principle of virtual powers can also apply to a system of n solid, rigid bodies, in motion under the action of directly applied forces and moments, $\bar{F}_j$, (j=1, 2,…, m) and $\bar{M}_i$, (i=1, 2,…, n), respectively.

Equation (6.26) remains valid, but virtual power is calculated taking into account directly applied forces and moments, as well as forces of inertia, expressed by the resultant vectors $\bar{R}_i^{in}$ and the resultant torque vectors, calculated with respect to the corresponding centers of mass, $\bar{M}_{C_i}^{in}$,

$$\begin{aligned} P' &= \sum_{i=1}^{n} \left(\bar{R}_i^{in} \cdot \bar{v}_{C_i}' + \bar{M}_{C_i}^{in} \cdot \bar{\omega}_i'\right) + \sum_{j=1}^{m} \bar{F}_j \cdot \bar{v}_j' + \sum_{i=1}^{n} \bar{M}_i \cdot \bar{\omega}_i' = \\ &= -\sum_{i=1}^{n} \left[m_i \bar{a}_{C_i} \cdot \bar{v}_{C_i}' + \left(\bar{\bar{J}}_{C_i} \bar{\varepsilon}_i + \bar{\omega}_i \times \bar{\bar{J}}_{C_i} \bar{\omega}_i\right) \cdot \bar{\omega}_i'\right] + \sum_{j=1}^{m} \bar{F}_j \cdot \bar{v}_j' + \sum_{i=1}^{n} \bar{M}_i \cdot \bar{\omega}_i', \end{aligned} \tag{6.28}$$

where:

- $\bar{\omega}_i$ – real angular velocity vector of the body i;
- $\bar{\varepsilon}_i$ – vector angular acceleration of the body i;
- $\bar{a}_{C_i}$ – acceleration of the center of mass C_i;
- $\bar{\omega}_i'$ – virtual angular velocity vector of the body i;
- $\bar{v}_{C_i}'$ – virtual velocity of the center of gravity C_i;
- $\bar{v}_j'$ – virtual velocity of the application point of the force $\bar{F}_j$.

To determine the motor torque M_{8z}, it is considered that O_8O_9 rotates with a virtual angular velocity ω_8', and all other control parameters are fixed. The virtual velocities of gravity centers C_8,..., C_{17} and virtual angular velocities of bodies 9,...,17, of finger 1 are determined. Then the corresponding virtual power is determined, P_8', and M_{8z} follows from the condition that it is equal to 0.

To determine the motor force F_{11dx}, produced by the linear motor of the finger d, it is considered that its rod moves with the virtual velocity v_{11d}', and all other control parameters are fixed. The virtual velocities of gravity centers C_{12},..., C_{17} and virtual angular velocities of bodies 1,...,17, of finger d are determined. Then the corresponding virtual power is determined, P_{11}' , and F_{11dx} follows from the condition that it is equal to 0.

6.3. Numerical applications

In this paragraph, the forces, and moments in the joints of the system were determined, if the laws of motion of the bodies that make up the system are known, as well as the dynamic parameters (i.e., inertia matrices and masses of bodies).

6.3.1. Study with the methods of classical mechanics

The study using the methods of classical mechanics of the problem boils down to solving the system with 270 equations and 270 unknowns presented in paragraph 6.1.

Following the resolution of this system, forces resulted in the global reference system R_1,...,R_7 (Fig. 6.13) and moments M_1,...,M_7 (Fig. 6.14) from the joints of the robotic arm, as well as forces R_8,...,R_{17}, R_A, R_B, R_D and R_F (Fig. 6.15) and moments M_8,...,M_{17} (Fig. 6.16) corresponding to finger 1. The moments M_A, M_B, M_D, and M_F are 0 because the joints A, B, D and F are spherical joints.

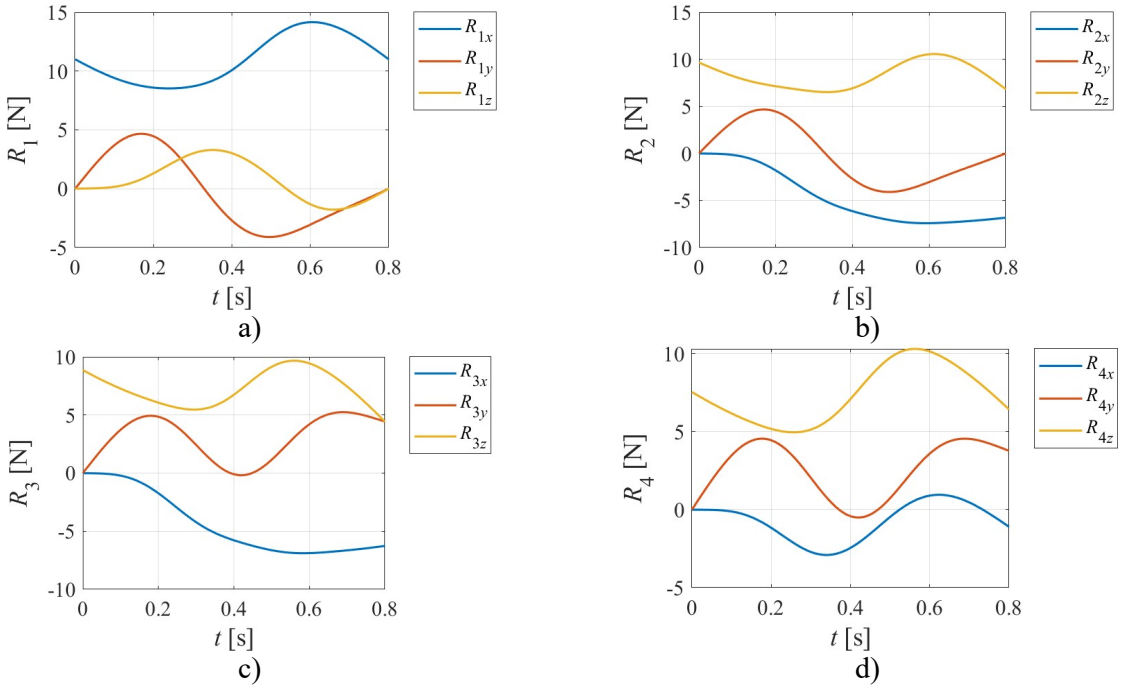

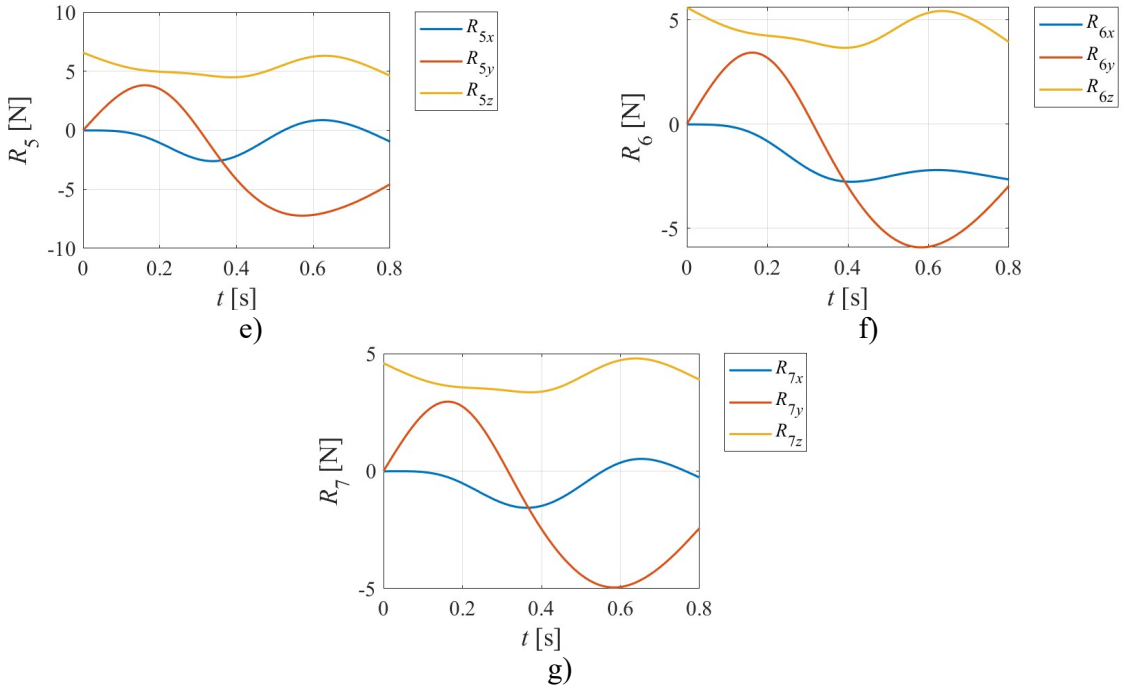

Fig. 6.13. Forces in the joints of the arm R_1,...,R_7, in the global reference system

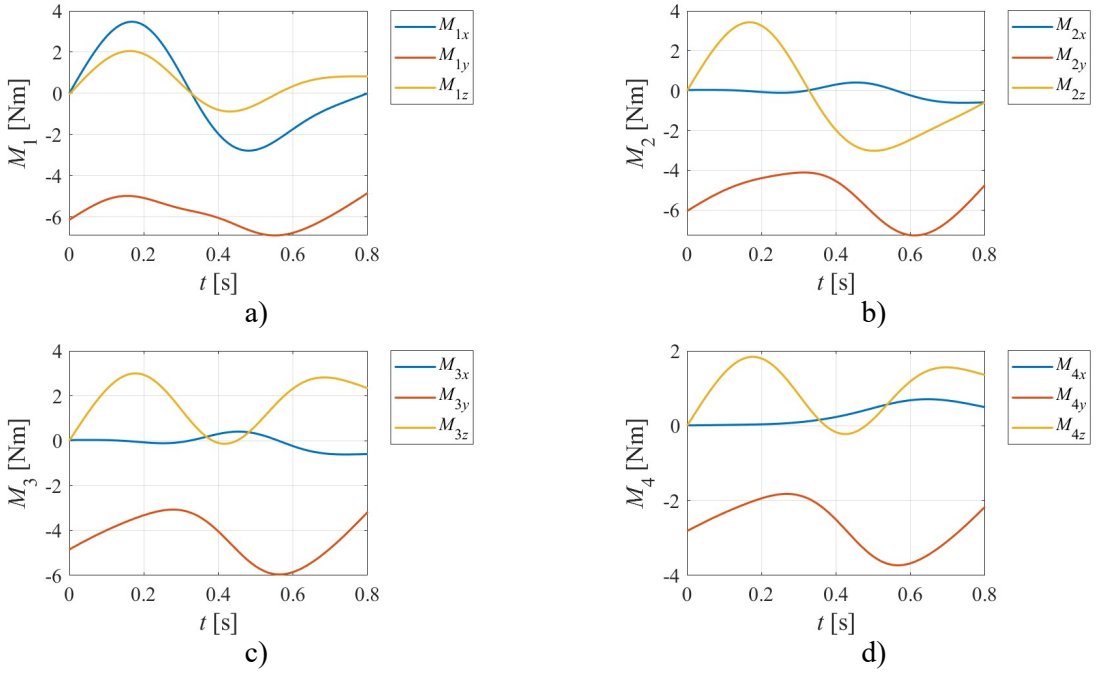

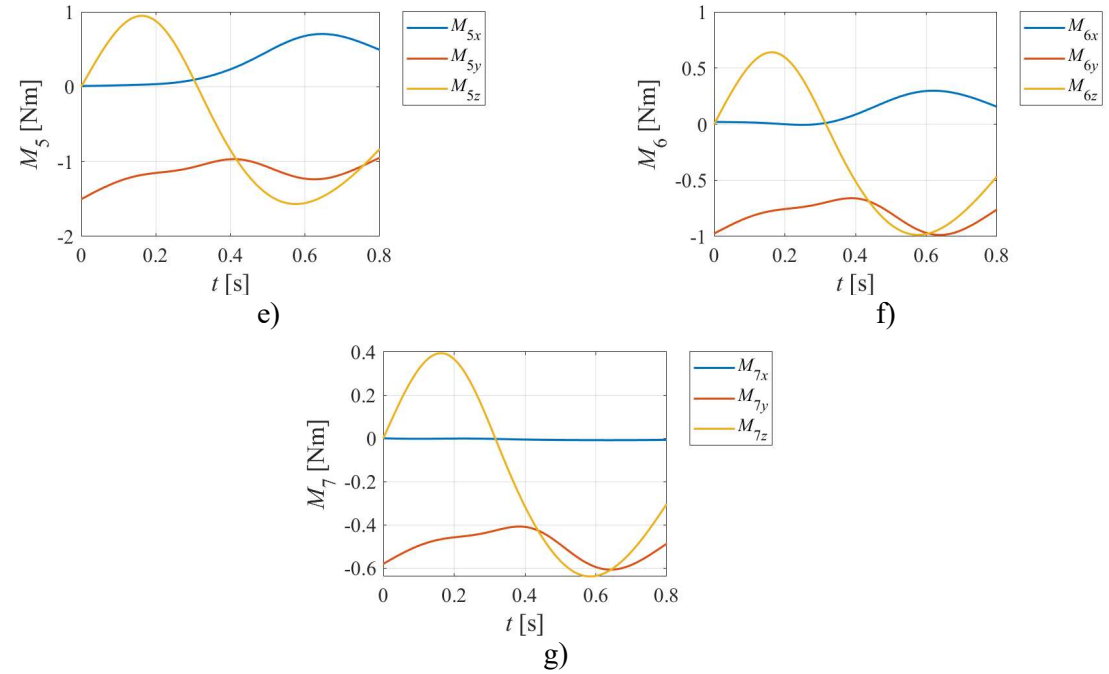

Fig. 6.14. Moments in the joints of the arm M_1,...,M_7, in the global reference system

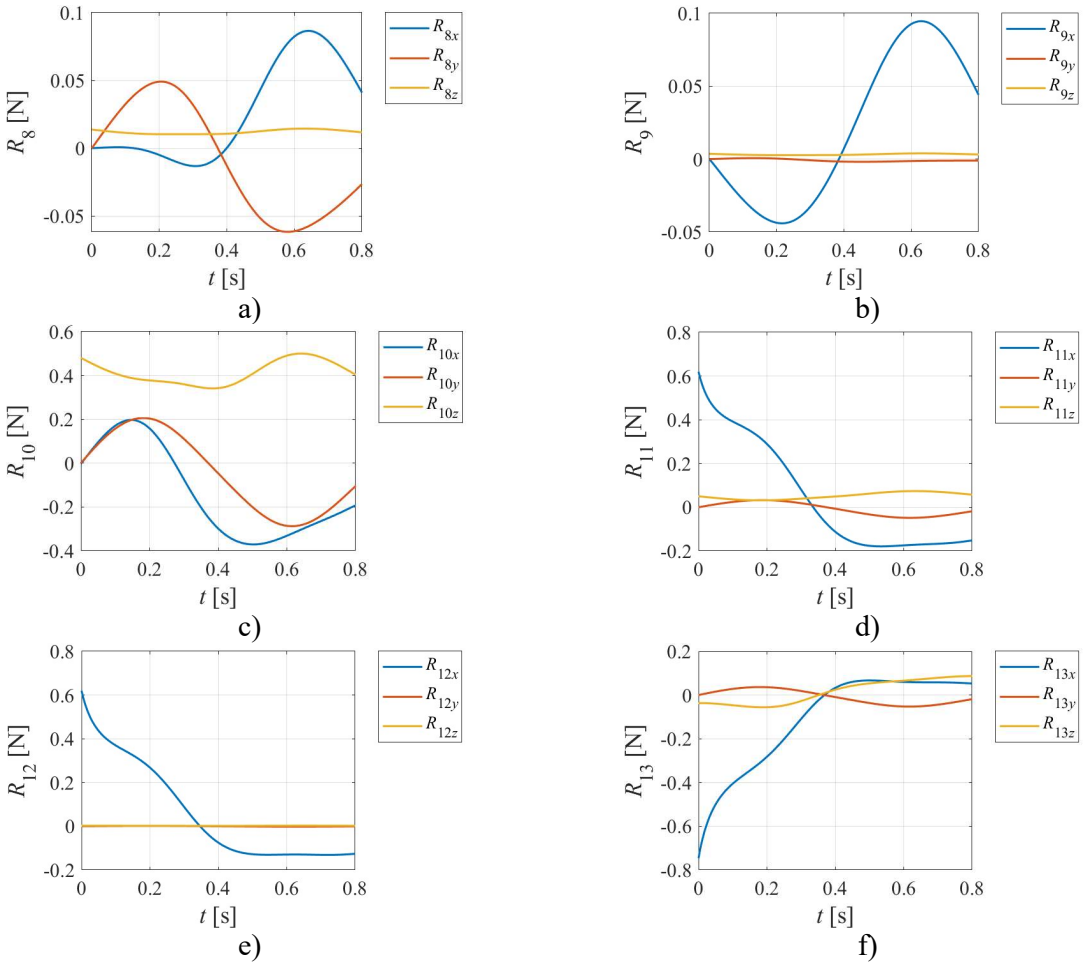

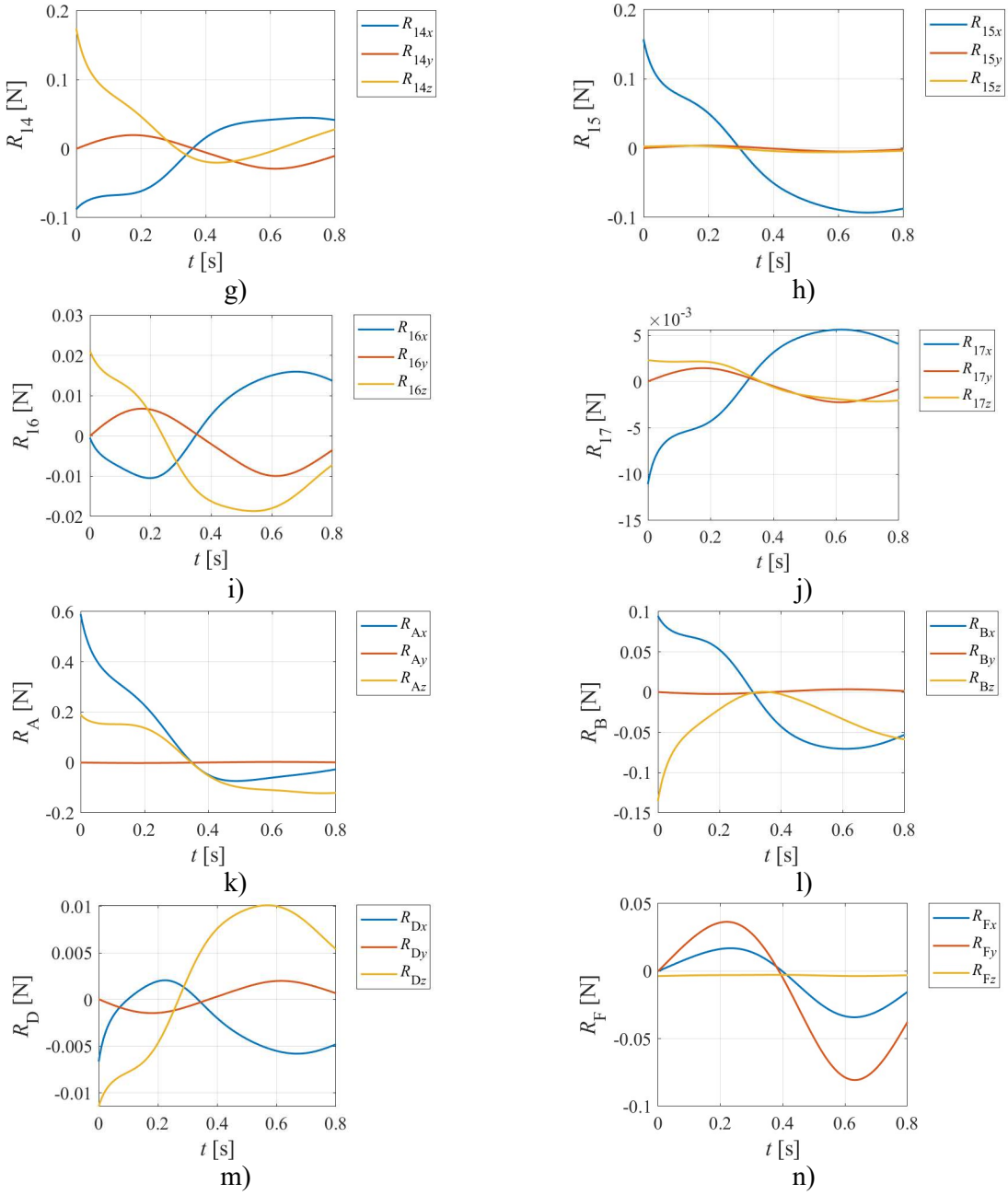

Fig. 6.15. Forces in the joints of finger 1 R_8,...,R_{17}, R_A, R_B, R_D, R_F in the global reference system

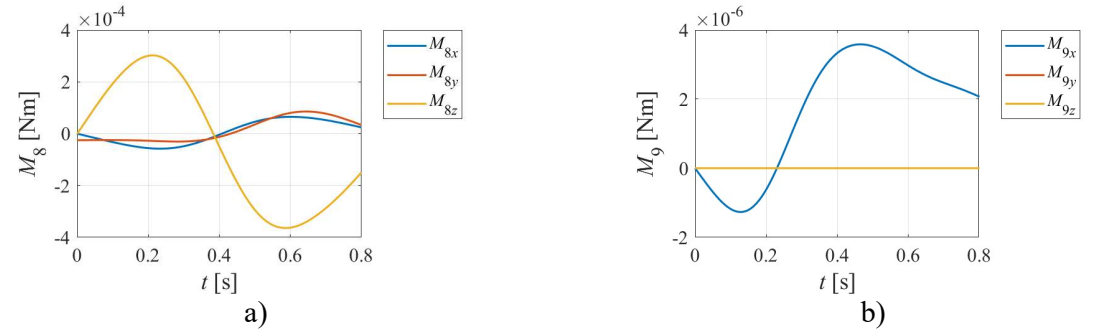

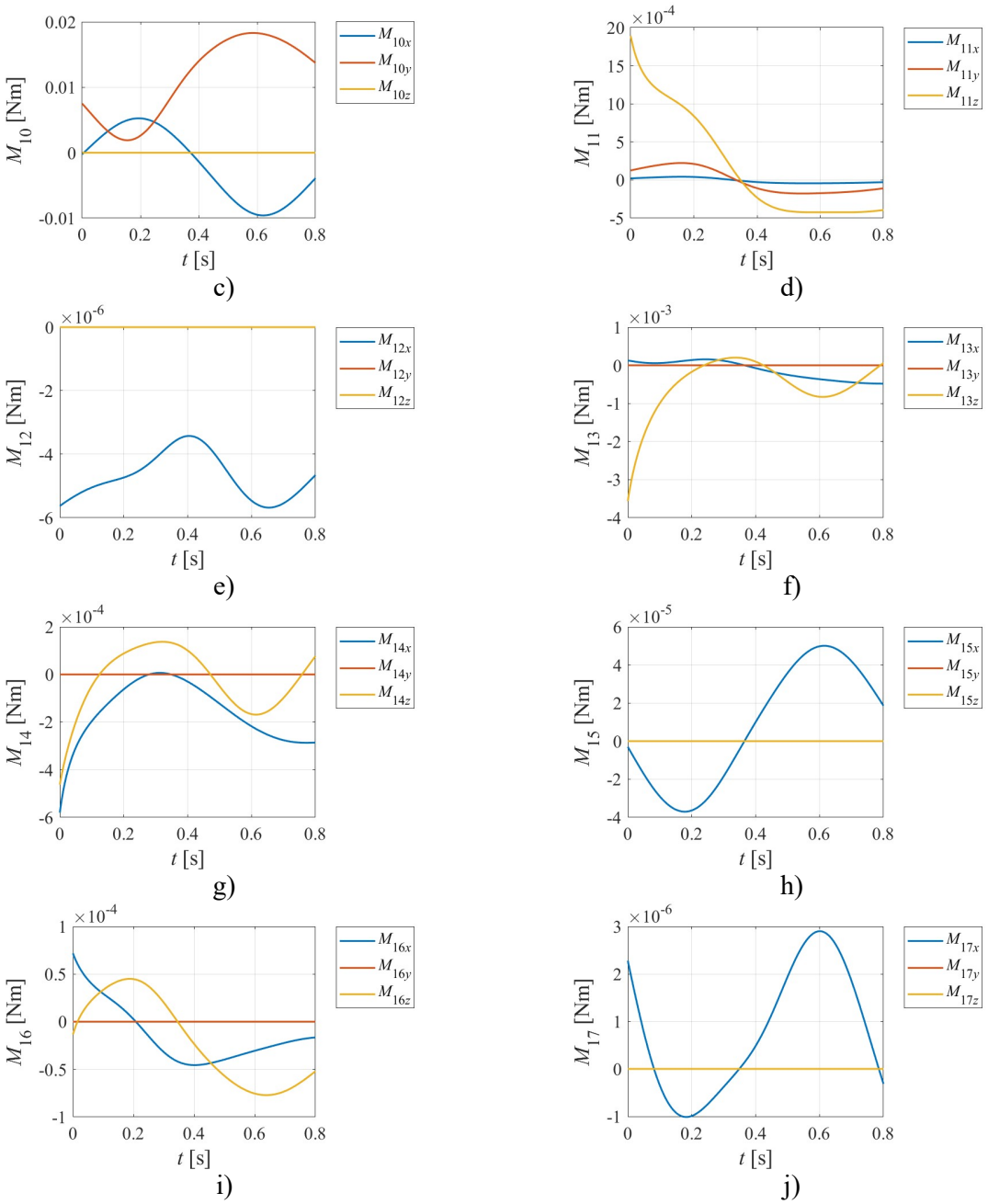

Fig. 6.16. Moments in the joints of finger 1 M_8,...,M_{17} in the global reference system

6.3.2. **Study with methods of analytical mechanics**

Calculating the virtual powers of subsystems O_8,O_9,...,O_{17},E for finger 1 and O_{11},O_{12},...,O_{17},E for each finger, the motor torque in body 8, as well as the motor forces in body 11, can be directly determined for each finger, without determining all the forces and moments in the other joints of the system.

Using this method, the motor forces were plotted along the axes on which the movement of bodies 11 occurs (Fig. 6.17), as well as the motor moments for the joints O_i (i=1...8)(Fig. 6.18),

comparingly to the values obtained from calculations performed using the methods of classical mechanics. As can be seen, the results are remarkably close in value, which is why the analytical method has been further used for direct dynamics due to its rapidity.

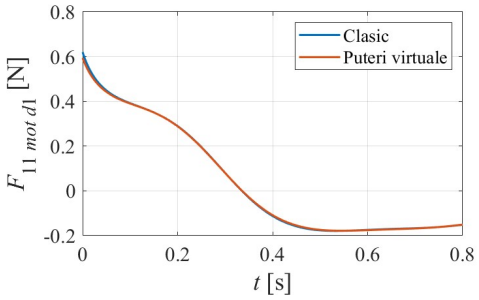

a) finger 1

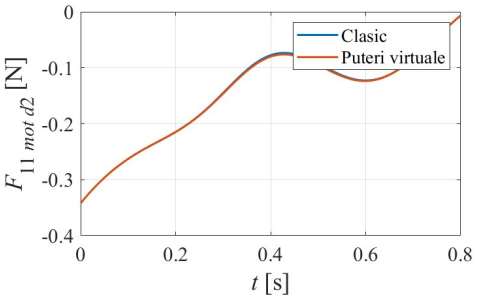

b) finger 2

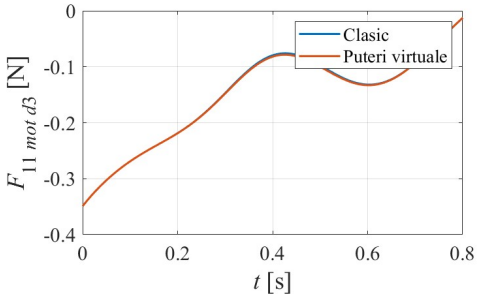

c) finger 3

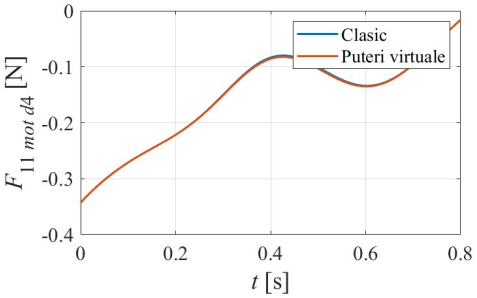

d) finger 4

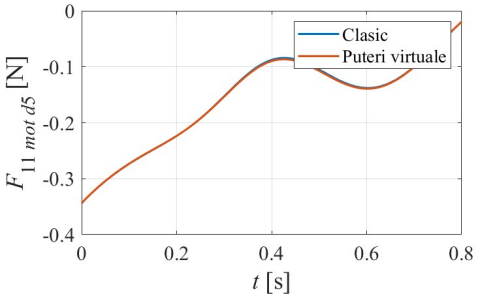

e) finger 5

Fig. 6.17. Motor forces in prismatic couplings 11

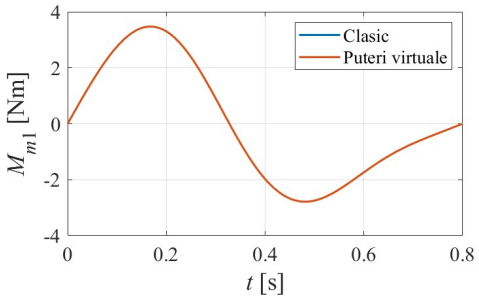

a)

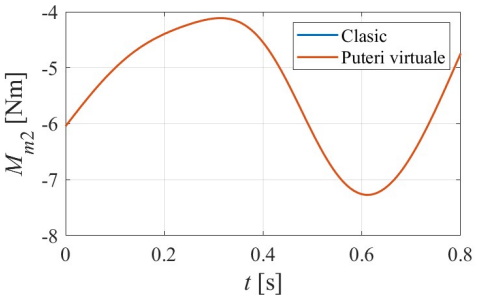

b)

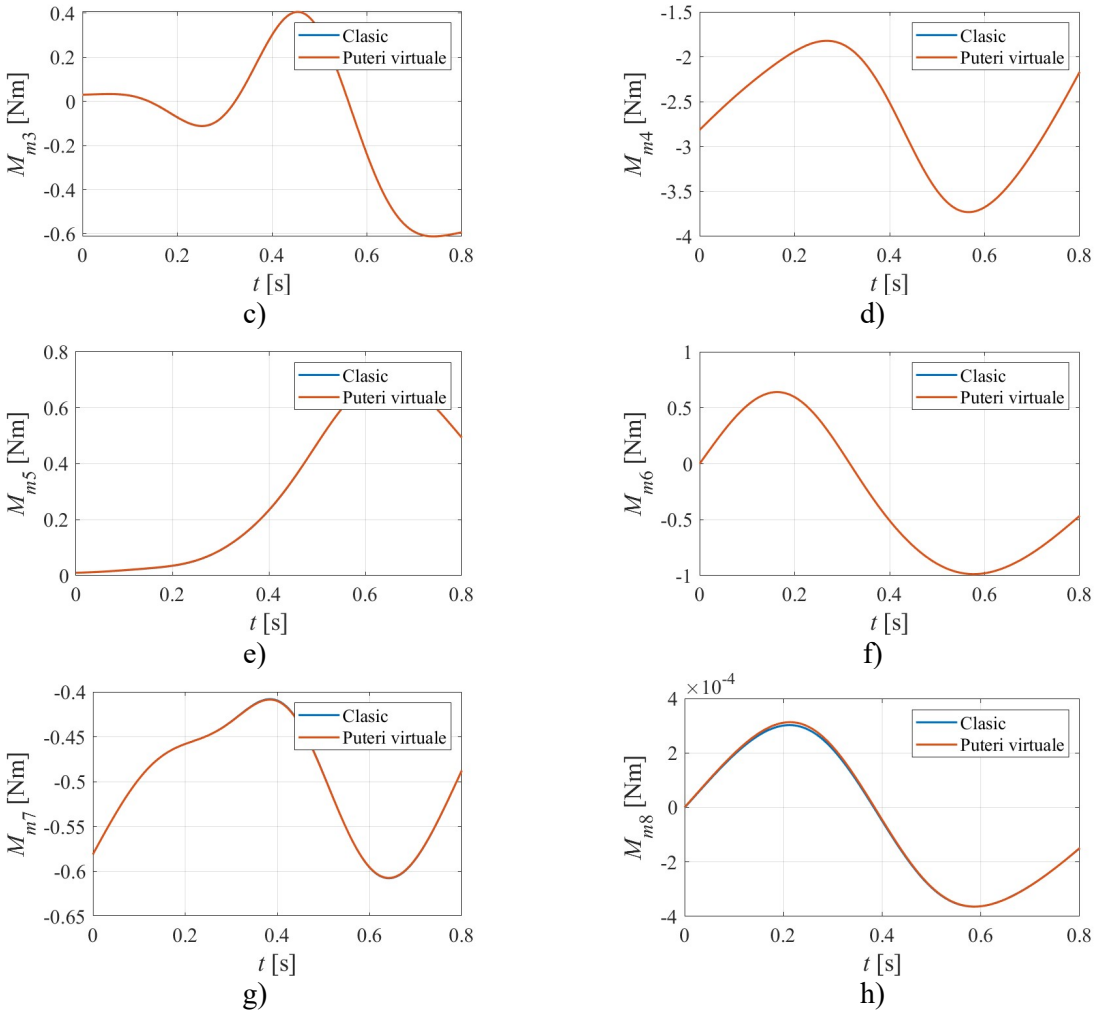

Fig. 6.18. Motor moments in the joints 1...8

6.4. Conclusions

In the chosen configuration, the required torque of the servo motor in joint 2 of the system is the highest, which is explained by the large arms of the weights of the components, relative to point O2. This result leads to the need either to use a sufficiently powerful actuator or to decrease the torque required to produce the movement, using a system of counterweights or a system of elastic elements.

The reaction couples in joints 1 and 3 are considerably larger than the others, which is why it is advisable to make more robust components of these joints.

Low values of torque components M_8 It is due to the small values of the inertia parameters of the 1st finger, as well as the arm O_8O_9.

Motor forces and torques were calculated by the methods of both classical mechanics and analytical mechanics, the results obtained overlapping the scale of representation.

Verifications performed by applying momentum theorem and angular momentum theorem on subsystems, thus analyzing all 5 fingers separately, also showed overlaps in the results obtained.

7. Direct dynamics

In robotics, direct dynamics deals with determining the motion of the system when motor forces and momentums are known, as well as inertial quantities (masses and moments of inertia).

Mathematically, this means considering the system of equations obtained in Chapter 6 with command parameters as unknowns, as well as non-driving forces and moments in the links, all as functions of time. Considered in this way, the system is differential in command parameters and algebraic in non-driving forces and moments.

However, solving systems of algebrodifferential equations is generally difficult and laborious [7], [35]. In the present application, an additional difficulty arises from the fact that the system is unexplained in second-order derivatives of control variables.

The solution of the present problem is simplified by using the methods of analytical mechanics to determine the driving forces F_{11dx} (d = 1, 2,…, 5) and the motor torque M_{8z}.

In the following, an original method of solving this system is presented, which is based on the observation that the dependence of differential equations of motion on second-order derivatives of command variables is linear.

7.1. Theoretical aspects

The general case of a holonomic system of material points is considered, P_i (i = 1, 2,…, n), described by independent generalized coordinates q_k (k = 1, 2,…, h).

The positioning vector of point P_i can be written according to generalized coordinates and time [9], [51], [68]:

$$\bar{r}_i = \bar{r}_i(q_k, t)\ (i = 1,2, \dots, n; k = 1,2, \dots, h). \tag{7.1}$$

It results the velocity of the point

$$\bar{v}_i = \frac{\mathrm{d}\bar{r}_i}{\mathrm{d}t} = \frac{\partial \bar{r}_i}{\partial q_1}\dot{q}_1 + \frac{\partial \bar{r}_i}{\partial q_2}\dot{q}_2 + \cdots + \frac{\partial \bar{r}_i}{\partial q_h}\dot{q}_h + \frac{\partial \bar{r}_i}{\partial \mathrm{t}} = \sum_{\mathrm{j}=1}^{\mathrm{h}} \frac{\partial \bar{r}_i}{\partial q_j}\dot{q}_j + \frac{\partial \bar{r}_i}{\partial \mathrm{t}}. \tag{7.2}$$

Considering the second order Lagrange's equations in the case of freely chosen forces,

$$\frac{\mathrm{d}}{\mathrm{d}t}\left(\frac{\partial E}{\partial \dot{q}_k}\right) - \frac{\partial E}{\partial q_k} = Q_k\ (k = 1,2, \dots, h), \tag{7.3}$$

into which the kinetic energy of the system has been introduced,

$$E = \sum_{i=1}^{n} \frac{1}{2} m_i {v_i}^2, \tag{7.4}$$

as well as the generalized force Q_k.

Substituting the expression (7.2) into equation (7.4), it results

$$E = \frac{1}{2}\sum_{j=1}^{h}\sum_{l=1}^{h} A_{jl}\dot{q}_j\dot{q}_l + \sum_{l=1}^{h} B_l\dot{q}_l + \frac{1}{2}C, \tag{7.5}$$

where the coefficients

$$A_{jl} = \sum_{i=1}^{n} m_i \frac{\partial \bar{r}_i}{\partial q_j} \cdot \frac{\partial \bar{r}_i}{\partial q_l}\ (j, l = 1,2, \dots, h)\ , \tag{7.6}$$

$$B_l = \sum_{i=1}^{n} m_i \frac{\partial \bar{r}_i}{\partial q_l} \cdot \frac{\partial \bar{r}_i}{\partial t} \ (l = 1,2, \dots, h) \ , \tag{7.7}$$

$$C = \sum_{i=1}^{n} m_i \frac{\partial \bar{r}_i}{\partial t} \cdot \frac{\partial \bar{r}_i}{\partial t}, \tag{7.8}$$

depend on generalized coordinates q_1, q_2, … , q_h and time t.

It results

$$\frac{\mathrm{d}}{\mathrm{d}t}\left(\frac{\partial E}{\partial \dot{q}_k}\right) - \frac{\partial E}{\partial q_k} = \sum_{l=1}^{h} A_{kl}\ddot{q}_l + D_k \ (k = 1,2, \dots, h), \tag{7.9}$$

where coefficients

$$D_k = \sum_{l=1}^{h}\sum_{j=1}^{h}\left(\frac{\partial A_{kl}}{\partial q_j} - \frac{1}{2}\frac{\partial A_{jl}}{\partial q_k}\right)\dot{q}_j\,\dot{q}_l + \sum_{l=1}^{h}\left(\frac{\partial A_{kl}}{\partial t} + \frac{\partial B_k}{\partial q_l} - \frac{\partial B_l}{\partial q_k}\right)\dot{q}_l + \\ + \frac{\partial B_k}{\partial t} - \frac{1}{2}\frac{\partial C}{\partial q_k}, (k = 1,2, \dots, h) \tag{7.10}$$

depend on generalized coordinates q_1, q_2, … , q_h, generalized velocities $\dot{q}_1$, $\dot{q}_2$, ... , $\dot{q}_h$ and time t.

Therefore the second order Lagrange's equations (7.3) become:

$$\sum_{l=1}^{h} A_{kl}\ddot{q}_l + D_k = Q_k \ (k = 1,2, \dots, h). \tag{7.11}$$

It follows that generalized forces depend linearly on second-order derivatives of generalized coordinates.

7.2. Explicating the system

The system (7.11) can be written in matrix form

$$[A]\{\ddot{q}\} + \{D\} = \{Q\}, \tag{7.12}$$

where the matrices

$$[A] = \begin{bmatrix} A_{11} & \cdots & A_{1h} \\ \vdots & \ddots & \vdots \\ A_{h1} & \cdots & A_{hh} \end{bmatrix}, \tag{7.13}$$

$$\{q\} = \begin{Bmatrix} q_1 \\ \vdots \\ q_h \end{Bmatrix}, \tag{7.14}$$

$$\{D\} = \begin{Bmatrix} D_1 \\ \vdots \\ D_h \end{Bmatrix}, \tag{7.15}$$

$$\{Q\} = \begin{Bmatrix} Q_1 \\ \vdots \\ Q_h \end{Bmatrix}. \tag{7.16}$$

were introduced.

Multiplying the system to the left (7.12) by the inverse of the matrix (7.13) yields the explicit form in the second-order derivatives of generalized coordinates,

$$\{\ddot{q}\} + \{D'\} = \{Q'\}, \tag{7.17}$$

where

$$\{D'\} = [A]^{-1}\{D\}, \tag{7.18}$$

$$\{Q'\} = [A]^{-1}\{Q\}. \tag{7.19}$$

The system (7.17) can be written in developed form

$$\ddot{q}_k = Q'_k - D'_k \ (k = 1,2, \dots, h). \tag{7.20}$$

The matrices (7.13), (7.15), (7.16), (7.18) and (7.19) depend on generalized coordinates q_k, generalized velocities $\dot{q}_k$ and time *t*.

7.3. Integration of the explicit system

If for known parameter values q_k, $\dot{q}_k$, $\ddot{q}_k$ and *t* generalized forces Q_k can be determined, them, for q_k, $\dot{q}_k$ and *t* given, the coefficients A_{kl} and D_k are calculated as follows:

1) we chose

$$\ddot{q}_k = 0 \ (k = 1,2, \dots, h), \tag{7.21}$$

we determine Q_k,

$$D_k = Q_k \ (k = 1,2, \dots, h); \tag{7.22}$$

2) successively, for $l = 1, 2, \dots, h$, we chose

$$\ddot{q}_l = 1, \ddot{q}_k = 0 \ (k = 1,2, \dots, h; \ k \neq l), \tag{7.23}$$

and we determine Q_k, as well as

$$A_{kl} = Q_k - D_k \ (k = 1,2, \dots, h). \tag{7.24}$$

With the coefficients (7.22) and (7.24) determine the matrices (7.13), (7.18) and (7.19) with which the explicit form (7.20) of the system is constructed.

This system consists of *h* second-order differential equations, which can be put in the form of a system of 2*h* first-order equations by introducing auxiliary variables

$$s_k = \dot{q}_k \ (k = 1,2, \dots, h). \tag{7.25}$$

With these variables, system (7.20) becomes

$$\{\dot{X}\} = [B]\{X\} + \{E\}, \tag{7.26}$$

where

$$\{X\} = \begin{Bmatrix} q_1 \\ \vdots \\ q_h \\ s_1 \\ \vdots \\ s_h \end{Bmatrix}, \tag{7.27}$$

$$[B] = \begin{bmatrix} 0 & \cdots & 0 & 1 & \cdots & 0 \\ \vdots & \ddots & \vdots & \vdots & \ddots & \vdots \\ 0 & \cdots & 0 & 0 & \cdots & 1 \\ A_{11} & \cdots & A_{1h} & 0 & \cdots & 0 \\ \vdots & \ddots & \vdots & \vdots & \ddots & \vdots \\ A_{h1} & \cdots & A_{hh} & 0 & \cdots & 0 \end{bmatrix}, \tag{7.28}$$

$$\{E\} = \begin{Bmatrix} 0 \\ \vdots \\ 0 \\ Q'_1 - D'_1 \\ \vdots \\ Q'_h - D'_h \end{Bmatrix}. \tag{7.29}$$

The system (7.26) can be numerically integrated with the Runge-Kutta method.

7.4. Numerical applications

The system of differential equations (7.26), of the first order, was numerically integrated using the Runge–Kutta method, using the time step Δt=0.00001 s.

In order to verify the method, the variations in driving forces and torques calculated in Chapter 6 were used as input and the laws of motion obtained by integration with those imposed in that chapter were compared.

The numerical integration of the system of differential equations was first performed with the *ode45* function, from the MATLAB program. In this case, the values obtained coincided to a good extent with those imposed in Chapters 4 to 5 only in a first sub-interval of approximately 30% of the time considered, $t = 0 \ldots 0.8$ s. In the latter part of the range, cumulative errors in the numerical integration method led to significant differences.

The functions *ode23*, *ode78*, *ode89* and *ode113* were then tried successively, but none brought significant improvements.

Finally, integration was performed with the *ode45* function, applied successively over 4000 subintervals $t = t_i \ldots t_i + 2 \cdot 10^{-4}$ s of the considered range , $t = 0 \ldots 0.8$ s. In this case, the accuracy has increased considerably, with the values obtained coinciding very well with those imposed in Chapter 6 for most of the time frame considered (approximately 88%).

Thus, variations in control parameters were obtained ($\varphi_{0\text{-}1}$, $\theta_{1\text{-}2}$, $\varphi_{2\text{-}3}$, $\theta_{3\text{-}4}$, $\varphi_{4\text{-}5}$, $\psi_{5\text{-}6}$, $\theta_{6\text{-}7}$, $\psi_{7\text{-}8}$, s_1, s_2, s_3, s_4 and s_5), and their first two derivatives illustrated in Figures 7.1 to 7.13, superimposed on those required in Chapters 4 and 5.

A further increase in accuracy can be achieved by reducing the time step, but the execution time lengthens considerably.

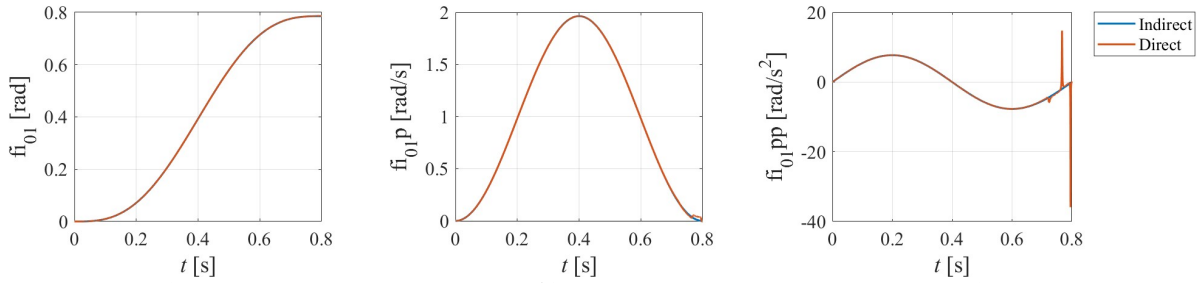

a) b) c)

Fig. 7.1. Angular displacement and its first and second derivatives respectively for the servomotor 1

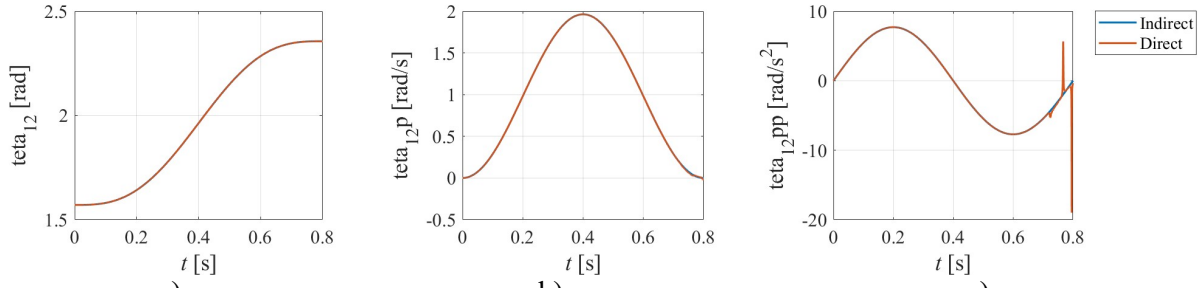

a) b) c)

Fig. 7.2 Angular displacement and its first and second derivatives respectively for the servomotor 2

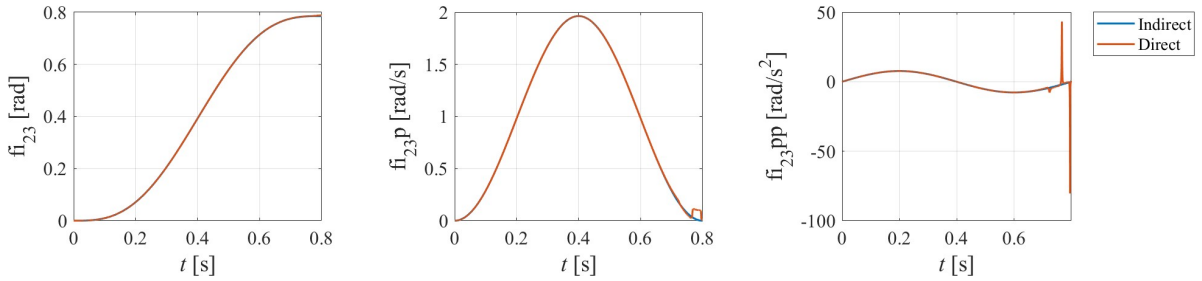

a) b) c)

Fig. 7.3. Angular displacement and its first and second derivatives respectively for the servomotor 3

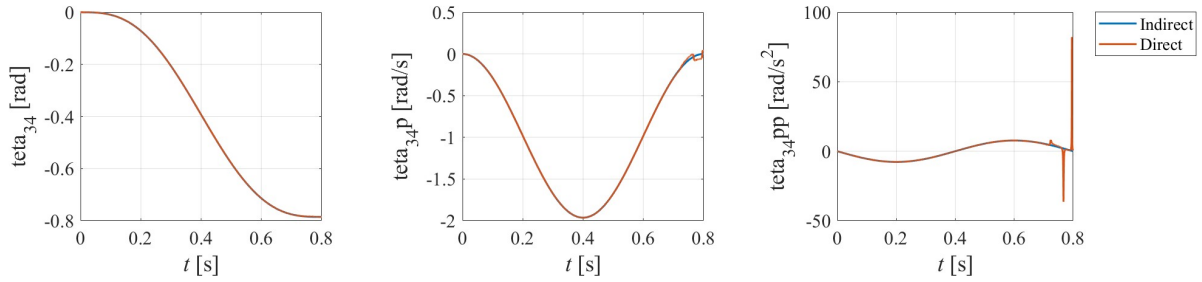

a) b) c)

Fig. 7.4. Angular displacement and its first and second derivatives respectively for the servomotor 4

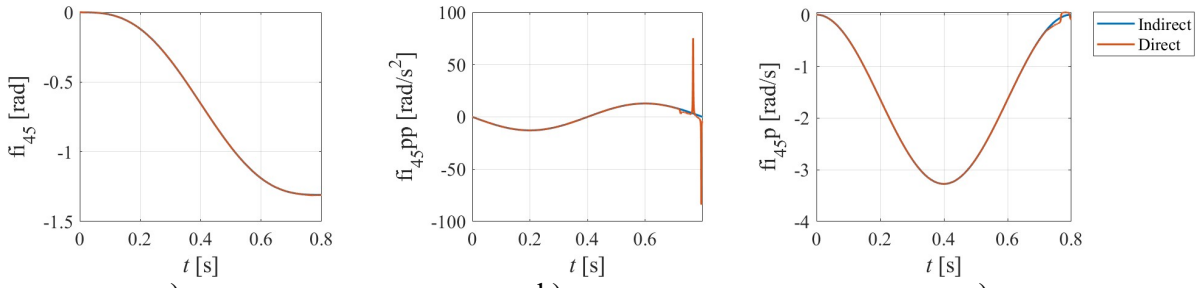

a) b) c)

Fig. 7.5. Angular displacement and its first and second derivatives respectively for the servomotor 5

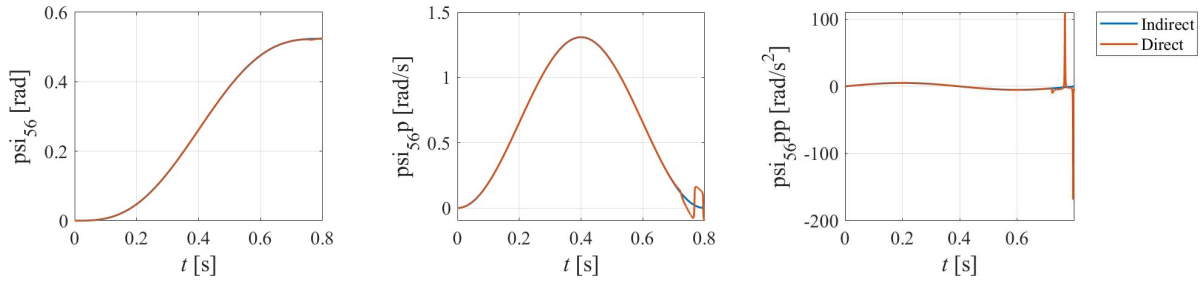

a) b) c)

Fig. 7.6. Angular displacement and its first and second derivatives respectively for the servomotor 6

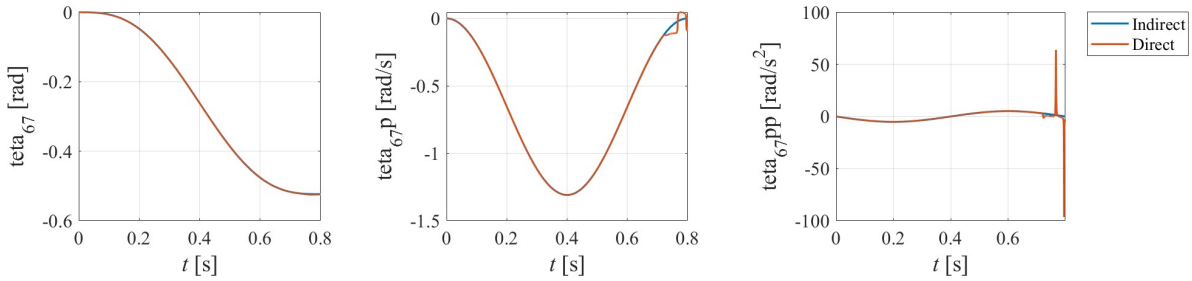

a) b) c)

Fig. 7.7. Angular displacement and its first and second derivatives respectively for the servomotor 7

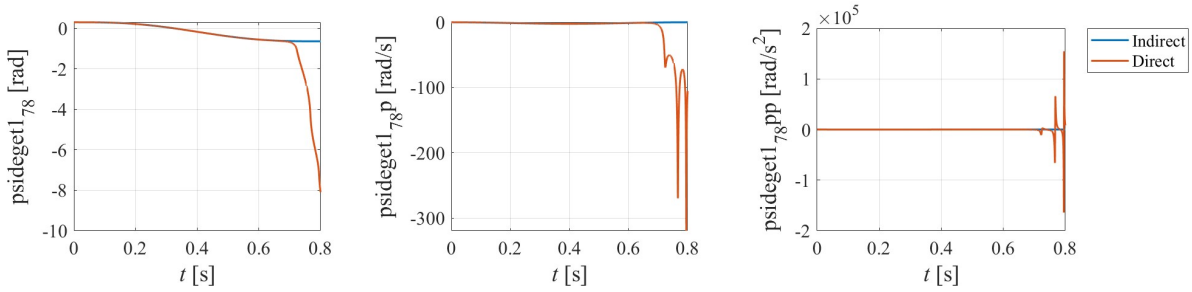

a) b) c)

Fig. 7.8. Angular displacement and its first and second derivatives respectively for the servomotor 8

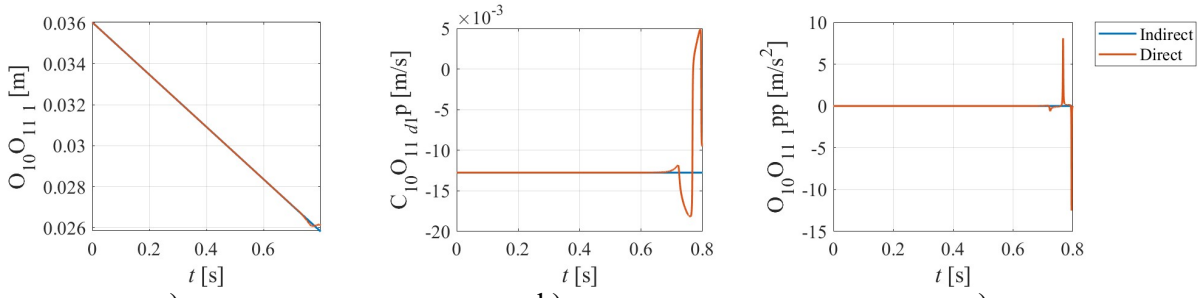

a) b) c)

Fig. 7.9. Displacement and its first and second derivatives respectively for the linear actuator 1

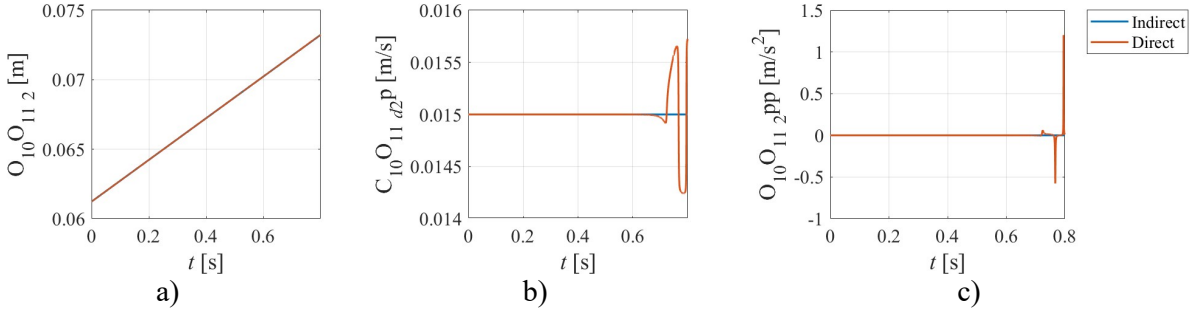

a) b) c)

Fig. 7.10. Displacement and its first and second derivatives respectively for the linear actuator 2

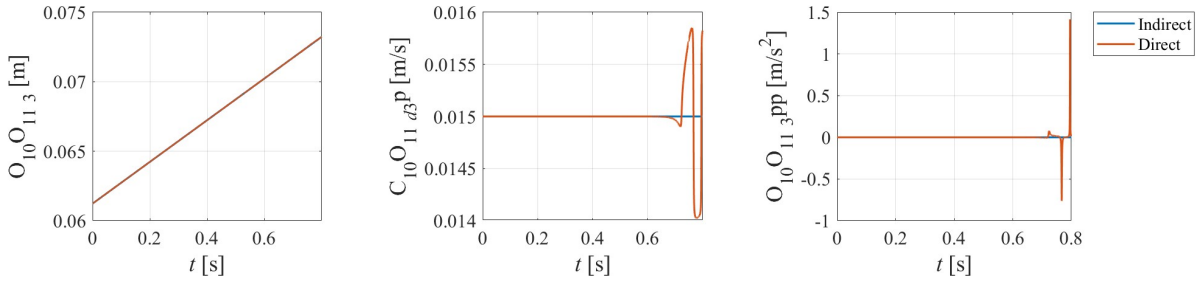

a) b) c)

Fig. 7.11. Displacement and its first and second derivatives respectively for the linear actuator 3

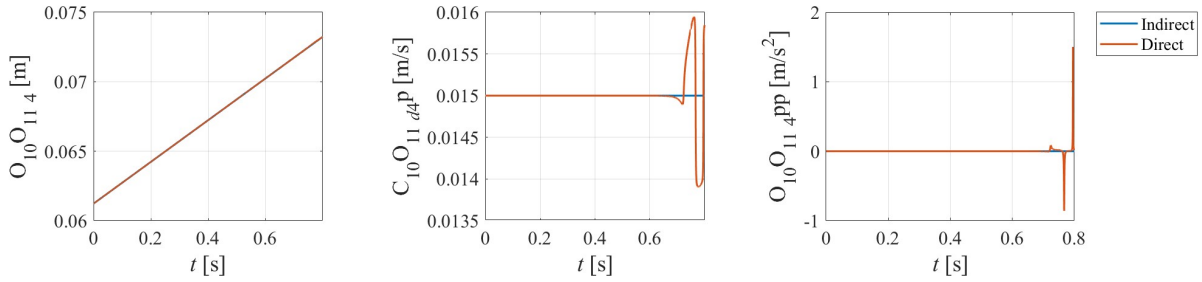

a) b) c)

Fig. 7.12. Displacement and its first and second derivatives respectively for the linear actuator 4

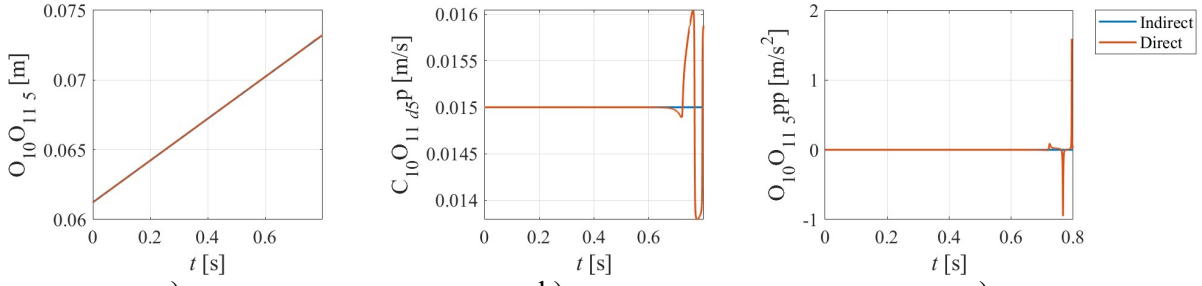

a) b) c)

Fig. 7.13. Displacement and its first and second derivatives respectively for the linear actuator 5

7.5. Conclusions

The values of displacements, velocities and accelerations of the linear actuators acting each finger, as well as the angular displacements, and their first two derivatives, obtained in the case of direct dynamics, largely coincide with the values given as input parameters for calculating the forces and moments in the joints in the case of reverse dynamics. This overlap of results confirms the correctness of the method of numerical solving of differential equations of motion of the robotic hand-arm system, presented in this chapter.

Errors occurring in the last eighth of the time interval in which the movement occurs are due to the numerical method of integration. A reduction of these errors can be achieved by choosing a smaller time step, which, however, considerably increases the running time.

8. Vibrations

The functionality of the anthropomorphic prehensor presented in Chapter 3 may be affected by vibrations arising from various mechanical interactions in the robotic hand-arm system, or due to external factors, depending on operating conditions.

Two types of studies were considered:

1. numerically, of 3D modeled fingers as rigidly bound elastic solids systems;
2. experimental, 1 finger, made with real joints.

8.1. Numerical study

The free, undamped vibrations of the following subsystems were analyzed using the finite elements method in CATIA V5:

1) thumb (finger 1), considered as a separate rigid system (fig. 8.1.a),
2) one of the fingers 2-5, considered as a separate rigid system (fig. 8.1.b),
3) the hand, considering that the fingers, considered rigid, are rigidly fixed on the palm.

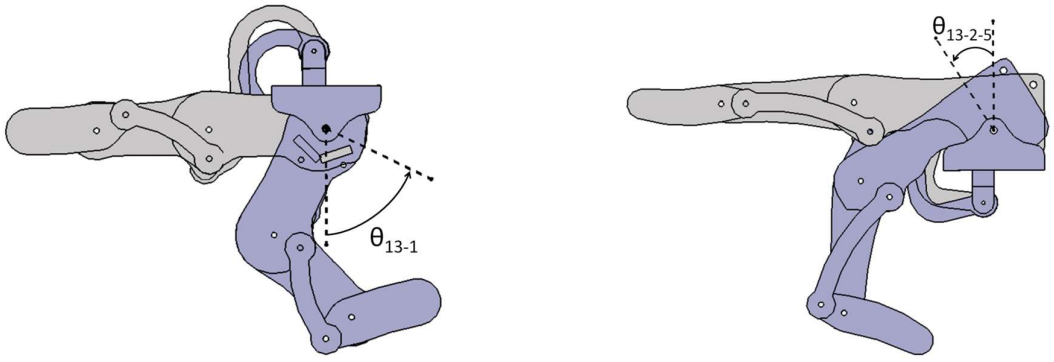

a) b)

4) Fig. 8.1. Fingers extended (light gray) and flexed (dark gray) [16]

Each of the three cases presented was studied for two configurations (Fig. 8.1) defined by the angle $\theta_{13\text{-}1}$ for the thumb, respectively by the angles $\theta_{13\text{-}2\text{-}5}$ for the other fingers:

- extended finger (light grey) - $\theta_{13\text{-}1}=0°$, $\theta_{13\text{-}2\text{-}5}=0°$,
- flexed finger (dark grey color) - $\theta_{13\text{-}1}=64°$, $\theta_{13\text{-}2\text{-}5}=32°$.

In addition, the proper frequencies of the fingers, considered as separate systems, were determined in seven intermediate configurations between the two above, with steps $\Delta\theta_{13\text{-}1}=8°$ (tab. 8.1) and $\Delta\theta_{13\text{-}2\text{-}5}=4°$ (tab. 8.2), respectively, as well as the system of the hand with outstretched and flexed fingers (tab. 8.3).

Variations with flexion angles $\theta_{13\text{-}1}$, and $\theta_{13\text{-}2\text{-}5}$, respectively, of the first two eigenfrequencies of finger 1 and one of the other fingers, respectively, considered as independent systems, are shown in figure 8.2.

The values of the first two proper frequencies are higher for finger 1 than for the other fingers. This is due to the smaller size of finger 1, compared to fingers 2-5. However, this observation is not true for higher modes of their own, which is explained by the different shape of the fingers.

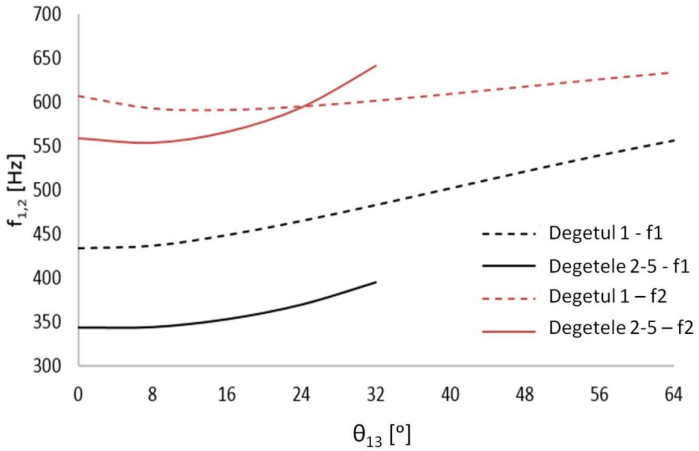

Fig. 8.2. Variation of the first two eigenfrequencies from the angle θ [16]

The first proper vibration mode of finger 1 (fig. 8.3), as well as fingers 2-5 (fig. 8.4), is to bend in a plane parallel to that of the plate, in which the flexibility of the body is greater.

The second proper mode of vibration of finger 1 (fig. 8.5), as well as fingers 2-5 (fig. 8.6), is to bend in a plane perpendicular to that of the plate.

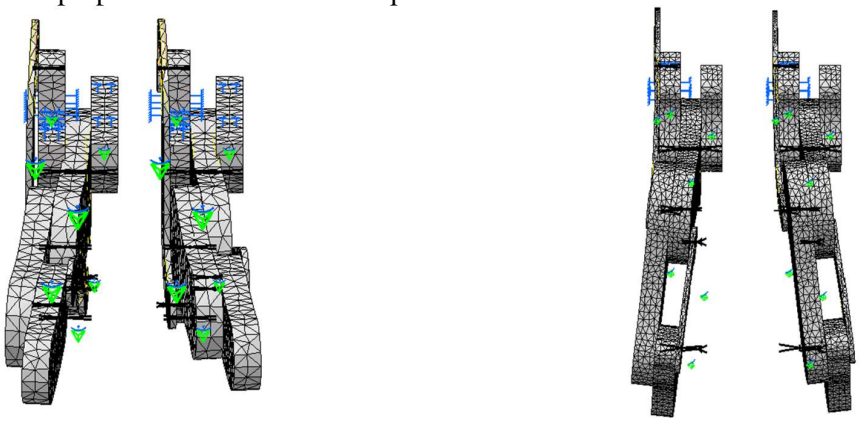

a) b)

Fig. 8.3. First vibration mode of finger 1: a) extended b) flexed [16]

a) b)

Fig. 8.4. First mode of vibration of fingers 2-5: a) extended b) flexed [16]

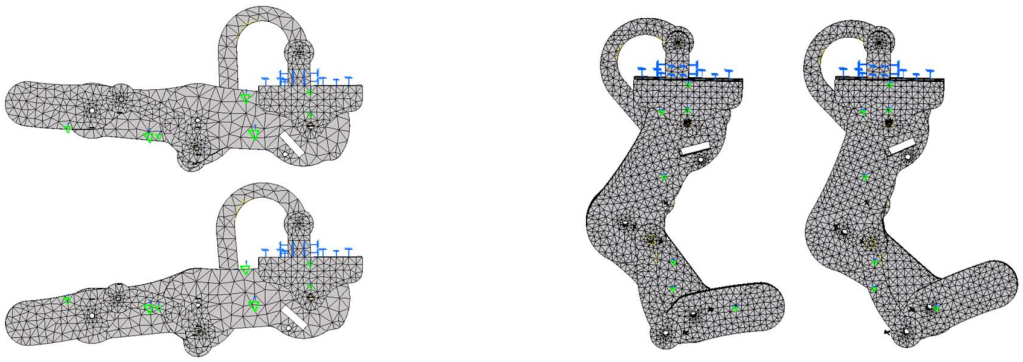

a) b)

Fig. 8.5. Second vibration mode of finger 1: a) extended b) flexed [16]

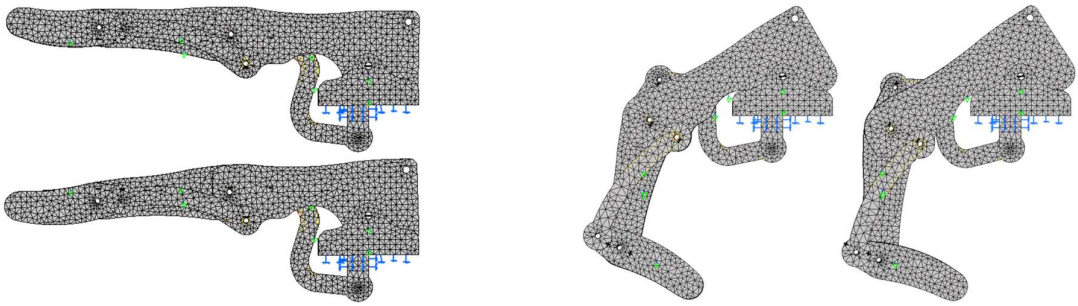

a) b)

Fig. 8.6. Second mode of vibration of fingers 2-5: a) extended b) flexed [16]

8.2. Experimental study

The experimental determinations were made using the laser vibrometer consisting of the Polytec OFV-5000 controller (fig. 8.33) and the Polytec OFV-505 laser head (fig. 8.34).

Fig. 8.33. Controller

Fig. 8.34. Laser head

The laser vibrometer measures the relative vibration speed of the body at which the laser beam is directed (fig. 8.35).

The thumb of the hand, together with the linear actuator attached to it, was fixed in the console on a support made by 3D printing (fig. 8.36).

Fig. 8.35. Laser head pointing at one of the fingers of the hand

Fig. 8.36. Assembly of finger 1, corresponding linear actuator and holder

Adjustments were made to measure low frequencies, and the amplitude of the output signal was used as a trigger, by gently hitting the system at various locations (fig. 8.37).

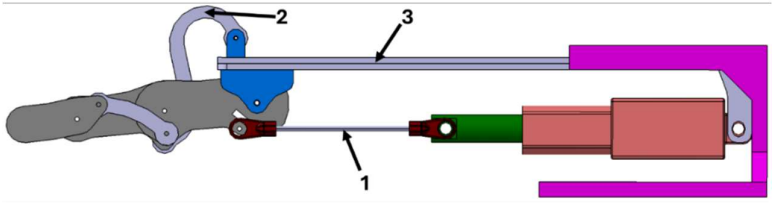

Fig. 8.37. Theoretical locations where it was desired to hit the

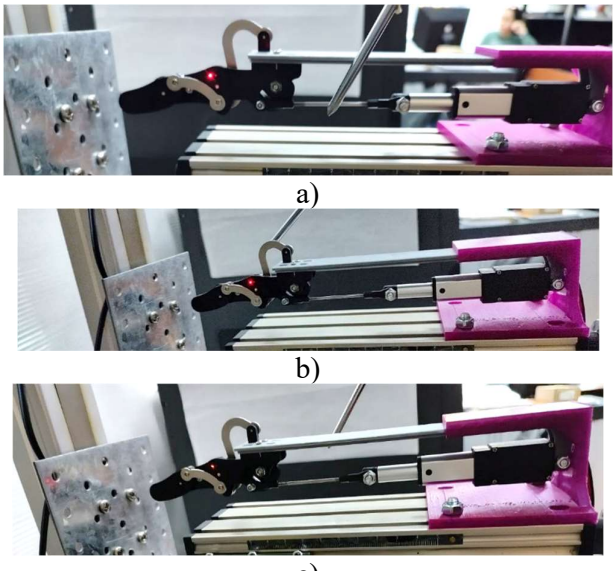

a) b) c)

Fig. 8.38. Actual locations where the system was hit to start measuring vibration

Measurements were made five times for each strike location (fig. 8.38 a-c), over a duration of 10s, with a sampling frequency of 1000Hz.

The signal analysis was performed using the fast Fourier transform, which calculates the discrete Fourier transform of the signal, thus obtaining the first proper frequency in the range 0...500Hz.

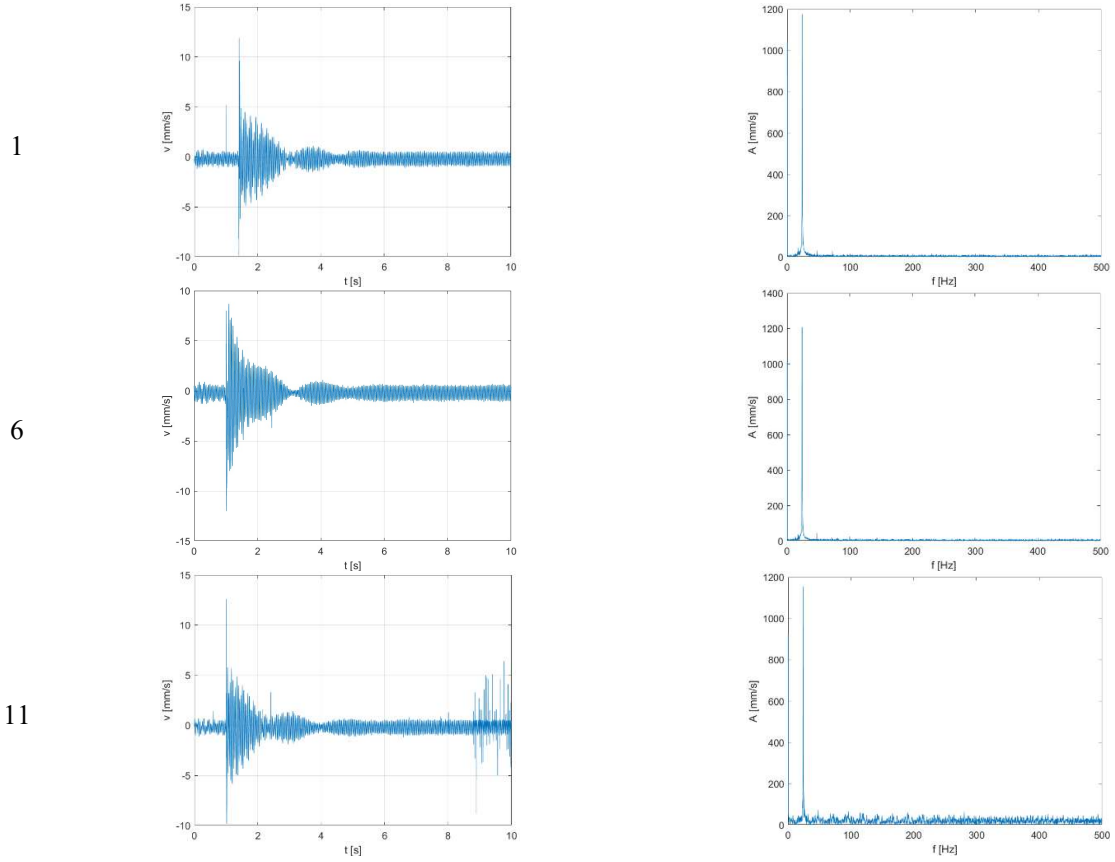

Fig. 8.39. Signal and corresponding spectrum

Thus, the signals in figure 8.39 and the corresponding spectra were obtained, with only 3 measurements being presented. All spectra show sharp maxima at 24.2 Hz.

8.3. Conclusions

The considered model in the numerical study differs significantly from the real system, in which the elements are articulated. The high flexibility of the joints in relation to that of the component bodies results in lower values of their own frequencies.

The studies presented in this chapter are only one step towards initiating more precise and complete studies, which could be the subject of further development.

9. Final considerations

9.1. Final remarks

The grasping device used is a mechanism with a reduced number of mobilities compared to that of a human hand, which makes it cheaper, lighter, and easier to build than a more realistic model.

To improve the functionality of the existing commercial hand, used as a starting point for the present doctoral thesis, additional mobility of the thumb was introduced, rotating it around an axis perpendicular to the plane of the palm. Additionally, an anthropomorphic arm was designed, which, together with the hand, forms a robotic hand-arm system.

Due to its simplicity and relatively small size, most parts of the device can be manufactured by 3D printing. Other parts are made directly from commercially available blanks. This design strategy easily allows further improvements to be made.

The study presents a kinematic analysis, an indirect dynamic analysis, as well as a direct dynamic analysis of the hand-arm robotic system.

The movement of the robotic hand-arm system was visualized through an animated graphical representation of its significant points, made with the help of the program developed for determining kinematic and dynamic calculations.

Several sets of kinematic calculation checks have been performed:

1. the angular velocities of analytically determined component copes were verified using Poisson's relations, where the unit vectors $\bar{\imath}, \bar{\jmath}$ and $\bar{k}$ were derived numerically;
2. the analytically determined significant point rates were compared with the values obtained by numerical derivation of position vectors;
3. the angular accelerations of analytically determined component copes were compared with the values obtained by numerical derivation of angular velocities;
4. analytically determined accelerations of significant points were compared with values obtained by numerical velocity derivation.

In all four sets of checks, the results obtained by the two methods are very well in agreement.

In the chosen configuration, the required torque of the servo motor in joint 2 of the system is the highest, which is explained by the large arms of the weights of the components, relative to point O2. This result leads to the need either to use a sufficiently powerful actuator or to decrease the torque required to produce the movement, using a system of counterweights or a system of elastic elements.

The reaction couples in joints 1 and 3 are considerably larger than the others, which is why it is advisable to make more robust components of these joints.

The small values of the torque components M_8 are due to the small values of the inertia parameters of the 1st finger, as well as the arm O_8O_9.

The results provide useful computational data for the basic design of a robotic hand-arm system as well as for an optimization process.

Motor forces and torques (forces required for linear finger motors and times required for actuators in joints providing degrees of mobility to the system) were calculated by two methods:

- using the methods of classical mechanics, isolating all 55 bodies of the system and using the momentum theorem and the angular momentum theorem with respect to the center of mass for each body;
- using the methods of analytical mechanics, using D'Alembert's principle and the principle of virtual powers.

The results obtained by the two methods are very well in agreement.

Another method of verification consisted in applying momentum theorem and angular momentum theorem on subsystems, thus analyzing all 5 fingers separately. And in this case, the results coincided with particularly good accuracy.

The values of displacements, velocities and accelerations of the linear actuators acting each finger, as well as the angular displacements, and their first two derivatives, obtained in the case of direct dynamics, largely coincide with the values given as input parameters for calculating the forces and moments in the joints in the case of reverse dynamics. This overlap of results confirms the correctness of the method of numerical solving of differential equations of motion of the robotic hand-arm system.

Errors occurring in the last eighth of the time interval in which the movement occurs are due to the numerical method of integration. A reduction of these errors can be achieved by choosing a smaller time step, which, however, considerably increases the running time.

9.2. Original contributions

The paper makes a number of original contributions to the study of anthropomorphic hand-arm robotic systems. These are reviewed below.

The 3D model of an anthropomorphic robotic arm was designed and made so that it could be made mainly of blanks.

The joints of the robotic arm have been designed so that they can be made by printing using a 3D printer.

The overall concept behind the robotic arm design has been developed so that the robot is modular, with new parts being added to improve system performance.

The means of action of the studied anthropomorphic hand have been modified to reduce its size and weight and a new degree of mobility has been added to it in order to achieve more complex movements and improve the ability to manipulate objects already grasped by it.

The connections between the constituent bodies of the robotic hand have been modeled in such a way as to avoid both underconstraint and overconstraint of the mechanical system, therefore so that the system of dynamic equations that calculate the forces and moments in the links is compatible and determined.

A complete kinematic analysis was performed by determining the equations of motion, the speeds, and accelerations of all points of the system, as well as the angular velocities and accelerations of the bodies composing the robot.

Inverse dynamic analysis was performed, both using the general theorems of classical mechanics and the methods of analytic mechanics, to determine the forces and momenta in the bonds of the system when motion is imposed. Some of these forces and moments are engines and others are reactions. Motor forces and torques are required for the choice of actuators, and reaction forces are used for dimensioning system elements.

Direct dynamic analysis of the system was carried out by an original method, based on the observation that the differential equations of motion of any mechanical system depend linearly on second-order derivatives of generalized coordinates. This analysis has been verified using the results obtained from reverse dynamic analysis and is the basis for determining the movement of the hand-arm system in any other configuration, as well as under the action of any other system of motor forces and torques.

A numerical analysis of the vibrations of 3D modeled fingers as rigidly bonded elastic solids systems was performed. The analysis was performed with the finite element method, from the design program, also used for designing the arm and hand elements, CATIA V5. The first ten proper vibration modes of the fingers of the grasping system as well as of the system with fingers

rigidly attached to the palm of the grasp in different configurations were determined. The study is a preliminary step to determine possible harmful own frequencies.

An experimental study was conducted to determine the true values of the first proper frequency of finger 1 using a remote vibration velocity acquisition system. The experimental data were processed with the fast Fourier transform to obtain the corresponding spectrum. Its analysis allowed to determine the fundamental eigenfrequency of the studied finger.

9.3. Development directions

The studies presented in this paper can be continued with a wide range of development directions.

A first direction consists in extending kinematic and reverse dynamic analysis for other laws of variation of control parameters of the presented robotic system.

A second direction is to determine optimal movements in terms of energy consumption and execution time.

Other systems can be studied, using both the knowledge gained and the calculation programs conducted in the framework of this work.

Another direction of interest is the implementation of algorithms based on artificial intelligence, to perform complex tasks.

The presented model can be made practically, with low costs, using the 3D printing process.

Successive improvements can also be made to the system by adding counterweights or elastic elements to reduce the driving torques required to make the hand-arm system lighter and more efficient.

Bibliography

1. Abdel-Malek, et al., *Towards a new generation of virtual humans*, International Journal of Human Factors Modelling and Simulation, vol. 1(1), pp. 2-39, 2006.
2. Abondance, S., Teeple, C. B., și Wood, R. J., *A dexterous soft robotic hand for delicate in-hand manipulation*, IEEE Robotics and Automation Letters, vol. 5(4), pp. 5502-5509, 2020.
3. Angeles J., *Fundamentals of Robotic Mechanical Systems: Theory, Methods, and Algorithms, Second Edition*, Editura Springer, Germania, 2002.
4. Bishop, R. H., (Editor), *The Mechatronic Handbook*, CRC Press Inc., Boca Raton, 2002.
5. Buondonno, G. și De Luca, Al., *A recursive Newton-Euler algorithm for robots with elastic joints and its application to control*, 2015 IEEE/RSJ International Conference on Intelligent Robots and Systems (IROS). IEEE, pp. 5526-5532, 2015.
6. Burger, M., Gerdts, M., *DAE aspects in vehicle dynamics and mobile robotics*, Campbell, S., Ilchmann, A., Mehrmann, V., Reis, T. (eds.) Applications of Differential-Algebraic Equations: Examples and Benchmarks. Differential-Algebraic Equations Forum. Springer, Cham, 2018.
7. Campbell, St., Lihn, V.H. și Petzold, L. Differential-algebraic equations. Scholarpedia, vol. 3(8), 2008., doi:10.4249/scholarpedia.2849.
8. Choi, D., Lee, D.-W., Shon, W. și Lee, H.-G., *Design of 5 D.O.F Robot Hand with an Artificial Skin for an Android Robot*, The Future of Humanoid Robots - Research and Applications, InTech, Rijeka, Croatia, pp. 81-96, 2012.
9. Craifaleanu, A., *Mecanica*, Editura MATRIXROM, București, 2021.
10. Cutkosky, M., *On Grasp Choice, Grasp Models, and the Design of Hands for Manufacturing Tasks*, IEEE Transactions on Robotics and Automation, vol. 5(3), pp. 269-279, 1989.
11. Daoud, N., Gazeau, J.P., Zeqhloul, S., Arsicault, M., *A real-time strategy for dexterous manipulation: Fingertips motion planning, force sensing and grasp stability*, Journal of Robotics and Autonomous Systems, vol. 60(2), pp. 377–386, 2012.
12. Deimel, R. și Brock, O., *A novel type of compliant and underactuated robotic hand for dexterous grasping,* The International Journal of Robotics Research, vol. 35(1-3), pp. 161-185, 2015.
13. Dragoș, L., *Principiile mecanicii analitice*, Ed. tehnică, București, 1976.
14. Dumitru, Șt., Craifaleanu, A., *Kinematic and dynamic analysis of an anthropomorphic hand-arm system*, U.P.B. Sci. Bull., Series D, vol. 85(4), pp. 27-42, 2023.
15. Dumitru, Șt., Craifaleanu, A., *Kinematic Model of an Anthropomorphic Robotic Arm*, ANNALS of Faculty Engineering Hunedoara – International Journal of Engineering, vol. 20(1), pp. 55-60, 2022.
16. Dumitru, Șt., Craifaleanu, A. și Petre R.A., *Vibratory analysis of a robotic hand*, Herisanu, N., Marinca, V. (eds) Acoustics and Vibration of Mechanical Structures – AVMS-2021, Springer Proceedings in Physics, vol. 274., Springer, Cham, pp. 213-221, 2022.
17. Farman, M., Al-Shaibah, M., Aoraiath, Z., și Jarrar, F., *Design of a three degrees of freedom robotic arm*, International Journal of Computer Applications, vol. 179(37), pp. 12-17, 2018.
18. Ferrolho, H., Ivan, V., Merkt, W., Havoutis, I., și Vijayakumar, S., *Inverse dynamics vs. forward dynamics in direct transcription formulations for trajectory optimization*, 2021 IEEE International Conference on Robotics and Automation (ICRA), IEEE, pp. 12752-12758, 2021.
19. Gasparetto, A., Scalera, L., *A Brief History of Industrial Robotics in the 20th Century.* Advances in Historical Studies, 8, Scientific Research Publishing, pp. 24-35, 2019.
20. Gonçalves, F., et al., *Dynamic Modeling of a Human-Inspired Robot Based on a Newton-Euler Approach*, Kecskeméthy, A., Parenti-Castelli, V. (eds) ROMANSY 24 - Robot Design, Dynamics and Control, ROMANSY 2022, CISM International Centre for Mechanical Sciences, vol. 606. Springer, Cham, pp. 79-90, 2022.
21. Hesse, S., Monkman, G. J., Steinmann, R., Schunk, H., *Robotergreifer: Funktion, Gestaltung und Anwendung industrieller Greiftechnik*, Hanser Verlag, München, 2007.
22. Hofer, M., și D'Andrea, R., *Design, fabrication, modeling and control of a fabric-based spherical robotic arm*, Mechatronics, vol. 68, 2020.
23. Ionescu, M., Borcoși, I., Gîlcă, Gh. și Bîzdoacă, N.G., *Description and control of a Lobot uHand STM 32 structure*, Annals of the „Constantin Brancusi" University of Târgu Jiu, Engineering Series, vol. 1, Târgu Jiu, pp. 14-19, 2019.
24. Ionescu, M., Gîlcă, Gh., Borcoși, I., Besnea (Petcu), F.L., Cismaru, S.I. și Bîzdoacă, N.G., *The Simulation of positioning of a Lobot uHand STM32 structure*, 2019 International Conference on Electromechanical and Energy Systems (SIELMEN), Craiova, pp. 1-6, 2019.
25. Iqbal, J., Islam, R. U., și Khan, H., *Modeling and analysis of a 6 DOF robotic arm manipulator*, Canadian Journal on Electrical and Electronics Engineering, vol. 3(6), pp. 300-306, 2012.
26. Jones, L. A., și Lederman, S. J., *Human hand function*, Oxford university press, 2006.

27. Kang, B., Chu, J., Mills, J. K., *Design of High Speed Planar Parallel Manipulator and Multiple Simultaneous Specification Control*, Proceedings - IEEE International Conference on Robotics and Automation, Vol. 3, pp. 2723-2728, 2001.
28. Kawasaki, H., Komatsu, T., Uchiyama, K. și Kurimoto, T., *Dexterous anthropomorphic robot hand with distributed tactile sensor: Gifu hand II,* IEEE International Conference on Systems, Man, and Cybernetics Proceedings, vol. 2, pp. 782-787, 1999.
29. Kivell, T. L., Baraki, N., Lockwood, V., Williams-Hatala, E. M., și Wood, B. A., *Form, function and evolution of the human hand*, American Journal of Biological Anthropology, vol. 181, pp. 6-57, 2023.
30. Kocin, N. E., *Calcul vectorial și introducere în calculul tensorial*, Ed. tehnică, București, 1954.
31. Küçük S. (Editor), *Serial and Parallel Robot Manipulators – Kinematics, Dynamics, Control and Optimization*, InTech: Rijeka, Croația, 2012.
32. Kurfess, T. R., (Editor), *Robotics and Automation Handbook*, CRC Press Inc., Boca Raton, 2005.
33. Kurosh, A., *Higher Algebra*, Mir Publishers, Moscow, 1975.
34. Lach, L., Lemaignan, S., Ferro, F., Ritter, H., și Haschke, R., *Bio-Inspired Grasping Controller for Sensorized 2-DoF Grippers*, IEEE/RSJ International Conference on Intelligent Robots and Systems (IROS), IEEE, pp. 11231-11237, 2022.
35. Lamour, R., März, R. și Tischendorf, C., *Differential-algebraic equations: a projector basedanalysis*, Springer Science & Business Media, 2013.
36. Lurie, A. I., *Analytical Mechanics*, Springer, 2002.
37. Luo, X., Mu, D., Wang, Z., Ning, P. și Hua, C., *Adaptive full-state constrained tracking control for mobile robotic system with unknown dead-zone input*, Neurocomputing, vol. 524, pp. 31-42, 2023.
38. Mahmoud, R., Ueno, A. și Tatsumi, S., *Dexterous Mechanism Design for an Anthropomorphic artificial hand: Osaka City University Hand I*, 10th IEEERAS International Conference on Humanoid Robots, Nashville, TN, 2010.
39. Mangeron, D., Irimciuc, N., *Mecanica rigidelor cu aplicații în inginerie*, vol. I-III, Ed. tehnică, București, 1978-1981.
40. Mataric, M. J., *The robotics primer*, The MIT Press, Cambridge, Massachusetts, 2007.
41. Meirovitch, L., *Fundamentals of vibrations*, McGraw-Hill International Edition, 2001.
42. Moran, M. E., *Evolution of robotic arms*, Journal of Robotic Surgery, vol. 1(2), Springer, Londra, pp. 103-111, 2007.
43. Murray, R. M., Li, Z., Sastry, S., *A mathematical introduction to robotic manipulation*, CRC Press Inc., Boca Raton, 1994.
44. Nurpeissova, A., Tursynbekov, T. și Shintemirov, A., *An Open-Source Mechanical Design of ALARIS Hand: A 6-DOF Anthropomorphic Robotic Hand*, Proceedings of the 2021 IEEE International Conference on Robotics and Automation (ICRA 2021), Xi'an, China, pp. 1077-1183, 2021.
45. Otten, E., *Inverse and forward dynamics: models of multi–body systems*, Philosophical Transactions of the Royal Society of London, Seria B: Biological Sciences, nr. 358(1437), pp. 1493-1500, 2003.
46. Pagoli, A., Chapelle, F., Corrales, J. A., Mezouar, Y., și Lapusta, Y., *A soft robotic gripper with an active palm and reconfigurable fingers for fully dexterous in-hand manipulation*, IEEE Robotics and Automation Letters, vol. 6(4), pp. 7706-7713, 2021.
47. Park, H. și Kim, D., *An open-source anthropomorphic robot hand system: HRI hand*, HardwareX, vol. 7, 2020, https://doi.org/10.1016/j.ohx.2020.e00100.
48. Pars, L.A., *A Treatise on Analytical Dynamics*, Heinemann Educational Books Ltd, London, 1965.
49. Plosceanu, B., Craifaleanu, A., Untăroiu, C., *Vibrațiile sistemelor cu un grad de libertate*, Ed. Bren, București, 2001.
50. Predoi, M. V., *Vibrații mecanice. Modele și aplicații în MATLAB*, Ed. MATRIX ROM, București, 2011.
51. Rădoi, M., Deciu, E., *Mecanica*, Ed. didactică și pedagogică R. A., București, 1993.
52. Reckhaus, M., Hochgeschwender, N., Paulus, J., Shakhimardanov, A., și Kraetzschmar, G. K., *An overview about simulation and emulation in robotics*, Proceedings of SIMPAR, pp. 365-374, 2010.
53. Săvescu, A.V., Cheze, L., Xuguang, W., Beurier, G., Verriest, J.P., *A 25° of freedom hand geometrical model for better hand attitude simulation*, SAE transactions, vol. 113(1) pp. 270-275, 2004.
54. Schlesinger, G., *Der mechanische Aufbau der kunstlichen Glieder in Ersatzglieder und Arbeitshilfen*, Springer, Berlin, 1919.
55. Schwarz, R. J. și Taylor, C., *The anatomy and mechanics of the human hand*, Artificial limbs, vol. 2(2), pp. 22-35, 1955.
56. Sireteanu, T., Solomon, O., Mitu, A.M., Giuclea, M., *A linearization method of piecewise linear systems based on frequency domain characteristics with application to semi-active control of vibration*, Journal of Vibration and Acoustics, vol 140(6), 061006, 2018.
57. Sireteanu, T., Solomon, O., Mitu, A.M.; Giuclea, M., *Application of a novel linearization method to compare the on–off control strategies modeled by piecewise linear systems*, Journal of Vibration and Control, vol. 26(23-24), pp. 2125-2135, 2020.
58. Spong, M. W., Hutchinson, S., Vidyasagar, M., *Robot Modeling and Control*, *First Edition*, John Wiley & Sons, Hoboken, NJ, 2006.
59. Stroe, I., Staicu, Șt. și Craifaleanu, A., *Internal forces calculus of compass robotic arm using Lagrange equations*, 10th ESA Workshop on Advanced Space Technologies for Robotics and Automation 'ASTRA 2011', ESTEC, Noordwijk, (pe CD-ROM), pp. 1-6, 2011.

60. Sutanto, G., et al., *Encoding Physical Constraints in Differentiable Newton-Euler Algorithm* Proceedings of the 2nd Conference on Learning for Dynamics and Control, Proceedings of Machine Learning Research, pp. 804-813, 2020.
61. Sutyasadi, P. și Wicaksono, M. B., *Joint control of a robotic arm using particle swarm optimization based H2/H∞ robust control on arduino*, TELKOMNIKA (Telecommunication Computing Electronics and Control), vol. 18(2), pp. 1021-1029, 2020.
62. Șabac, I. Gh., *Matematici speciale*, vol. I-II, Ed. didactică și pedagogică, București, 1981, 1983.
63. Touvet, F., Daoud, N., Gazeau, J. P., Zeghloul, S., Maier, M. A., Eskiizmirliler, S., *A biomimetic reach and grasp approach for mechanical hands*, Journal of Robotics and Autonomous Systems, vol. 60(3), pp. 473–486, 2012.
64. Tsai, L. W., *Robot analysis: the mechanics of serial and parallel manipulators*, John Wiley & Sons, 1999.
65. Voinea, R., Deciu, E., Dragomirescu, C., *Technische Mechanik*, ed. ALMA, Craiova, 2009.
66. Voinea, R., Stroe, I., *Introducere în teoria sistemelor dinamice*, Ed. Academiei Române, București, 2000.
67. Voinea, R., Stroe, I., Predoi, M. V., *Technical mechanics*, Ed. POLITEHNICA PRESS, București, 2010.
68. Voinea, R., Voiculescu, D. și Ceaușu, V., *Mecanica*, Editura didactică și pedagogică, București, 1983.
69. Wahit, M. A. A., Ahmad, S. A., Marhaban, M. H., Wada, C., și Izhar, L. I., *3d printed robot hand structure using four-bar linkage mechanism for prosthetic application*, Sensors, Basel, vol. 20(15), 2020.
70. Wallén J., *The history of the industrial robot*, Linköping University Electronic Press, Linköping, 2008.
71. Wang, S., et al., *Dynamic simulation analysis and experimental study of an industrial robot with novel joint reducers* Multibody Syst Dyn vol. 57(2, pp. 107–131), 2023, https://doi.org/10.1007/s11044-022-09864-7.
72. Xu, J., et al., *Efficient tactile simulation with differentiability for robotic manipulation*, Conference on Robot Learning, pp. 1488-1498, PMLR, 2023.
73. Ye, T., Ling, J., Yao, T., și Xiao, X., *Design of a 2-DOF constant force compliant microgripper for optical switch assembly*, The 46th Annual Conference of the IEEE Industrial Electronics Society, IEEE, pp. 4403-4408, 2020.
74. Zhang, D., Ma, W. și Zhang, H., *Analysis and Simulation of Mechanical Arm Dynamics Model Based on Simulink* 2nd International Conference on Algorithms, High Performance Computing and Artificial Intelligence (AHPCAI), Guangzhou, pp. 416-419, 2022.
75. *** - *A Glossary of Terms for Robotics* pregătit pentru Air Force Materials Laboratory, Wright-Patterson Air Force Base, Ohio. Biroul Național de Standardizare a Statelor Unite, Washington, D.C., 1980.
76. *** - ISO 8373:2012, *Robots and robotic devices - Vocabulary*.
77. *** - https://math.stackexchange.com/questions/569856/function-with-zero-first-to-nth-derivative-at-end-points, accesat 15.09.2023.
78. *** - https://uk.banggood.com/LOBOT-uHand-STM32-Open-Source-RC-Robot-Right-Arm-APP-or-Stick-or-Glove-Control-Educational-Robot-Arm-Kit-p-1403202.html?cur_warehouse =CN, accesat 15.09.2023.
79. *** - https://www.amazon.com/ELEPHANT-ROBOTICS-Collaborative-Programming-Applications/dp/B0C2CXTP52/ref=sr_1_1_sspa?adgrpid=1340307075889385&hvadid=83769455604490&hvbmt=bb&hvdev=c&hvlocphy=140908&hvnetw=o&hvqmt=b&hvtargid=kwd-83770243317663&hydadcr=7668_13583979&keywords=wearable%2Brobotic%2Barm&msclkid=097173ab178f181487d316156dd93ca5&qid=1706982017&sr=8-1-spons&sp_csd=d2lkZ2V0TmFtZT1zcF9hdGY&th=1, accesat 03.01.2024.
80. *** - https://www.amazon.com/dp/B094FRPJ16/ref=sspa_dk_detail_0?psc=1&pd_rd_i= B094FRPJ16&pd_rd_w=23Tj6&content-id=amzn1.sym.eb7c1ac5-7c51-4df5-ba34- ca810f1f119a&pf_rd_p=eb7c1ac5-7c51-4df5-ba34-ca810f1f119a&pf_rd_r=ZC33CZPCFZM XJS73NZTZ&pd_rd_wg=u9l5M&pd_rd_r=2fdd8a4b-a0a0-4cea-8c58-9a12e77682e4&s=toys-and-games&sp_csd=d2lkZ2V0TmFtZT1zcF9kZXRhaWw, accesat 03.09.2023.
81. *** - https://www.amazon.com/dp/B0BX52FSX8/ref=sspa_dk_detail_0?psc=1&pd_rd_i =B0BX52FSX8&pd_rd_w=6AwCV&content-id=amzn1.sym.eb7c1ac5-7c51-4df5-ba34-ca810f1f119a&pf_rd_p=eb7c1ac5-7c51-4df5-ba34-ca810f1f119a&pf_rd_r= JFZTPKKTCV12FGQAZV6M&pd_rd_wg=32e6B&pd_rd_r=140a3dca-4d1d-4811-82ee-bfea78a33e5a&s=toys-and-games&sp_csd=d2lkZ2V0TmFtZT1zcF9kZXRhaWw
82. *** - https://www.aliexpress.com/i/1005004514454645.html, accesat 03.09.2023.
83. *** - https://www.rmigo.com/shop/platforms/arduino/lobot-uhand-arduino-gestrure-recognition-bionic-mechanical-hand/, accesat 15.09.2023.
84. *** - https://www.sutori.com/en/item/1963-the-rancho-arm-is-developed-at-rancho-los-amigos hospital-in-downey-cal, accesat 02.08.2023.